DEMONSTRATION OF ROBOTIC DEBURRING PROCESS MOTOR SKILLS FROM MOTION PRIMITIVES OF HUMAN SKILL MODEL

A THESIS SUBMITTED TO
THE GRADUATE SCHOOL OF NATURAL AND APPLIED SCIENCES
OF
MIDDLE EAST TECHNICAL UNIVERSITY

BY

PAYAM PARVIZI

IN PARTIAL FULFILLMENT OF THE REQUIREMENTS
FOR
THE DEGREE OF MASTER OF SCIENCE
IN
MECHANICAL ENGINEERING

JANUARY 2018

Approval of the thesis:

DEMONSTRATION OF ROBOTIC DEBURRING PROCESS MOTOR SKILLS FROM MOTION PRIMITIVES OF HUMAN SKILL MODEL

submitted by **PAYAM PARVIZI** in partial fulfillment of the requirements for the degree of **Master of Science in Mechanical Engineering Department, Middle East Technical University** by,

Prof. Dr. Gülbin Dural Ünver
Dean, Graduate School of **Natural and Applied Sciences**

Prof. Dr. M. A. Sahir Arıkan
Head of Department, **Mechanical Engineering**

Assoc. Prof. Dr. E. İlhan Konukseven
Supervisor, **Mechanical Engineering Dept., METU**

Examining Committee Members:

Prof. Dr. Reşit Soylu
Mechanical Engineering Dept., METU

Assoc. Prof. Dr. E. İlhan Konukseven
Mechanical Engineering Dept., METU

Assist. Prof. Dr. Ali Emre Turgut
Mechanical Engineering Dept., METU

Assist. Prof. Dr. Kıvanç Azgın
Mechanical Engineering Dept., METU

Assist. Prof. Dr. Andaç T. Şamiloğlu
Mechanical Engineering Dept., Başkent University

Date: ______________

I hereby declare that all information in this document has been obtained and presented in accordance with academic rules and ethical conduct. I also declare that, as required by these rules and conduct, I have fully cited and referenced all material and results that are not original to this work.

Name, Last Name: PAYAM PARVIZI

Signature :

ABSTRACT

DEMONSTRATION OF ROBOTIC DEBURRING PROCESS MOTOR SKILLS FROM MOTION PRIMITIVES OF HUMAN SKILL MODEL

Parvizi, Payam
M.S., Department of Mechanical Engineering
Supervisor : Assoc. Prof. Dr. E. İlhan Konukseven

January 2018, 107 pages

This study presents a new method to learn motor skills of robotic deburring process from a human expert who is performing manual deburring operation. By utilizing this method, it is possible to automate the robotic deburring process of a workpiece with an unknown shape. In this work, the task-related movements of the human expert are recorded using 6DOF and 1DOF haptic devices. Then, the intrinsic movement primitives are parametrized by using Dynamic Movement Primitive (DMP) method. By collecting dataset of parameters and weights of this method, trajectories of complex behaviors can be generated. Moreover, this method can adapt itself with respect to different start and goal positions. In order to move from one position to other position in two-dimensional space, rhythmic movements of human expert are extracted by using two-dimensional DMPs.

In addition, different fundamental studies have been done on general concentrated-position DMP and local DMP. In general concentrated DMP, the experiments are conducted on 6DOF haptic device, in which the manual deburring processes on a workpiece are imitated and the results are used as primitives to accomplish general automatic deburring on the workpiece. Furthermore, Local DMP performs like the human automatic controller which its aim is to control force using movement primitives of the skills of a human expert in one dimension. The experiments of local DMP are conducted on 1DOF haptic device interacted with 6DOF grinding robot and piezoelectric actuator.

Moreover, automation of robotic deburring process on unknown workpiece requires studies on tool deflection, collision, optimal velocity and surface shape search. Different experiments have been performed in order to eliminate collision and reduce form error on a workpiece. The results of experiments are analyzed by scanning the surface of workpieces. Finally, our process is compared with an alternative process and the time duration of each process is analyzed.

Keywords: Deburring Process, Industrial Robotic, Motion Primitives, Learning from Demonstration, Motion and Path Planning

ÖZ

İNSAN BECERİSİNİN HAREKET İLKELERİYLE ROBOTİK TAŞLAMA İŞLEMİNDE GÖSTERİMİ

Parvizi, Payam
Yüksek Lisans, Makina Mühendisliği Bölümü
Tez Yöneticisi : Doç. Dr. E. İlhan Konukseven

Ocak 2018, 107 sayfa

Bu çalışma manuel çapak alma işlemini gerçekleştiren operatörün, robotik çapak alma işleminin motor becerilerini öğrenmesi için yeni bir yöntem sunmaktadır. Bu yöntemi kullanarak bilinmeyen şekle sahip bir iş parçasının robotik çapak alma işleminin otomasyonunu gerçekleştirmek mümkündür. Bu çalışmada, operatörün görevle ilgili hareketleri 6 ve 1 serbestlik dereceli haptik cihazlar kullanılarak kaydedilir. Ardından, içsel temel hareketler Dinamik Hareket Primitifleri (DMP) yöntemi kullanılarak parametrelendirilir. Bu yöntemin parametrelerinin ve ağırlıklarının veri kümesini toplayarak, karmaşık davranışların yörüngeleri oluşturulabilir. Dahası, bu yöntem kendisini farklı başlangıç konumlarına göre uyarlayabilir. İki boyutlu uzayda bir konumdan diğer pozisyona geçmek için operatörün ritmik hareketleri iki boyutlu DMP kullanılarak çıkarılır.

Buna ek olarak, genel konum odaklı DMP ve yerel posizyonlama odaklı DMP üzerinde farklı temel çalışmalar yapılmıştır. Genel konum odaklı DMP'de, deneyler, iş parçasındaki manuel çapak alma işlemlerinin taklit edildiği ve iş parçasındaki çapak alma işlemini gerçekleştirmek için ilkel olarak kullanılan 6 serbestlik dereceli haptik cihaz üzerinde yürütülür. Ayrıca, yerel posizyonlama odaklı DMP, operatörün becerilerinin bir boyutta hareketinin temel ilkelerini kullanarak kuvveti kontrol etmeyi amaçlayan insanın kontrol komutlarını taklit eder. Yerel posizyonlama odaklı DMP deneyleri 6 serbestlik dereceli çapak alma robotu ve pizoelektrik aktüatör ile etkileşimli 1 serbestlik dereceli haptik cihaz üzerinde yürütülmüştür.

Ayrıca bilinmeyen iş parçası üzerinde robotik çapak alma işleminin otomasyonu için takım sapması, çarpışma, optimum hız seçimi ve yüzey şeklinin belirlenmesi üzerine daha ileri araştırmalara ihtiyaç duyulmaktadır. Bu amaca yöneklik, çarpışma kuvvetini ortadan kaldırmak ve iş parçasındaki yüzeydeki form hataları azaltmak için farklı deneyler gerçekleştirildi. Deney sonucu, iş yüzeyi taranarak analiz edildi. Son olarak, işlemimiz alternatif süreçle karşılaştırıldı ve sürecin süresi incelendı.

Anahtar Kelimeler: Robotik çapak alma prosesi, Endüstriyel robotik, Hareket İlkeleri, Gösterimden Makine öğrenimi, Hareket ve yol planlaması

To my parents
and my brother

ACKNOWLEDGMENTS

First and foremost, I would like to express my endless appreciation to my supervisor Assoc. Prof. Dr. Erhan İlhan Konukseven for his guidance and support during this study. Despite my slight experience in the beginning of this study, he gave me a chance to be part of his lab and get knowledge about this field to put one more step further to reach my goals.

I would like to thank my lab mates, Kemal Acikgoz, Masoud Latifi Navid, Musab Cagri Ugurlu, Abdulhamit Donder, Ugur Mengilli and Omer Okumus for their immense supports and fruitful knowledge they shared. They were always available to discuss my academic questions regardless of time and condition. I appreciate the sleepless nights we shared to carry on our project.

I am deeply grateful to my friends Yashar Badienia, Arif Badem, Arvin Hoseinnejad, Golden Nadimi and Ashkan Soltani for their friendship and encouragements. During all these years far from hometown, they were always with me like a family.

Finally, yet importantly, I would like to express my profound gratitude to my parents and my brother. Their enlightened vision helped me to choose my goals and pursue them. This study would not be finished without their patience and encouragements.

I also would like to thank the Scientific and Technological Research Council of Turkey for their financial support of this research under Grant TÜBİTAK-114E274

TABLE OF CONTENTS

ABSTRACT v

ÖZ vii

ACKNOWLEDGMENTS x

TABLE OF CONTENTS xi

LIST OF TABLES xvi

LIST OF FIGURES xvii

LIST OF ABBREVIATIONS xxii

LIST OF SYMBOLS xxiii

CHAPTERS

1 INTRODUCTION 1

  1.1 Deburring Process 1

  1.2 Robot Imitation 3

  1.3 Thesis Motivation and Objective 4

1.4 Thesis Outline 6

2 LITERATURE SURVEY 9

3 EXPERIMENTAL SETUP 17

3.1 6DOF Haptic Device and related setup 19

3.2 Deburring/Grinding robot 23

3.3 1DOF Haptic Device and related setup 25

4 METHODOLOGY OF DMP 29

4.1 Development of Model 29

4.2 Learning Dynamics from demonstration 33

4.3 Global Optimization algorithm 34

4.4 Conclusion 37

5 GENERAL POSITION CONCENTRATED DMP 39

5.1 Methodology of General Position Concentrated DMP . . 39

5.2 Experiments 41

5.3 Results 41

5.4 Conclusion 43

6 TELEOPERATION IN GRINDING PROCESS 45

6.1 Methodology of Local Control with DMP 45

6.1.1 Force Control 46

6.1.2 Local DMP 49

6.2 Experiment Procedure 50

6.3 Model Verification 53

6.4 Conclusion 58

7 BASIC CONCEPTS 61

7.1 Tool deflection 61

7.2 Collision 62

7.3 Optimal feed-rate selection 63

7.3.1 Grinding Model 63

7.3.2 Artificial Neural Network model 67

7.4 Generating DMP 67

7.5 Conclusion 70

8 BASIC EXPERIMENTS AND RESULTS 71

8.1 Tool Deflection 71

8.2 Cleaning pass 72

8.3 Collision and burr size relation 74

8.4 ANN training for optimal F_R selection 75

8.4.1 ANN training for L_p and forces 76

8.4.2 Overall ANN training 77

8.5 Dynamic Movement Primitives generation 78

8.5.1 Experiments related to DMP generation 79

8.5.2 Elliptical fit from hand movements 80

8.5.3 Extraction of DMP 82

8.6 Conclusion 84

9 EXPERIMENTAL PROCEDURE 85

9.1 Ramp step search 86

9.2 Generation of DMP 87

9.3 Touching motion 88

9.4 Grinding on the layers 88

9.5 F_R selection by using ANN 89

9.6 Overall experimental procedure 89

10 RESULTS AND DISCUSSION 91

10.1 Duration of process 91

10.1.1 Process with zigzag movement 91

10.2 Form error of workpiece 93

10.2.1 Experiment with last layer D_c of 150 μm . . . 94

10.2.2 Experiment with last layer D_c of 300 μm . . . 95

10.2.3 Experiment with last layer D_c of 450 μm . . . 95

11 CONCLUSION AND FUTURE WORK 97

11.1 Conclusion 97

11.2 Future work 98

REFERENCES 99

APPENDICES 103

A MATLAB SIMULINK MODEL 103

B DATA OF EXPERIMENTS 105

LIST OF TABLES

TABLES

Table 8.1 Maximum normal force and related maximum form error on workpiece 72

Table 8.2 Maximum form error before and after cleaning pass 73

Table 8.3 Maximum and average resultant force of specific task 75

LIST OF FIGURES

FIGURES

Figure 1.1 Manual deburring process on medical component 2

Figure 1.2 Movement primitives of human for shaking hand 4

Figure 1.3 Learning by demonstration 5

Figure 2.1 Left: The human generated paths. Right: The DMP generated paths 12

Figure 2.2 Obstacle avoidance example. Red line: A DMP generated path. Black dot: An obstacle 13

Figure 2.3 Combination of two demonstration 14

Figure 3.1 Two haptic devices are being used for surgery in virtual environment 18

Figure 3.2 6DOF haptic device, deburring tool, workpiece, and F/T sensor 19

Figure 3.3 A close up of workpiece, F/T sensor, and the heavy metal block 20

Figure 3.4 Different workpiece profiles 20

Figure 3.5 Scanned figure of deburring tool of 6DOF haptic device . . . 21

Figure 3.6 Cylinders are fitted to the point cloud data using SolidWorks to obtain the orientations and offsets 22

Figure 3.7 Overall setup of the deburring robot 23

Figure 3.8 P-602 piezoelectric actuator. 24

Figure 3.9 1DOF haptic device figure 26

Figure 3.10 Relative clockwise or counterclockwise 1DOF haptic motion with respect to piezoelectric actuator 27

Figure 4.1 Phase variable as a function of time (s) of specific experiment 31

Figure 4.2 40 exponential kernels as a function of time (s) of specific experiment 32

Figure 4.3 Generation of trajectory using DMP in 1-dimension 32

Figure 4.4 psudo code of PSO algorithm 34

Figure 4.5 Example of conceptual diagram of PSO 35

Figure 4.6 Example of position and velocity of swarms through fitness value 35

Figure 4.7 Example of the trajectory with different start and end positions and sizes 37

Figure 5.1 2D movement of the tool on workpiece with PSO optimization 42

Figure 5.2 Movement of tool on Workpiece in x-direction with respect to time in PSO optimization 42

Figure 5.3 Movement of tool on workpiece in y-direction with respect to time in PSO optimization 43

Figure 6.1 Wrist motions of participant while trying to fix normal force on $10N$ 46

Figure 6.2 Example of the deburring/grinding operation on a flat surface 47

Figure 6.3 Example of the deburring/grinding operation on a wavy surface 47

Figure 6.4 The connectivity diagram of the overall system 51

Figure 6.5 Upper front view of the workpiece and the tool tip 52

Figure 6.6 Example of the segmentation for the 1st participant in a random normal force of experiment 53

Figure 6.7 Example of the segmentation for the 2nd participant in a random normal force of experiment 54

Figure 6.8 All normal force reactions of 1st Participant 55

Figure 6.9 All normal force reactions of 2nd Participant 55

Figure 6.10 Best reaction of 1st Participant for 11.5 N disturbance force . 56

Figure 6.11 Best reaction of 2nd Participant for 11.5 N disturbance force 57

Figure 6.12 Best reaction of normal force for each participants with respect to random disturbance force (each color represent each participant) 57

Figure 6.13 Best reaction of normal force for all participants with respect to random disturbance force 58

Figure 7.1 Normal force with and without collision on same characteristic experiments 62

Figure 7.2 Normal force profile in time domain 65

Figure 7.3 Example of regime 1 65

Figure 7.4 Example of regime 2 66

Figure 7.5 Example of regime 3 66

Figure 7.6 Feed-rate selection by using ANN 68

Figure 7.7 Block diagram of DMP generation 69

Figure 8.1 Surface scanning setup 72

Figure 8.2 Form error due to interaction force of 150 μm depth of cut . 73

Figure 8.3 Form error due to interaction force of 300 μm depth of cut . 73

Figure 8.4 Form error due to interaction force of 450 μm depth of cut . 74

Figure 8.5 Example of the relation between L_p and $F_{resultant}$ 76

Figure 8.6 ANN block digram of force inputs and L_p output 77

Figure 8.7 ANN prediction of L_p and trained L_p 77

Figure 8.8 Block diagram of overall ANN for feed-rate selection 78

Figure 8.9 ANN prediction of F_R and trained F_R 78

Figure 8.10 Participant holding spindle of 6-DOF haptic device 79

Figure 8.11 sinusoidal profile 79

Figure 8.12 Example of elliptic fit of rhythmic movement of experienced participants 81

Figure 8.13 Example of elliptic fit of rhythmic movement of deburring expert 81

Figure 8.14 DMP with elliptical trajectory generation 82

Figure 8.15 Generating trajectory of experienced participant 83

Figure 8.16 Generating trajectory of deburring expert 83

Figure 8.17 Example training to choose DMP in the desired range for experienced participants 84

Figure 9.1 The Y-direction movement of the tool on the workpiece . . . 85

Figure 9.2 Ramp step search in order to find profile shape 86

Figure 9.3 wall shaped workpiece 87

Figure 9.4 DMP generation of the tool with respect to the desired depth of cut 87

Figure 9.5 Layer selection 88

Figure 9.6 overall flowchart of the experiments 90

Figure 10.1 Example of zigzag movement 92

Figure 10.2 Significant zigzag motion on workpiece 92

Figure 10.3 Nonsense zigzag motion on workpiece 93

Figure 10.4 DMP trajectory on the workpiece 93

Figure 10.5 profile scanning in two different paths 94

Figure 10.6 Workpiece before and after experiment with last layer of 150 μm 94

Figure 10.7 Workpiece before and after experiment with last layer of 300 μm 95

Figure 10.8 Workpiece before and after experiment with last layer of 450 μm 96

Figure A.1 Matlab Simulink of F/T sensor, Piezoelectric actuator and spindle speed (Work simultaneously) 103

Figure B.1 Scanned surface of experiment of figure 10.7 105

Figure B.2 Scanned surface of experiment of figure 10.8 106

Figure B.3 Scanned surface of experiment of figure 10.9 107

LIST OF ABBREVIATIONS

F_t	Tangential force
F_n	Normal force
ω	Weight of nonlinear learn-able function
τ	Temporal scaling factor
α	Time constant
β	Time constant
D_c	Depth of cut
F_R	Feed-rate
S_s	Spindle speed
L_p	Load percent
$f(x)$	Nonlinear learn-able term
$\psi(x)$	Basis function
y_0	Initial state of a trajectory
α_x	Constant value
τ_x	Constant value
x	Phase variable
h_i	Width of basis function
c_i	Center of basis function

LIST OF SYMBOLS

$6DOF$	6 Degrees of freedom
$1DOF$	1 Degree of freedom
cBN	Cubic Boron Nitride
F/T	Force/Torque
DMP	Dynamic Movement Primitive
DAQ	Data Acquisition card
PSO	Particle Swarm Optimization
$1-D$	One-Dimensional
$3-D$	Three-Dimensional

CHAPTER 1

INTRODUCTION

1.1 Deburring Process

After machining operation with different manufacturing methods, burrs that are undesirable small pieces of material, remain attached to the edge and surface of a material. Burr formation is one of the most critical issues that appear during manufacturing. Although burrs are small in size, they can increase early corrosion of the material, injury during assembly, failure in precision instruments and increase stresses on the edge and surfaces of a machined part [1].

Deburring or burr removal is finishing process that removes burrs, increases the functionality, performance, safety and quality of the machined part. Precisely deburred machined parts are usually used for aircraft structures and medical implants which the surface of these parts should be functionalized by micro-structuring and better compatibility to get more efficient performance [2]. There are many types of deburring processes which most common of them are Mechanical, Manual, Electrical, Thermal and chemical deburring [1]. Nowadays, by increasing the demand for high quality and precisely machined parts, robotic deburring also gained attention in the industry.

Manual deburring is the most extensively used deburring process in the industry. In this process, tools are low-cost and human expert is able to accustom him/herself to many different parts. Also, he/she has inherent added inspection effect [1]. Human expert performs the process by using his/her three senses, simultaneously. Human expert has special wrist and hand motions when using the tool which is the optimal motion on the workpiece, Figure 1.1. Also, by touching the workpiece, the expert understands the surface roughness while deburring on the workpiece. Besides, by hearing the sound of the process, he/she can figure out the burr size and hardness of the material. In addition, an expert can understand the roughness of the workpiece by using the vision. Besides a lot of advantages of manual deburring, this process has many disadvantages. Human expert has the lack of repeatability and mass processes which the performance can change due to physical and psychological fatigue. In addition, the requirement of micron-size resolution deburring/grinding process cannot be performed by expert dexterity. Human senses are incapable of recognizing surface roughness in micron-size resolution.

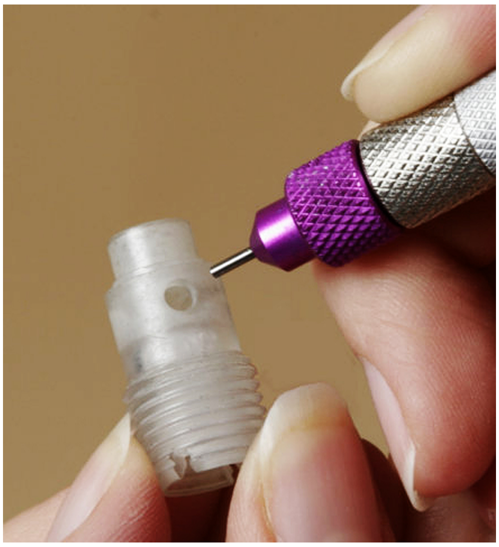

Figure 1.1: Manual deburring process on medical component

Over the past years, by increasing the necessity of repeatability, mass production and high precision machined materials, robotic deburring become widespread. Although deburring robots have possible senses of vibration, vision, sound and Force/Torque (F/T) sensors, in precise robotic deburring processes, these senses are not preferred because of the high value of noise with respect to burr size. For this reason, there is a complete lack of understanding of the burr removal.

Since the generation of a path for a task cannot be programmed for every situation (or robot-environment interactions), a higher level decision-making approach based on an already expert system's internal model of its environment might be extracted through a proper mathematical method and be replaced with the traditional methods. Therefore, the best choice is to associate the advantages of manual and robotic deburring processes. Accordingly, the optimal alternative is to develop a robot that can mimic human expert skills by using Force/Torque sensors.

1.2 Robot Imitation

The study of imitation in robotics has been developed to produce machines which are flexible in different circumstances and able to utilize skills of human expert. Robot that imitate human expert has to know what to imitate and be able to map its perceptions onto its actions. Moreover, a capability of the joints and links of the robot to imitate the extracted skills from the expert who has unique set of joints and link structure with associated dexterity, must also be determined.

In order to imitate a human, foremost, robot needs to detect the demonstrator and percept his/her actions. The general solution to percept human movements is perceptual-motor primitives (Movement primitives) to provide basic information on how a human is moving. Movement primitives are a representation of action sequences for generalized movements that conclude to goal [3]. By using parameters in the form of a parameterized motor controller, a movement primitives can be formalized as a control policy to obtain an intended task.

Secondly, once the actions of human expert have been perceived, robot has to map the perceptions of movement primitives in a sequence of motor actions with the same outcome. The problem of mapping the perception and action is "correspondence problem". The human and robot body are not the same; which links and joints of human and robot are different and have diversified link and

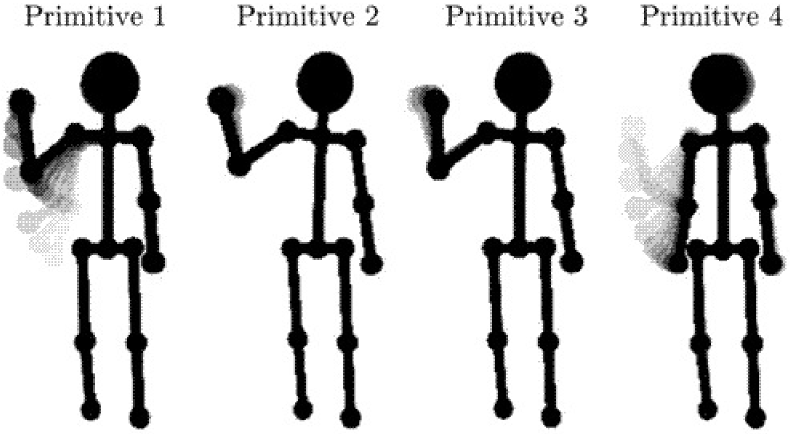

Figure 1.2: Movement primitives of human for shaking hand

actuator responses. Correspondence problem can be solved by giving a robot the ability by "Learning by demonstration" and "Learning to imitate". In Learning by demonstration, a new task is acquired by the robot. The robot learns how to perform the physical task of the demonstrator, shown in figure 1.3. For this, robot has been neutralized and demonstrator tries to perform a task by driving the robot structure to perform the task directly or teleoperation can be performed which solves the correspondence problem. However, in "Learning to Imitate", when the ability to imitate is learned, robot learns how to solve the "correspondence problem" through experience using learning algorithms [4].

1.3 Thesis Motivation and Objective

Going through the introduction of the manual and robotic deburring process and robot imitation, one can realize that the main concern is to transfer the skills of human expert while performing manual deburring to robot in micron-size resolution. In order to provide robot to imitate human expert, some problems must be stated.

As the generation of wrist movements cannot be adapted for every task, the

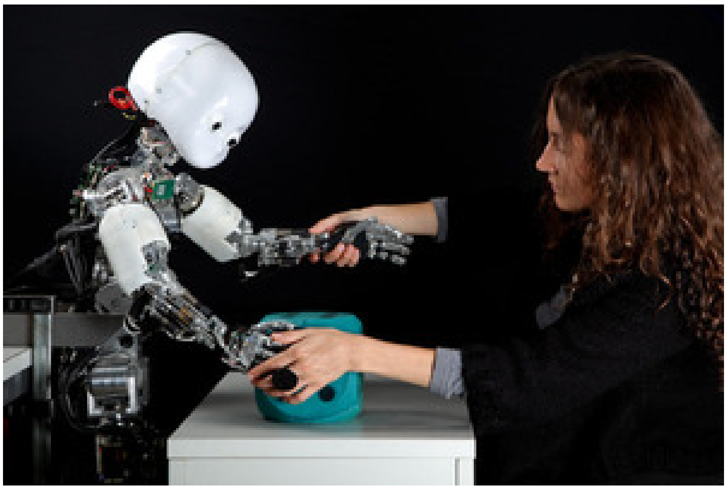

Figure 1.3: Learning by demonstration

useful representation of a task should be indicated. The mathematical model represented for a task has to have proper parameters, commands, controls and state representation. Also, model of task must be in the form of generalization. Primitives of a specific task create a family of movements that all converge to the same goal. In addition, In order to transfer the model of specific task, there has to be a setup to record wrist movements, quickness and exerted forces of human expert on the workpiece. Furthermore, after modeling a specific task of human expert, it must be transferred to robot. However, robot actuators, links, motion and speed constraints are not the same as human expert which is correspondence problem. Therefore, the movement derivatives have to be scaled and controlled, and after experiments with robot, trial and error learning must be performed.

General motivation of this study is to develop a mathematical system by using Dynamic Movement Primitives. In order to do this, we build a setup which contains the force/torque sensor under workpiece to measure 3-D forces coming from expert and haptic device to measure movements of the wrist of human expert. Also, by using this information, dynamic movement primitive method is considered. Dynamic Movement Primitive (DMP) is a method of trajectory modeling motivated by the desire to find a way to represent complex motor actions. DMP is generally implemented in grasping, placing movements of the robot arm and the movement of locomotion robot in dynamic environment. However, in this study, DMP is going to be implemented in robotic deburring process at micron-size resolution. Finally, correspondence problem is going to be solved by taking advantage of grinding model that is implemented for robot before [5]. In addition, our motivation is to have automatic robot that is able to perform deburring/grinding process on the unknown workpieces with different shapes.

It is necessary to state that, the aim of this study is to transfer the hand movements of human expert, recorded with haptic device, to a robot.

1.4 Thesis Outline

The main chapters of this thesis are about the development of robotic deburring process with motor skills from movement primitives of human skill model.

Subsequent to the introduction of the study in chapter 1, chapter 2 deals with a literature review of previous similar studies. Literature survey includes the presentation of similar studies and studies that are not related but inspiring.

Chapter 3 deals with the experimental setup used in this work. In order to transfer skills of a human expert to the robot, the setup has to be built to record human movements and forces. Also, the robotic deburring/grinding setup which contains a parallel manipulator (hexapod), spindle, workpiece and a piezoelectric actuator is presented.

Chapter 4 is the main conceptual chapter of this thesis. The general method that has been inspiring for us on doing this thesis work is presented in this chapter. This method helps us to model movement primitives of skills of a human expert for a specific task. Also, parametrization of DMP is studied.

In chapter 5, the method of DMP is modified with respect to generation of interaction force between tool and workpiece in deburring/grinding process. These interaction forces affect the trajectory. Therefore, in this study, nonlinear differential equation part of DMP method is modified using deburring force.

In Chapter 6, we dealt with the correspondence problem by utilizing a teleoperation scheme. An experimental setup consisting of F/T sensor and a 1DOF haptic device has been constructed and discussed in this Chapter. We obtained human expert's hand movements in one dimension and extracted the movement primitives. DMP method is modified to accommodate a force trajectory rather than a movement trajectory.

Another task of this study is to automatize the robotic deburring/grinding process. The DMP method is not enough alone to cover automation. The remaining studies are discussed in chapters 7 and 8 include tool deflection, collision, layer selection, ramp step search and ANN for feed-rate selection. In chapter 7, the aforementioned concepts have been introduced and in chapter 8 experiments and results associated with them have been shared. In addition, in chapter 9, the experimental procedure for automatic robotic deburring/grinding process is explained.

Finally, in chapter 10, an alternative obvious process other than our main approach has been investigated. The time duration for cutting in each process is compared. In addition, the surface of the workpiece before and after grinding process is scanned and discussed.

CHAPTER 2

LITERATURE SURVEY

In industry; tasks, such as deburring/grinding, requires adaptation to constantly changing part geometries. Evidently, skillful human workers do these tasks for any possible geometry. The setbacks of manual deburring and implications of a successful autonomous deburring cell for industry have already been discussed in chapter 1. In order to achieve high level of autonomy, robotic deburring needs to be more adaptable than its current state of the art. The bottleneck of adaptability for such tasks is all about the difficulty of generating a solution trajectory dynamically and correctly. An important observation on this is stated in [6] as *"Many control problems take place in continuous state-action spaces, e.g., as in manipulator robotics, where the control objective is often defined as finding a desired trajectory that reaches a particular goal state. While reinforcement learning offers a theoretical framework to learn such control policies from scratch, its applicability to higher dimensional continuous state-action spaces remains rather limited to date"*.

As a trajectory generation method, Dynamic Movement Primitives (DMPs) are suitable for general applicability in robotics. It concerns with how to formalize complex nonlinear dynamic equations without the need of manual parameter tuning and the danger of instability [7]. The mainstream DMP equation is based on nonlinear attractors where a linear mass-spring-damper system is coupled with a nonlinear term. The mass-spring-damper system acts as an attractor where the attraction is the target or the goal point. Depending on the start position, the trajectory is generated converging to the goal point. Combining all the joint DMPs and applying necessary torques can generate an end-effector movement that is required to perform a task. This approach alleviates the danger of instability while allowing generation of complex nonlinear dynamics. Before reviewing the main approaches on DMPs that can be applied to deburring, let's digress and talk about a mobile robot case and the importance of human demonstrations. There are mobile robot path generation methods that use Artificial Intelligence (AI) concepts such as Decision Trees, Bayesian Networks, Searching, and Neural Networks. The most prominent example is driver-less cars for this type of tasks, where a car senses the environment and dynamically generates a path to follow. This is a too broad and unrestricted task. However, traffic rules, models of general human behavior on traffic, reactions of real human drivers, and experience can be useful to restrict the search space and make the problem tractable. Also, real human driver demonstrations can be utilized for the solution of such a task. In fact, the human approach on driving a car is the most valuable piece of knowledge for a driver-less car AI since humans already solved how to drive a car and the traffic environment requires inevitable human interactions (unless until a completely driver-less future). In this example, the requirement of human demonstrations stems from both the difficulty of the problem (immense search space) and the environment.

Broadly speaking, the robotic deburring task is an interaction control topic. Hogan's [8] and [9] papers on interaction control is the root of similar studies. However, in a more specific study [9], Hogan identifies the types of movements as sub-movements, oscillations and mechanical impedance. Sub-movements are basic mathematical functions and can be used to generate any discrete movement. The oscillations are special combinations of sub-movements and can be used to generate rhythmic movements. The mechanical impedance is a relation between interaction forces and the motion. It is a dynamic operator defined as a mapping from given displacement, velocity and acceleration to the forces.

In deburring, reaction forces (cutting forces) plays a crucial role in the end quality. Thus, the trajectory is expected to be adaptable based on the force feedback. For force dependence, in [10], learning movement primitives for force interaction tasks is investigated. The approach relies on kinesthetic teach-in where correspondence problem is not presented. The problem they worked was a “pull and flip” task. In their work, control modalities (position control and force control) are decided based on movement primitives. They also worked on composition of movement primitives. In [11], the human deburring expert’s hand movements are modeled via Artificial Neural Networks (ANNs). Force inputs and orientation of the tool on the workpiece is used for generating a control strategy.

In the exciting work of Pastor, [12], human grasping and placing movements imitated by a robot. The author addressed correspondence problem, generalization, and robustness against perturbations. The correspondence problem occurs if the robot link and joint structure differ from that of the human arm. The generalization concerns with the ability to suit a demonstration to different start and goal positions. The robustness is important due to changing environment conditions (consider grasping a water bottle at different positions of a table). These problems are solved using Dynamic Movement Primitives (DMPs) method. DMPs solve generalization and robustness problems inherently, however correspondence problem requires further elaborations. For comparison of the DMP performance versus human performance, [13] contains a very explanatory figure (Figure 2.1). In the figure, DMPs generalization capabilities are emphasized. On the right-hand side, a single DMP is used for generating paths with same dynamics but different goal positions. On the left-hand side, human demonstrations are shown. Assuming extraction of the DMP from blue curves, the DMPs can generate the red curve on the right figure.

In [14], learning aggressive maneuvers for obstacle avoidance for UAVs is considered. Human remotely pilots the UAV and avoids obstacles. These maneuvers are recorded and modeled using DMPs. In this study, DMPs are extended using nonlinear contraction theory. Then, for different start and end positions, complex trajectories generated without considering the flight model of the UAV.

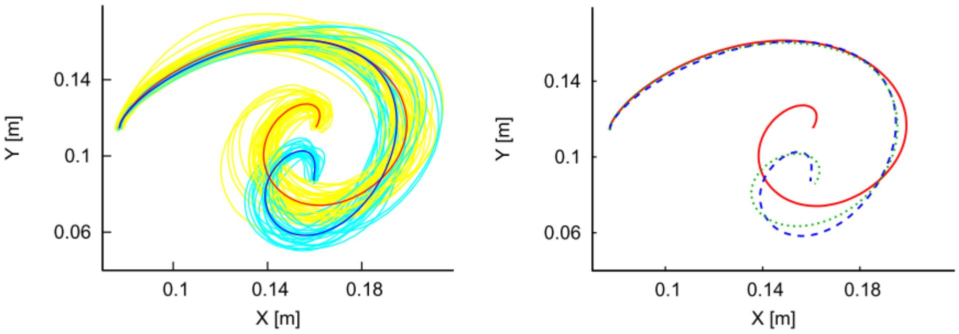

Figure 2.1: Left: The human generated paths. Right: The DMP generated paths

Also, simple DMP based obstacle avoidance is considered in [13], Figure 2.2. It can be extended to multiple obstacle avoidance and avoidance of moving obstacles as well. In robotic deburring, the forces change abruptly during a deburring task based on local hardness of the burrs. These forces can be considered as obstacles and avoiding them might be possible using DMPs following the aforementioned studies. More importantly, human experts need to reach the edge with burrs in order to perform the task. Thus, they need to avoid hitting other edges or the part. The segments of DMPs used for reaching to the burred region needs also obstacle avoidance not only for end-effector but also for the entire body of the robot.

An extension of DMPs using probability theory is given in [15]. It concerns with batches of movement primitives. In that respect, the authors conjecture on applicability of probability theory for many desired mathematical operations on DMPs. These operations are given as co-activation, modulation, optimality, coupling, learning, temporal scaling, and rhythmic movements. The corresponding probabilistic operations are identified as a product, conditioning, encode variance, mean-covariance, maximum likelihood, modulate phase and periodic basis.

The idea of extending trajectory generation problems into Hilbert spaces is com-

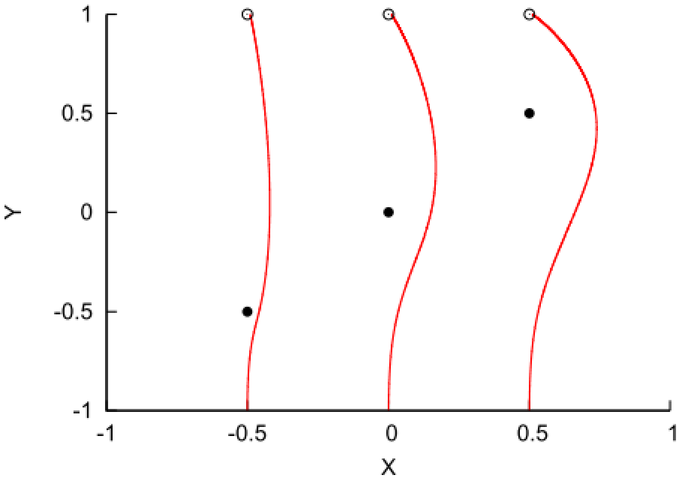

Figure 2.2: Obstacle avoidance example. Red line: A DMP generated path. Black dot: An obstacle

bined with DMPs concept in [16]. The norm and relationship with DMPs are explained and choosing a suitable norm is defined as an optimization problem (Hilbert Norm Minimization).

Since in DMPs every joint moves in tandem and has its own DMPs; thus, dimensionality reduction becomes an important subject. In [17], dimensionality reduction for probabilistic movement primitives is given (ProDMPs). They used expectation maximization to extract the unknown synergies from a given set of demonstrations. They showed their ProDMP method is more efficient both for encoding the learned trajectories and for applying Reinforcement Learning with Relative Entropy Policy Search (REPS). This work is an extension of [15].

In most of the DMP research, learning is carried out for a single or a few demonstrations. This results in poor generalization capabilities. In [18], learning DMPs from multiple demonstrations is considered. Their approach efficiently encodes multiple demonstrations by shaping a parametric attractor landscape in a set of differential equations. In other words, it focuses on what can additionally be learned from each demonstration instead of recording every demonstration and encoding them inefficiently.

Combining learned primitives is also an important problem. A task can be solved by combining different movement primitives smoothly without actually altering their dynamics. This induces two questions. How a movement primitive can be segmented? And how they can be combined even though their dynamics are different? In [19], a planning methodology for sequencing movement primitives is given. Their approach relies on a search tree where each node represents a reachable valid configuration, and edges represent a path between parent and child nodes. Joining a node to one of the subsequent child nodes is done using concatenation of paths. They used A* search method to traverse the tree and select locally optimal combinations of movement primitives. In [15], as we already discussed, the probability theory helps smoothly construct paths based on multiple movement primitives. An example of combining different DMPs taken from [15] is given in Figure 2.3.

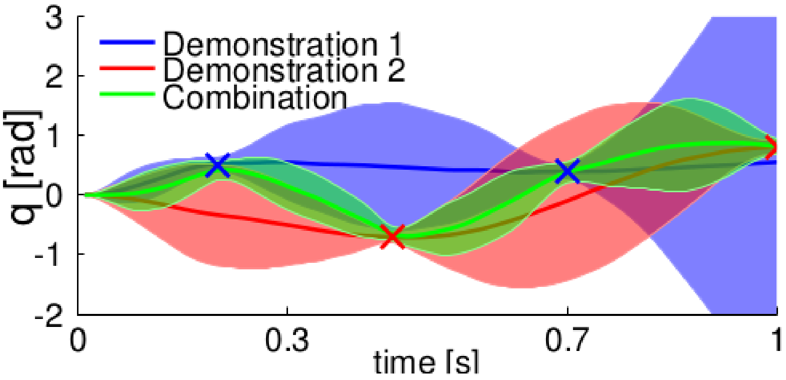

Figure 2.3: Combination of two demonstration

In [20], we introduced the specified DMPs (sDMPs) approach. The sDMPs use a contact term in the nonlinear part specific to deburring task (can be extended to any interaction task) to include the effect of tool part interaction. This coupling term is multiplied with the resultant force exerted on the tool tip. As the literature review suggests, the DMPs are more common in locomotion of robots and humanoid robot arm tasks. In these tasks, the environment is highly dynamic but the robots do not need to be precise. However, in robotic deburring, the environment can be considered static but the movements have to be precise. Thus, the aim of the study was to introduce the coupling term and apply the DMPs on deburring task. A haptic interface is utilized to capture the human participants' hand movements as demonstrations on an experimental setup.

In [21], a concept called Interaction Primitives (IP) is investigated. The IP is used for learning multiple interaction patterns between two agents (i.e. robot and human) from unlabeled demonstrations. The IPs are DMP based. This approach can be useful for robot-human collaborative tasks.

There are also Beta Process Auto Regressive Hidden Markov Model (BP-AR-HMM) methods [22]. It is also a DMP based framework for representing dynamical systems. They showed in [22], that the proposed approach helped a robot to learn a multi-step task from unstructured demonstrations. [23] also employed BP-HMM for teaching a complex sequential task, pizza dough rolling to a robot. They separated the motion into reach, roll and reach back segments (action primitives rather than motion primitives) and calculated their transition probabilities. Then, they trained the model on human demonstrations to learn robot controller parameters. However, they used manually tuned parameters.

In deburring process, qualified surfaces in micron-size resolution operations have to be obtained. A specific motivation of this paper is to introduce a new trajectory model by taking inspiration from DMP methods used in literature survey, then, after the necessary modifications, introduce new trajectory model.

CHAPTER 3

EXPERIMENTAL SETUP

In order to determine the deburring skills of operators', various experimental setups are required. Since the mathematics explained in chapter 4 requires recording of movements (e.g., position, velocity, acceleration) as well as force, setups are facilitated to allow these measurements. Recording movements of hand motion of operators' dictates usage of some sort of a haptic device. A haptic device, in general, records human hand (or other limbs) movements and provides force feedbacks to reply a virtual environment. The virtual environment can be, for instance, a virtual surgery on a tissue. The operator moves the end-effector of the haptic device and this results in the movement of the surgical tool in virtual environment. This tool, when interacted with the tissue, generates forces. These forces are then conducted to the operator in real world via haptic device's motors. Force feedback is an integral part of all haptic devices. However, in our study, we only require the haptic device's measurements of hand movements and its derivatives, since we eliminate the virtual environment and deal with real world. A representative pictorial description of haptic devices is provided in Figure 3.1.

Since commercial haptic devices provide a fair amount of accuracy, we utilized a Phantom 6DOF haptic device. However, since the stiffness of the haptic device as well as its calibration validity in its entire workspace is debatable for our micron-size resolution deburring operations, we also came up with a 1DOF haptic device which provides more precise but single degree of freedom measurements. This 1DOF device allows us to manipulate the piezoelectric actuator, i.e. in teleoperation mode, as will be explained in Section 3.3. The

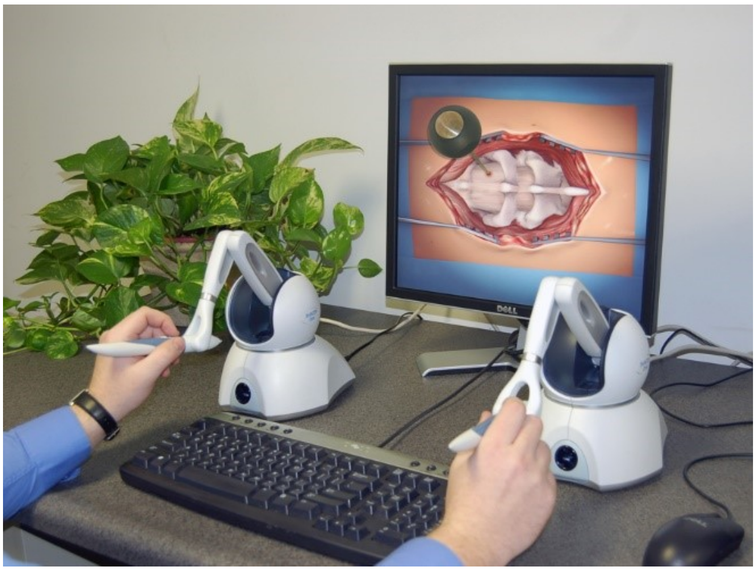

Figure 3.1: Two haptic devices are being used for surgery in virtual environment

subject of "General concentrated position DMPs" is related to 6DOF haptic device and "Local DMPs" is related to 1DOF haptic device. These concepts are explained in chapter 5 and chapter 6 respectively.

Apart from measurements, a controlled environment is required for conducting the experiments. This environment has been provided in our laboratory from previous studies [24]. This experimental setup consists of a hexapod parallel manipulator (PI M-824), a piezoelectric actuator (P-602), a high speed spindle (BMR Z42-M160.19 K1S2), a cBN tool, 6DOF F/T sensor (ATI GAMMA IP60 SI-130-10), a tool changer (3R-600.24-S), and a hand driven precision linear stage. The purpose of this deburring setup was to obtain a deburring/grinding model for cBN tool bits.

Since we have used several experimental setups, it is necessary to summarize the above-mentioned devices and give their names here:

1. 6DOF haptic device and related setup
2. Deburring/Grinding robot enumerate environment
3. 1DOF haptic device and related setup

In the remainder of this chapter, we will provide detailed descriptions of the aforementioned experimental setups and their components.

3.1 6DOF Haptic Device and related setup

The human operator moves the deburring tool in 6 directions and angles (i.e., in 6DOF). In order to record these movements, we constructed the experimental setup shown in Figure 3.2. A deburring tool is instrumented with a spindle that is attached to the end of a haptic device. In this configuration, the haptic device is used to measure the displacement, velocity and acceleration of the tool. The human expert grasps the deburring tool and moves it against a workpiece to perform the deburring operations [11].

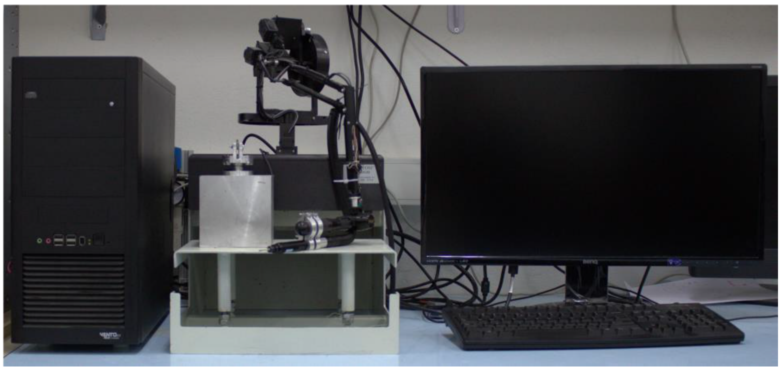

Figure 3.2: 6DOF haptic device, deburring tool, workpiece, and F/T sensor

The workpieces which are used in this study are fixed to a fixture under which a six-axis F/T sensor ATI FT07638 is placed to measure the force and torque acting on them, Figure 3.3.

Our workpieces have different surface profiles with a varying height, Figure 3.4. Also, the deburring tool is a cBN abrasive bit from PFERD Company. These workpieces provide standardized study material for repeated experiments.

The haptic device end effector is standardized and its dimensions and mounting points can be found in the producer's datasheet. However, we mounted a

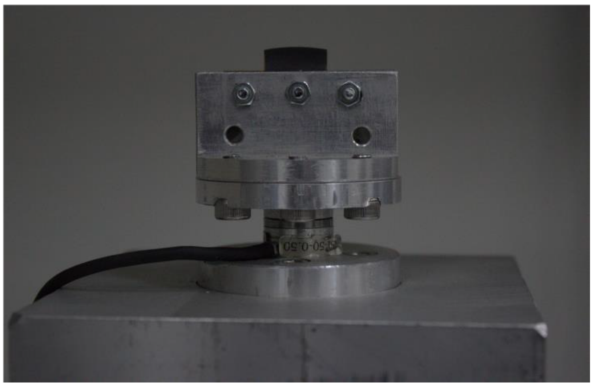

Figure 3.3: A close up of workpiece, F/T sensor, and the heavy metal block

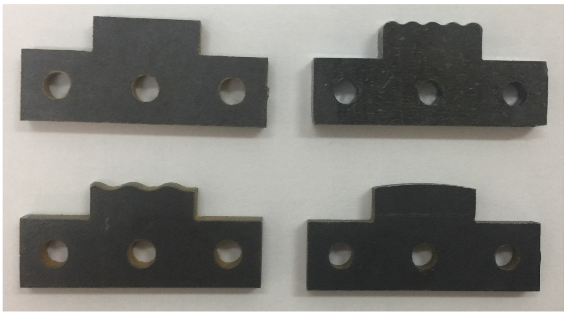

Figure 3.4: Different workpiece profiles

different tool (a deburring tool) to the end-effector. This tool has relative position with respect to the haptic device's end-effector. In order to obtain the tool tip position after mounting the cBN tool bits, we scanned the end-effector and the deburring tool simultaneously and obtained the tool tip position from the point-cloud data as shown in Figure 3.5 (point cloud data is obtained using Artec Spider scanner). After that, as it can be seen in Figure 3.6 cylinders and planes are fitted to obtain the geometrical properties of the system in SolidWorks. This provides an accurate tool tip position and orientation with respect to the standard haptic device end-effector. After obtaining offsets (in position and orientation), we obtained the transformation matrix and incorporated this matrix in the software we developed for measurements.

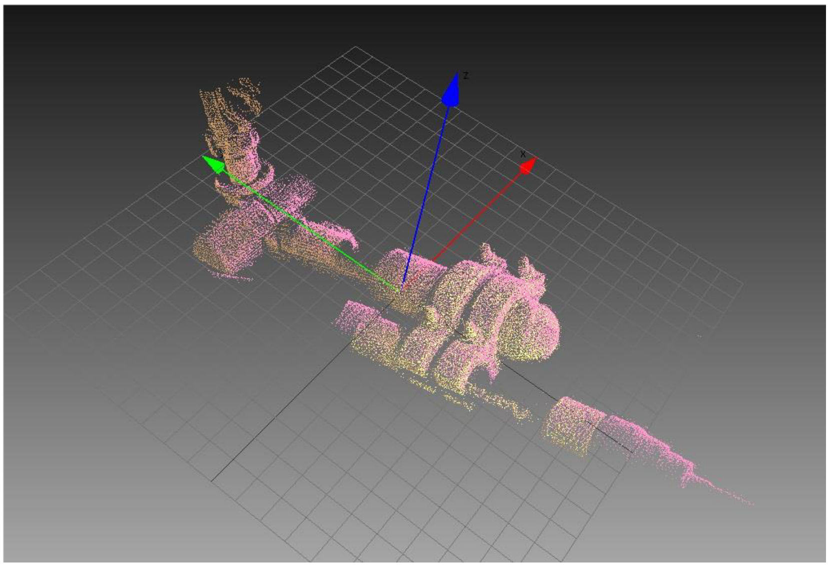

Figure 3.5: Scanned figure of deburring tool of 6DOF haptic device

Data of the wrist coming from the haptic device is obtained, then by calculating the translation and the rotation of the tool tip coordinate frame with respect to the wrist coordinate frame and obtaining the transformation matrix, the position and the velocity of the tool tip can be validated. Forces on the F/T sensor and the position of the haptic device are measured simultaneously. These data are then used in DMP model for parametrization.

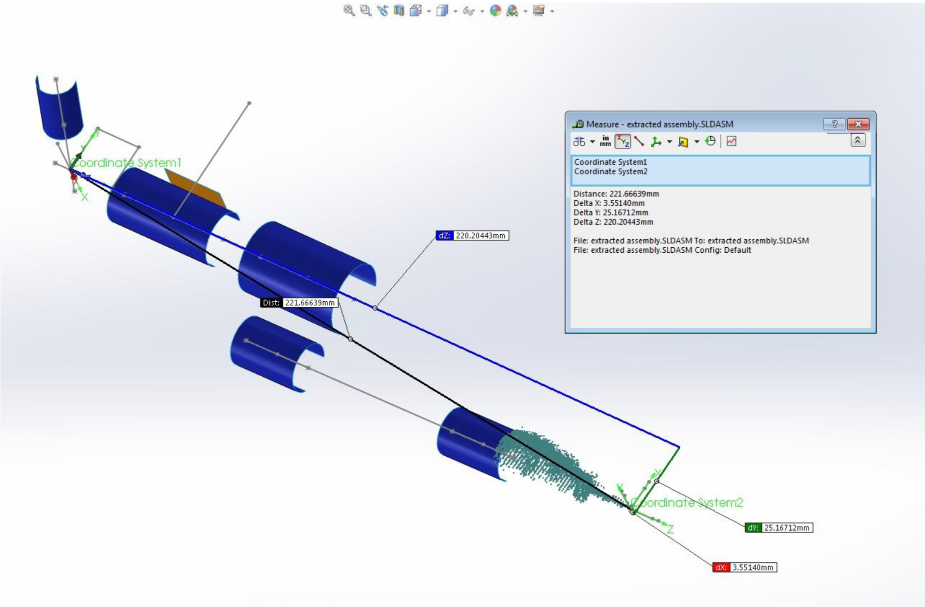
Measure - extracted assembly.SLDASM

Coordinate System1
Coordinate System2

Distance: 221.66639mm
Delta X: 3.55140mm
Delta Y: 25.16712mm
Delta Z: 220.20443mm

File: extracted assembly.SLDASM To: extracted assembly.SLDASM
File: extracted assembly.SLDASM Config: Default

Figure 3.6: Cylinders are fitted to the point cloud data using SolidWorks to obtain the orientations and offsets

As can be deduced by the reader, the 6DOF hand movements are unique set of movements that may or may not be transferred to the deburring/grinding robot directly. As we will explain shortly, the deburring robot utilizes a Hexapod parallel manipulator which has limited position, velocity, and acceleration range and has very different joint and link structure and geometry from human's (i.e., their kinematics and dynamics are completely different). This particular problem is referred to as the correspondence problem occurring in most imitation learning tasks. In order to resolve this problem, we studied towards learning by demonstration via teleoperation (i.e., imitation from demonstration). To this end, a 1DOF haptic device and related experimental setup are devised. Teleoperation completely eliminates the correspondence problem since it only allows compatible movements by restricting the human operator to perform the movements that robot can do.

3.2 Deburring/Grinding robot

The deburring/grinding robot was developed for modeling the deburring/grinding tasks for cBN tool bits. It is a controlled environment with which we can perform deburring/grinding tests on defined workpiece surfaces. Hexapod parallel manipulator is the main component of this setup. It provides 6DOF movement with high accuracy and repeatability. However, it is too slow to imitate human hand movements (1 mm/s). Hexapod is fixed on a heavy block of metal and the moving surface is free and connected to F/T sensor and spindle. On the other hand, the workpiece is connected to piezoelectric actuator and the piezoelectric actuator is connected to the heavy metal block. The spindle is moved by hexapod and the motion is near the workpiece. Similarly, the piezoelectric actuator can move the workpiece near the spindle. Therefore, cutting action can be obtained either by movements of hexapod or piezoelectric actuator. Furthermore, the spindle is high speed and speed regulated (thus provides constant speed regardless of the torques on the tool). The overall picture of the deburring setup is shown in figure 3.7.

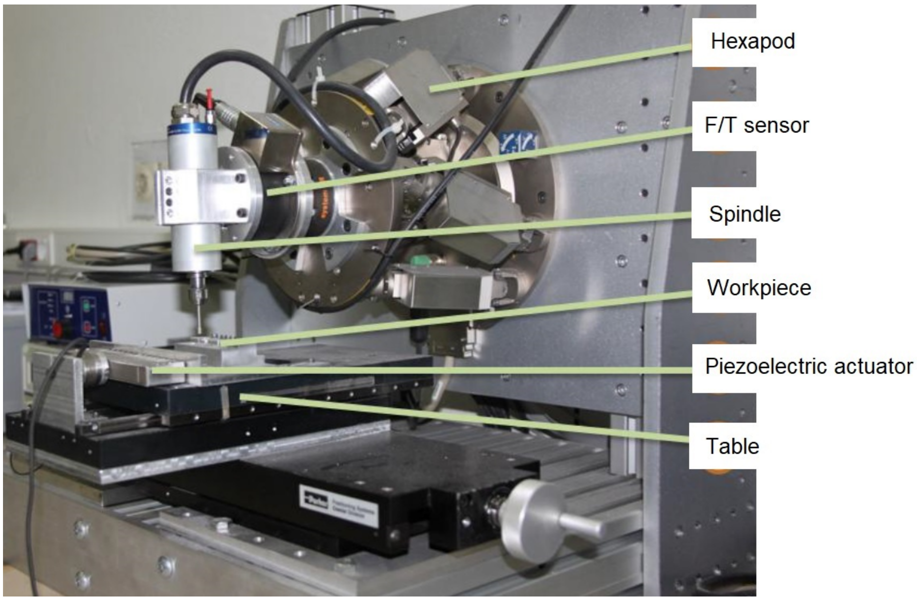

Figure 3.7: Overall setup of the deburring robot

In our teleoperation experiments explained in section 3.3 in conjunction with the 1DOF haptic device setup, requires fast and accurate movements of either the tool or the workpiece. In this case, the piezoelectric actuator provides the necessary speed and accuracy. Therefore, we chose to move the workpiece via piezoelectric actuator.

Figure 3.8: P-602 piezoelectric actuator.

The piezoelectric actuator is the main component we focus on from this previously developed setup, figure 3.8. Therefore, it is mandatory to provide information regarding its capabilities. For this matter, the actuator is P-602 Piezo-Move flexure-guided piezo actuator from PI Company. Mainly, a piezoelectric actuator utilizes a piezoelectric crystal which is an active material that can respond to electricity and pressure. When provided with electrical current, it elongates and with the help of the flexural mechanism, it can quickly return to its default position when the current is removed. Conversely, when provided with pressure, it produces electricity. In this setup, a linear guide restricts the motion of the piezoelectric actuator from one end, but, the other end is connected to the workpiece. So, the workpiece slides with the linear guide and controlled solely by piezoelectric actuator.

The piezoelectric actuator requires PI E-610.S0 LVPZT motion amplifier/ controller circuit board. This board has proportional-integral type control mechanism ready to use. The piezoelectric actuator can move 1 mm only. Despite its short range, the resolution is approximately 7 nm in closed loop control mode.

The control input of the piezoelectric actuator is the voltage provided from a Data Acquisition card (DAQ NI6052e) and results in displacement (0 to 1 mm).

The remaining main components are Hexapod, Force/Torque sensor, and the spindle. Hexapod is a parallel manipulator capable of moving in 6DOF. The model we have in our setup is H-824 from PI Company. Since the spindle and the F/T sensor are connected to the moving end of the Hexapod, it provides the main motion for the modeling purposes required by the previous studies. Thus, it moves the cBN tool in a desired position and orientation on a trajectory. However, in this study, we only used a one-directional constant speed movement to carry the spindle in perpendicular to the direction of piezoelectric actuator motion. The interaction between the tool and the workpiece results in cutting forces and these forces are recorded using the F/T sensor.

3.3 1DOF Haptic Device and related setup

The idea of utilizing DMPs in metal cutting and finishing operations is a new concept and humbly we provide the first steps towards this novelty. There are other similar works related to more general tasks such peg-in-hole placement, grasp-and-replacement etc. that utilize also teleoperation with DMPs [25]. However, such an approach is not tested on high precision processes such as deburring. Thus, in this study, we developed a teleoperation system utilizing a 1DOF haptic device for deburring operations to prove conceptual viability of this approach.

The haptic device consists of a motor attached to a knob via a timing belt. When the operator rotates the knob, a rotation angle is resolved from the encoder embedded within the motor. Also, a torque sensor is mounted between the knob and the setup that allows measurement of the torque applied by the operator. This device is connected to the computer using a DAQ. A MATLAB Simulink© model is developed for receiving and transmitting information between the deburring/grinding robot and the 1DOF haptic device. The workpiece is attached to the piezoelectric actuator within the deburring robot. When the operator rotates the knob which is shown in figure 3.9, piezoelectric actuator moves back and forth accordingly, thus moves the workpiece. This is the teleoperation part of the setup.

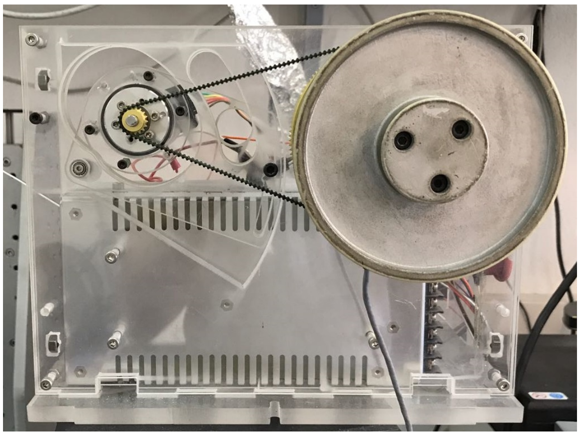

Figure 3.9: 1DOF haptic device figure

Since the piezoelectric actuator is very fast and withstands a fair amount of load, we are free to rotate the knob in a natural way comfortable to human operator physiology (i.e., it doesn't restrict the speed or acceleration of human hand during the operation). However, we also utilize force feedback mechanism. In the deburring robot, we measure forces and torques. Therefore, the cutting forces are fed back to the operator via the motor of the haptic device. This way, the operator is aware of the cutting forces, thus provides better cutting action. On the Simulink model, a display shows the instantaneous cutting force. The operator both look at the cutting force shown in the monitor and feel the force from the haptic device simultaneously.

Knob is at zero angle (relative) when starting an experiment. A 60° clockwise rotation of knob corresponds to 1 mm (limit of elongation of the piezoelectric actuator) movement of piezoelectric actuator towards the tool. At zero angle, a counterclockwise rotation does not result in movement of piezoelectric actuator since the actuator is at its minimum elongation, shown in figure 3.10. During the operation, for the purpose of post-processing and DMP model extraction,

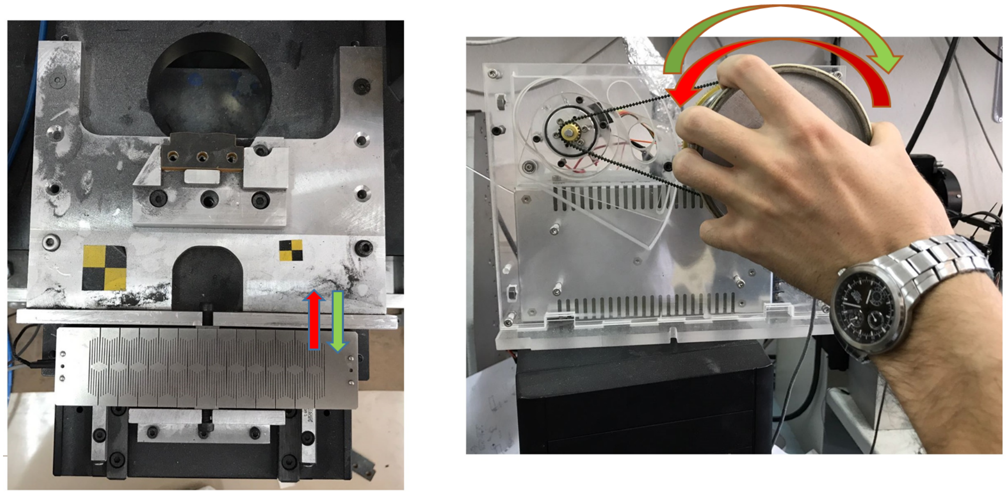

Figure 3.10: Relative clockwise or counterclockwise 1DOF haptic motion with respect to piezoelectric actuator

we recorded the knob movements, piezoelectric actuator movements, time in nanosecond, and the force data in a dataset.

CHAPTER 4

METHODOLOGY OF DMP

In order to model complex behaviors of human movements and maybe force interactions coming from the experiments, nonlinear dynamical systems are suitable. They have been used to model discrete and rhythmic movements, such as biological motor control and robotics. Both discrete and rhythmic movements are point attractive and independent of the initial conditions of the trajectory.

The aim of this chapter is to model point attractive discrete and rhythmic movements by using weak nonlinear dynamical systems and then strengthen it with the added nonlinear learn-able term. Also, This model has to be independent of start and goal stations of the trajectory taken from experiments. The model that is explained in this chapter is published by S.Schaal from [7].

4.1 Development of Model

The simplest possible model which has most convenient dynamical system and also dependent to movements and its derivatives is mass-spring-damper model. The mass-spring-damper model with nonlinear learn-able form is,

$$\tau \ddot{y} = \alpha(\beta(g-y)-\dot{y})+f(x) \tag{4.1}$$

This model can be converted to first order model with nonlinear dynamical system,

$$\tau \dot{z} = \alpha(\beta(g-y)-z)+f(x),$$
$$\tau \dot{y} = z \tag{4.2}$$

Equation 4.2 is the transformation system where y,$\dot{y}$ and $\ddot{y}$ correspond to desired trajectory position, velocity and acceleration, α and β are time constants. τ is a temporal scaling factor and g is the desired end position. Also, $f(x)$ is the nonlinear learn-able term added to mass-spring-damper model [18].

Values of α and β are proportional to each other. If $\beta/\alpha = 1/4$, the system becomes critically damped. This means that, when the system is critically damped, the movements are going to the point attractor g without any oscillations. In addition, If the nonlinear learn-able term $f(x)$ is removed from equations 4.1 and 4.2, the trajectory of y will be directly toward point attractor g without any changes on the landscape of the arbitrary movements.

In order to generate more complex trajectories and change the landscape of the arbitrary movements, the nonlinear learn-able differential equation term can be added.

$$f(x) = \frac{\sum_{i=1}^{k} \omega_i \psi_i(x)}{\sum_{i=1}^{k} \psi_i(x)} x(g-y_0) \tag{4.3}$$

where ψ_i is the basis function of a system which every nonlinear function can be represented as a linear combination of a basis function of a system. This can create complex movements out of a simple parametrization. Also, ω_i's are elements of the nonlinear term which each of them has different influence to generate arbitrary movement. Weights help the nonlinear term to change the landscape of the arbitrary movement to the desired intended shape. Also, y_0 $(y=0)$ is the initial state of the trajectory.

In addition, time dependency of a nonlinear function creates a non-autonomous dynamical system and does not permit coupling with other systems in differential times. The intended dynamical model should be an autonomous system, without explicit time dependence [26]. Thus x, which has a first-order dynamics is preferred instead of time. Figure 4.1 shows the relation between time and x.

$$\tau_x \dot{x} = -\alpha_x x \tag{4.4}$$

Here α_x is a constant value and x is the phase variable determined by an extra dynamic system which is also called canonical system. When $x = 1$ indicates the start of the time of trajectory and when $x = 0$ means the trajectory is on the point attractor g. Also, τ_x is constant value which designates the duration of movement and works in place of time.

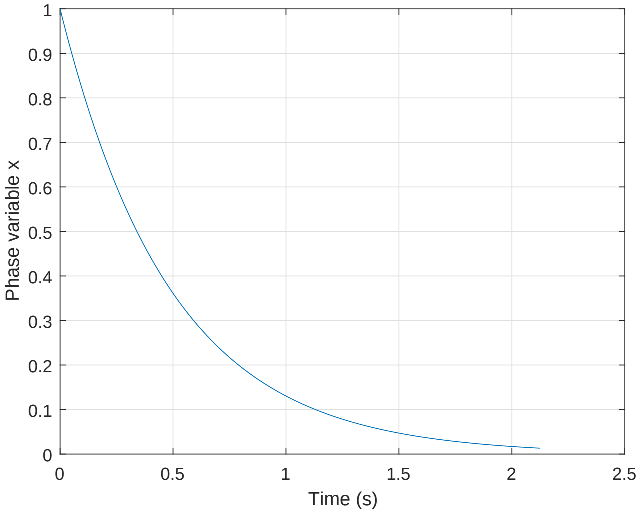

Figure 4.1: Phase variable as a function of time (s) of specific experiment

Considering a canonical system, the basis function ψ_i has to be phase variable dependent with k exponential kernels. Figure 4.2 shows the example of 40 exponential kernels as a function of time.

$$\psi_i(x) = exp(h_i(x - c_i)^2)$$

where h_i and c_i are constant values that determine the width and the centers of the basis function [26].

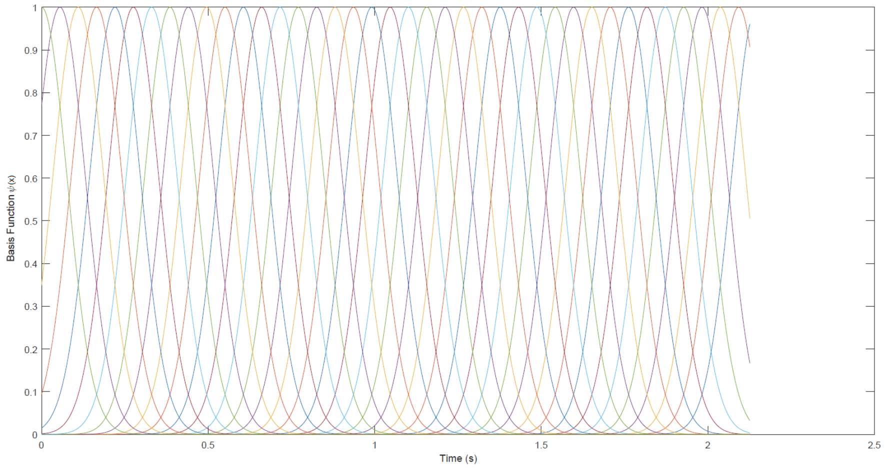

Figure 4.2: 40 exponential kernels as a function of time (s) of specific experiment

By taking the data of canonical system and ω_is we can obtain the values of nonlinear learn-able differential equation. Also, by taking parameters of transformation system of specific experiment and nonlinear learn-able equation from previous procedure, we can generate a trajectory model of Dynamic Movement Primitives (DMPs), figure 4.3.

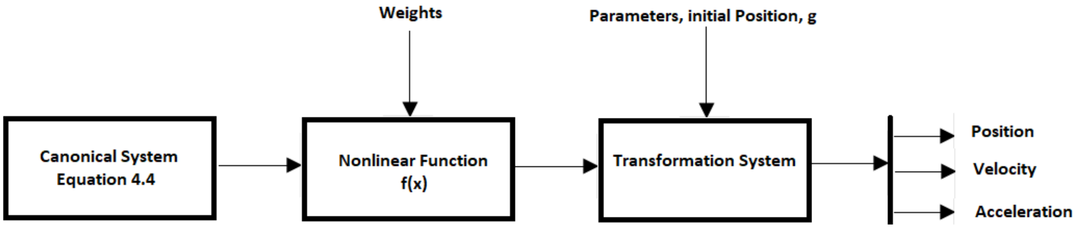
Weights
Parameters, initial Position, g
Canonical System
Equation 4.4
Nonlinear Function
f(x)
Transformation System
Position
Velocity
Acceleration

Figure 4.3: Generation of trajectory using DMP in 1-dimension

The main concern is, how we are going to find parameters and weights of the transformation system and nonlinear learn-able function. Section 4.2 is the answer to this question.

4.2 Learning Dynamics from demonstration

In order to formulate a function approximation problem, we have to rearrange equations 4.2 and 4.3. By taking mass-spring-damper model to one side of equation and nonlinear learn-able differential equation to the other side of the equation we equate them,

$$f_{target}(x) = \tau^2 \ddot{y} - \alpha(\beta(g - y) - \tau\dot{y}) \tag{4.5}$$

By inserting the value of position, velocity and acceleration coming from the trajectory experiment, the value of ω_i can be obtained using equation 4.3,

$$b_i(x) = \frac{f_{target}\sum_{i=1}^{k}\psi_i(x)}{x(g - y_0)} \tag{4.6}$$

b_i does not have any meaning. This is just for showing the process of the calculation of ω_i in detail.

$$\begin{pmatrix} \psi_i(x) \end{pmatrix} \begin{pmatrix} \omega_{i,target} \end{pmatrix} = \begin{pmatrix} b_i(x) \end{pmatrix} \tag{4.7}$$

By solving the system of linear equations, ω_i can be achieved. Putting $\omega_{i,target}$ in equation of nonlinear learn-able differential equation 4.3 of experiment;

$$f_{target}(x) = \frac{\sum_{i=1}^{k}\omega_{i,target}\psi_i(x)}{\sum_{i=1}^{k}\psi_i(x)} x(g - y_0) \tag{4.8}$$

By inserting equation 4.8 in equation 4.5, we will have parameters of equation 4.9 that have to be solved with a global optimization algorithm.

$$\frac{\sum_{i=1}^{k}\omega_{i,target}\psi_i(x)}{\sum_{i=1}^{k}\psi_i(x)} x(g - y_0) = \tau^2 \ddot{y} - \alpha(\beta(g - y) - \tau\dot{y}) \tag{4.9}$$

4.3 Global Optimization algorithm

PSO is an evolutionary optimization method inspired by simulations of bird flocks' movements [27]. Since its first appearance in literature, many studies and modifications were made on PSO. The working principle of PSO is to use particles and their movements in order to achieve their optimal positions that correspond to the optimal solution. The pseudo code for the PSO algorithm is as figure. 4.4 [28]. In this optimization algorithm, no gradient information is required for which derivatives may not be available.

```
Initialize a finite number of particles with randomly set positions and velocities on the parameter hyperspace
Do
For each particle
    Calculate the fitness value, (equation 4.14)
    If a better fitness value is obtained than pbest
        Set pbest as the current fitness value
End
Set the best one among all pbests as gbest
For each particle
    Determine particle velocity according to the velocity update equation, (equation 4.10)
    Calculate new particle position according to the position update equation, (equation 4.11)
End
While the maximum iteration or the convergence is not attained
```

Figure 4.4: psudo code of PSO algorithm

At the beginning, a finite number of particles are generated randomly, that is, the particles are spread to the hyperspace randomly with random velocities. In the beginning of the search, swarms are spread out randomly with various positions and velocities as shown in Figure 4.5 [29]. Then, an iterative process starts by evaluating fitness values of each particle according to the fitness criterion specified by a cost function. After finding the fitness values, the best ones (**pbest**) are selected for each particle at each iteration. At the end of each iteration, the global best fitness value (**gbest**) is selected among **pbest** values and particles are updated according to the following velocity and position update equations as shown in Figure 4.6 [30].

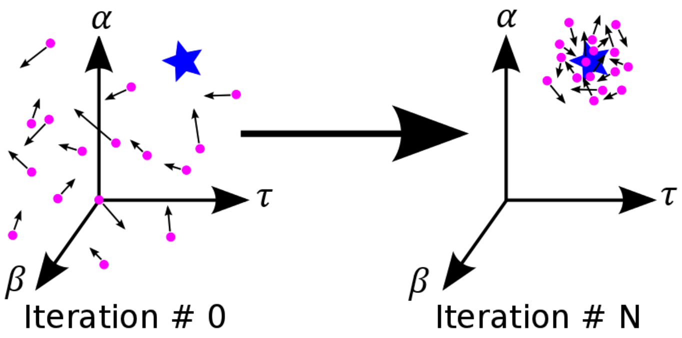
α
τ
β
Iteration # 0
α
τ
β
Iteration # N

Figure 4.5: Example of conceptual diagram of PSO

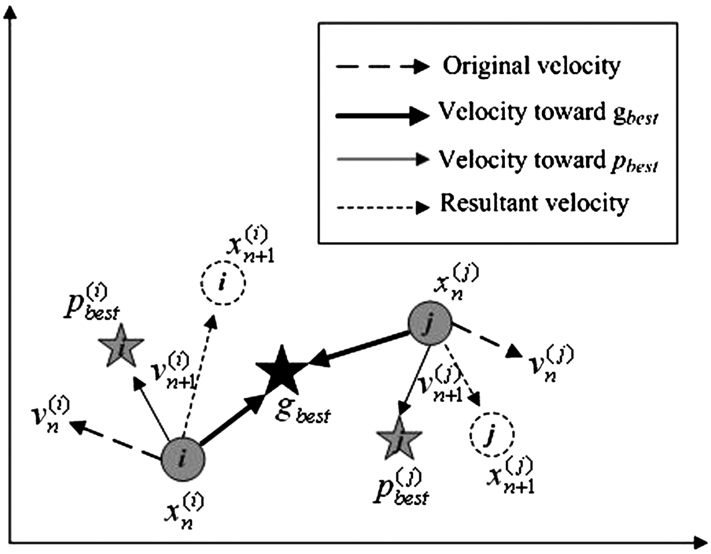
Original velocity
Velocity toward g_{best}
Velocity toward p_{best}
Resultant velocity
$x_{n+1}^{(i)}$
i
$p_{best}^{(i)}$
i
$v_{n+1}^{(i)}$
$v_n^{(i)}$
i
g_{best}
$x_n^{(i)}$
$x_n^{(j)}$
j
$v_n^{(j)}$
$v_{n+1}^{(j)}$
j
j
$p_{best}^{(j)}$
$x_{n+1}^{(j)}$

Figure 4.6: Example of position and velocity of swarms through fitness value

$$\mathbf{v}_i(n+1) = \chi(\mathbf{v}_i(n) + \varphi_1 r_1(\mathbf{pbest}_i - \mathbf{P}_i(n)) + \varphi_2 r_2(\mathbf{gbest}_i - \mathbf{P}_i(n))) \quad (4.10)$$

$$\mathbf{P}_i(n+1) = \mathbf{P}_i(n) + \mathbf{v}_i(n+1) \quad (4.11)$$

where, $\mathbf{P}_i(n)$ is the position and $\mathbf{v}_i(n)$ is the velocity of i^{th} particle at the n^{th} iteration, r_1 and r_2 are random values between 0 and 1, φ_1 and φ_2 are constants and χ is defined as,

$$\chi = \frac{2}{\left|2 - \varphi - \sqrt{\varphi^2 - 4\varphi}\right|} \quad (4.12)$$

$$\varphi = \varphi_1 + \varphi_2,$$
$$\text{where } \varphi > 4$$

Then, a new iteration starts unless the maximum iteration or the convergence is attained.

In this work, PSO is used to determine the parameters of DMP that follows a known trajectory generated in an optimal way. Here the optimization criterion is the minimization of error of the trajectory generated via DMP from the known trajectory.

Optimization of DMP parameters using PSO is held with a particle structure of,

$$\mathbf{P}_i = [\alpha \quad \beta \quad \tau]^T \quad (4.13)$$

In order to evaluate the fitness values, mean squared error (MSE) is used as the cost function and expressed as,

$$MSE = \frac{1}{N}\sum_{i=1}^{N} e^2(i) \qquad (4.14)$$

where, $e(i)$ is the trajectory error of tool tip of i^{th} sample of N time samples.

4.4 Conclusion

DMP method presents an ordinary differential equation for modeling human expert skills for different movements on the workpiece from any start position to desired end position. Adding the learn-able nonlinear equation to transformation system of mass-spring-damper system can generate complex behaviors and change the landscape of the arbitrary movements to the desired trajectory. Also, we have to mention that, not only DMP is able to adapt itself for different start and end positions, but also, it is able to change its size by changing the value of scaling factors and constant values of the equation, shown in figure 4.7. By performing experiments and creating the dataset of time constants α, β, temporal scaling factor τ and weights of nonlinear equation ω of each task, we can generate desired trajectories and utilize them in deburring/grinding processes.

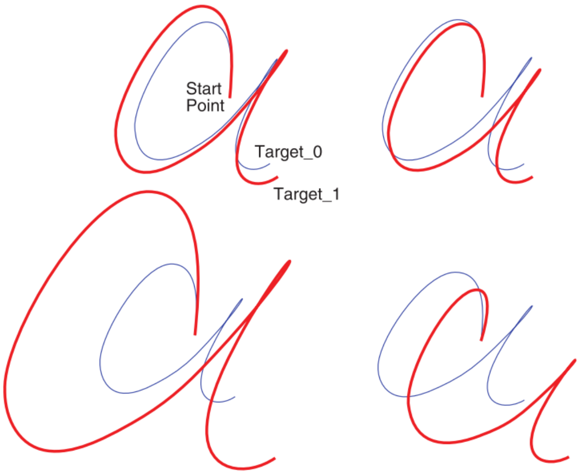

Figure 4.7: Example of the trajectory with different start and end positions and sizes

CHAPTER 5

GENERAL POSITION CONCENTRATED DMP

As it is known from the literature survey analyzed before, DMP is more common in locomotion of robots and humanoid robot arm tasks, such as jumping robots, grasping and placing movements. In these tasks, there is a dynamic environment and the movements of robots do not need to be highly precise. However, in deburring process used in this work, the environment is static and the trajectory of the tool tip must perform high precision machining on the workpiece due to the millimeter-sized burrs. In addition, obstacle avoidance is not required in deburring process, but, there is a contact between the tool and workpiece that effects the trajectory. Therefore, in this case, nonlinear differential equation part of DMP method is modified using deburring forces.

5.1 Methodology of General Position Concentrated DMP

In [12], the motion primitives are found using weighted summation of the kernel functions, time constants, and time scaling factor were used as the guidance on how to generate the given trajectory. Here, as an alternative, we propose to augment DMP equation and try to fit the characteristics of the trajectory to the time constants and time scale factors under the influence of current deburring forces. Therefore, DMP algorithm can be modified to:

$$\tau_z \ddot{y} = \alpha_z(\beta_z(g-y)-\dot{y}) + Fr_z(x) \tag{5.1}$$

F is the resultant force exerted to the workpiece by the tool tip. The magnitude of the force can be measured by the F/T sensor available on the fixture manufactured for the workpiece. Also, r_z is the Gaussian coupling term that is used for contact effect between workpiece and tool tip, which nonlinear part of DMP is replaced with a gaussian function of force exerted. Moreover, there is multiplication between force and coupling term of contact r_z instead of addition. That is because of the direct relation between them.

Nonlinear term which changes the landscape of the arbitrary movement can be presented as

$$r_z(x) = \frac{\sum_{i=1}^{k} w_i \psi_i(x)}{\sum_{i=1}^{k} \psi_i(x)} x(g - y_0) \tag{5.2}$$

where w_is are weights and $\psi_{\mathbf{i}}(x)$s are the basis functions of a system which mentioned in chapter 4. Here, the weights are determined using locally weighted regression as proposed in [26].

$$\psi_i(x) = exp(h_i(x - c_i)^2) \tag{5.3}$$

And x is the phase variable determined by an extra dynamic system which is also called canonical system and has the following form, where τ_x and α_x are the constant values.

$$\tau_x \dot{x} = \alpha_x x \tag{5.4}$$

These basis functions can create complex movements out of simple parameterization.

5.2 Experiments

In this section, the trajectory of the tool tip of haptic device on the smooth profile of workpiece is examined by asking a participant to have rhythmic hand motions on workpiece and imitate the hand motions of human expert. The task which is given to participant is to obtain a horizontal flat surface. In each experiment parameters are recorded. Then, parameterization of the system is used in modified DMP for imitation. The parameters of the task are analyzed for each experiment. For simplicity, we have considered tool tip movement only in the tangential and Normal direction and F/T sensor in tangential and normal direction. We are to validate the trajectory coming from the experiment and the trajectory gained from DMP model and also, comparison of trajectory errors of DMP and modified DMP models with respect to experimental results. The aim of these experiments is to show that, modified DMP works slightly better and less error than DMP. Another aim is to show that expert changes depth of cut and feed-rate according to force on the tool tip.

5.3 Results

Particle Swarm Optimization method is tested in this part. Figs. 5.1-3 show DMP, modified DMP and actual path of one of the conducted experiments using PSO. As it can be observed, modified DMP works extremely satisfactory in curve fitting operations and has slightly smaller error than classical DMP. MSEs for feed position are 2.05e-3 and 5.40e-5 for standard DMP and modified DMP, respectively. MSEs for depth of cut are 1.22e-4 and 1.03e-4 for standard DMP and modified DMP, respectively. Here, we can say that feed of the tool is effected by the force more significantly. Alternatively, modified DMP is more effective and accurate when representing motions with force interactions.

By using parameters of experiments, we will be able to show participant's characteristics. This can help to understand the variance and repeatability of a

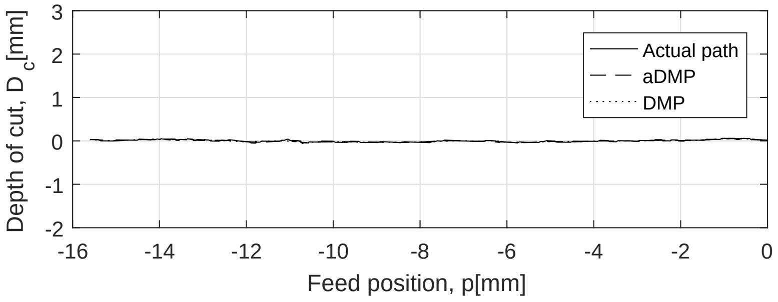

Figure 5.1: 2D movement of the tool on workpiece with PSO optimization

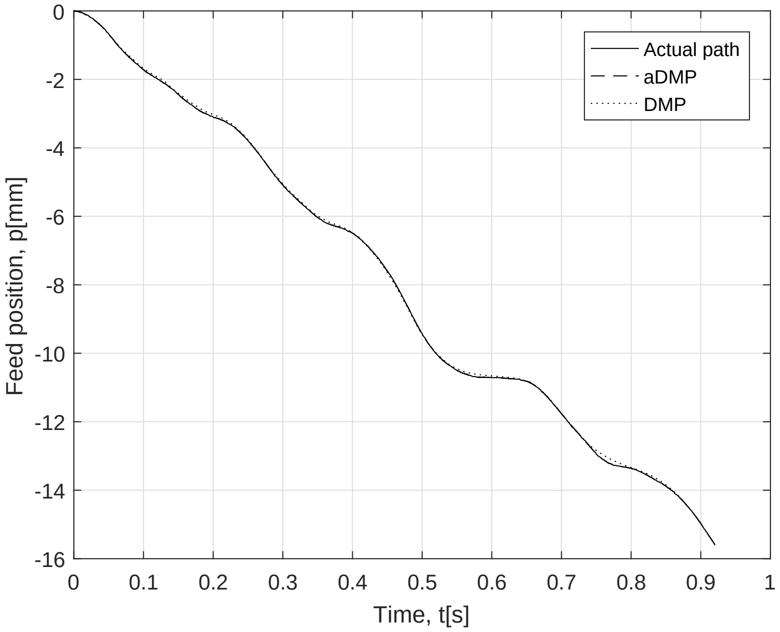

Figure 5.2: Movement of tool on Workpiece in x-direction with respect to time in PSO optimization

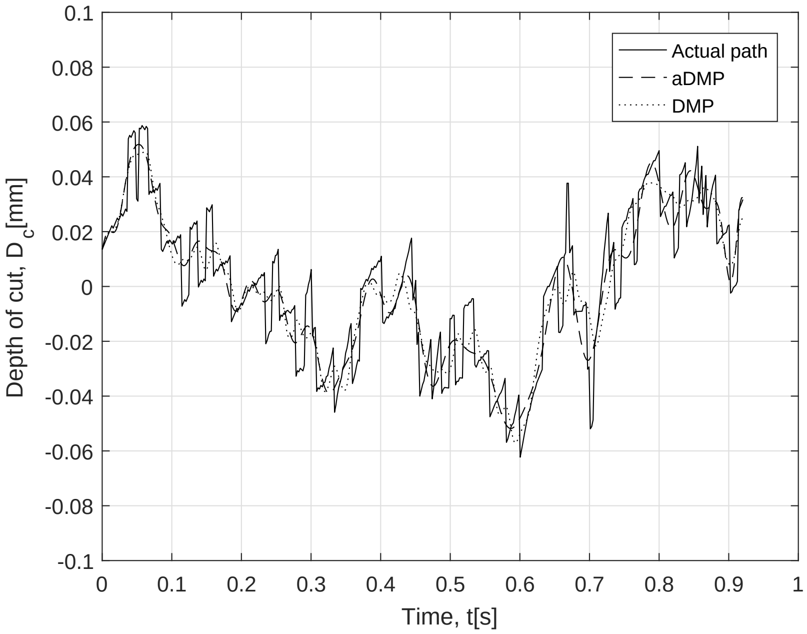

Figure 5.3: Movement of tool on workpiece in y-direction with respect to time in PSO optimization

participant in rhythmic motions.

5.4 Conclusion

Expert human agent performs almost perfect deburring process based on his/her set of given limbs and perception. An expert, internally develops an interaction model (i.e., the model regarding the interaction between tool and burrs or workpiece) by time (or experience) in his/her mind. This model, due to expert's immense neural network, adapts to changing environment accordingly. Instead of developing an explicit interaction model for deburring, that is a daunting task; the idea of utilizing a human expert's already developed internal model in generating trajectories of a robot for deburring is the main theme of this study. This is elaborated by a modified DMP which is an important proposition in this study.

CHAPTER 6

TELEOPERATION IN GRINDING PROCESS

The aim of this study is to control force using movement primitives of the skills of a human participant while doing a high precise deburring process. By analyzing the movements of the participant in specific task, the ordinary differential equation is used to investigate dynamic movement primitives (DMP). In this study, DMP, that assists the trajectory of human interaction behavior is altered to extract human movement primitives in 1DOF deburring process. Human participant tries to control force during the task of deburring process by using local movements of haptic device's knob. Using these local movements of human participant as DMPs, transfer them to deburring robot and making dataset of group of sub-movements, we will have automatic system which imitates human participant characteristics. Figure 6.1. shows the wrist motion of the participant while trying to fix normal force on 10 N.

6.1 Methodology of Local Control with DMP

General methodology of this study is to build a setup which contains the F/T sensor to measure normal forces coming from human participant actions and 1-D knob setup to measure movements of the wrist of human participant. By using this setup, human participant can be able to change movements by considering the force displayed on setup screen in specific task. Then, by using force and wrist movements, dynamic movement primitive method can be considered. DMP

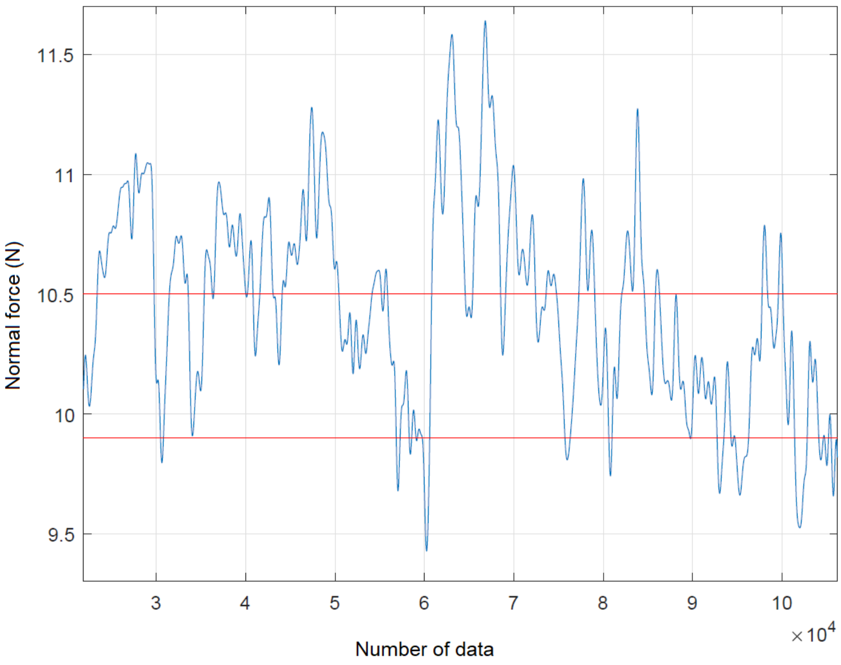

Figure 6.1: Wrist motions of participant while trying to fix normal force on $10N$

helps to characterize each human participant with respect to his/her movement primitives with respect to reaction forces.

6.1.1 Force Control

In machining processes, the exerted force components on workpieces in deburring/grinding have significant influence on surface quality. While performing a deburring/grinding process, the direction which is tangent to the surface of the workpiece is the tangential direction and the force exerted in this direction is tangential force F_t. Also, the direction which is normal to the tangential direction is normal direction, and the force in this direction is normal force F_n. Therefore, the forces that are exerted to the tool of spindle from surface of workpiece is a combination of tangential and normal forces. Figure 6.2 shows the example of deburring operation.

In Figure 6.3, the red circle represents the cutting tool; “md” is short for moving direction of the tool. Tangential force is shown by F_t and the normal force is shown by F_n.

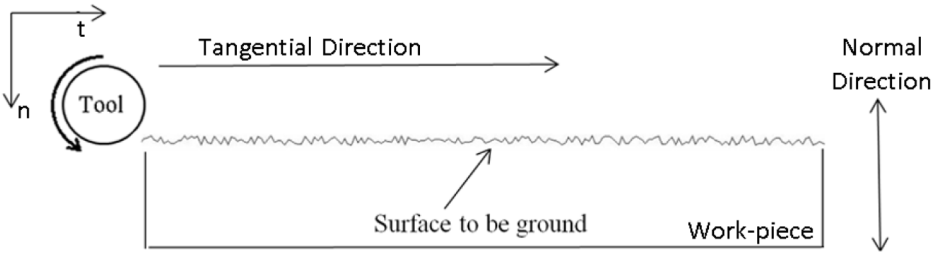
t
n
Tool
Tangential Direction
Normal Direction
Surface to be ground
Work-piece

Figure 6.2: Example of the deburring/grinding operation on a flat surface

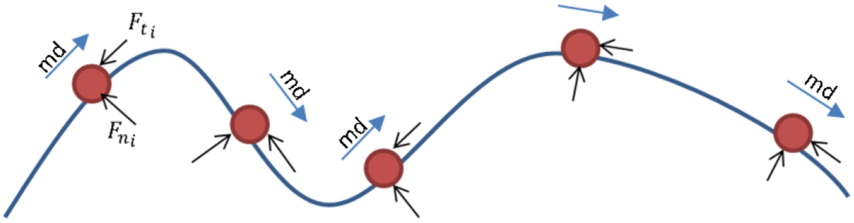
md
F_{t_i}
F_{n_i}
md
md
md

Figure 6.3: Example of the deburring/grinding operation on a wavy surface

In order to obtain constant depth of cut from variable surface, the key strategy that should be implemented is imposing appropriate normal force and tangential velocity. That is, classical explicit hybrid force/velocity control should be implemented [31]. In order to obtain the actual local normal force from measured X and Y force components, the algorithm which is explained in [32] was implemented.

The local tangential force is as follows:

$$F_t = \frac{M_{zSpindle}}{r_{tool}} \tag{6.1}$$

where, $M_{zSpindle}$ the measured moment around the Z axis of the spindle and r_{tool} is the radius of the cutting tool. However, with the used setup, measured moment around Z axis of the F/T sensor, M_z, is not the moment around the axis of the spindle since the F/T sensor has an eccentricity with respect to the spindle. Therefore, local tangential force is calculated as follows:

$$F_t = \frac{M_{zSpindle}}{r_{tool}} = \frac{M_z - F_x\Delta_y - F_y\Delta_x}{r_{tool}} \tag{6.2}$$

where, F_X is the measured force in X direction, F_y is the measured force in Y direction, Δ_x is the eccentricity of the force/torque sensor with respect to spindle axis in Y direction, and Δ_x is the eccentricity of the force/torque sensor with respect to spindle axis in X direction.

After the calculation of F_t, the local normal force F_n is calculated by the utilization of the following equality:

$$\sqrt{{F_x}^2 + {F_y}^2} = \sqrt{{F_n}^2 + {F_t}^2} \tag{6.3}$$

therefore,

$$F_n = \sqrt{{F_x}^2 + {F_y}^2 - {F_t}^2} \tag{6.4}$$

Constant velocity control is performed by the controller of the hexapod robot. However, when the piezoelectric actuator is in action, the resultant feed-rate increases since it is defined as:

$$F_R = \sqrt{{V_{Hex}}^2 + V_{Pzo}^2} \tag{6.5}$$

where, V_{Hex} is the velocity of the Hexapod, V_{Pzo} is the velocity of the piezoelectric actuator.

However, since the amplitude of the sinusoidal profile of the used workpiece is very low compared to the length of the workpiece, the effect of the V_{Pzo} was neglected. In order to control the normal force, the movement of the piezoelectric actuator was utilized [33].

6.1.2 Local DMP

Since the deburring process in local movements is dependent on normal force F_n of the surface of the workpiece, Dynamic movement primitives of the process has to be as a function of F_n.

DMP model as a function of F_n is no longer a trajectory model of position, but the trajectory of the force and its gradients. The point attractor of the system is the desired force which we want to keep constant in order to have better surface quality.

Therefore, transformation system of the normal force can be presented as,

$$\tau_F \dot{z}_F = \alpha_F(\beta_F(F_n^{set} - F_n) - z_F) + f_F(x) + P \tag{6.6}$$

$$\tau_F \dot{F}_n = z_F \tag{6.7}$$

Here, P is the set movement of the tool of spindle with respect to the normal force. These movements can be obtained from piezo movements or the radial movements of knob during an experiment. F_n^{set} is defined as the intended constant force that we need to have same profile.

DMP of local control in this section is changed to force trajectory instead of motion trajectory. This is because of the importance of desired force and the force exerted by the tool tip on the surface of the workpiece. This DMP is not the mass-spring-damper system anymore, however, it is still useful for imitation learning.

For formulating a function approximation problem, we rearrange equations 6.6 and 6.7 as

$$\tau_F^2 \ddot{F}_n = \alpha_F(\beta_F(F_n^{set} - F_n) - \tau_F \dot{F}_n) + f_F(x) + P \tag{6.8}$$

and the learn-able nonlinear term can be obtained from below equation,

$$f_F(x) = \frac{\sum_{i=1}^{k} \omega_i \psi_i(x)}{\sum_{i=1}^{k} \psi_i(x)} x(F_n^{set} - F_n(0)) \tag{6.9}$$

By performing above equations and methods, the imitation of local control on the surface of the workpiece can be obtained.

6.2 Experiment Procedure

In this study, the following main devices are utilized:

1. An experimental precision grinding robot (utilizing a 6DOF Hexapod from PI company) with 6DOF F/T sensor,
2. A 1DOF haptic device with force feedback,
3. A piezoelectric actuator with 1-mm stroke for moving the workpiece,
4. Workpiece (St37) with known geometry,
5. A high-speed spindle.
6. A 4-mm diameter cBN tool from Pferd company

In Figure 6.4, the connection of the devices is summarized. In order to combine all these devices, a prototypical MATLAB/SimulinkTM model is developed (with Windows target machine, targeting 1000 Hz sampling frequency for all measurements and control action in pseudo-real-time).

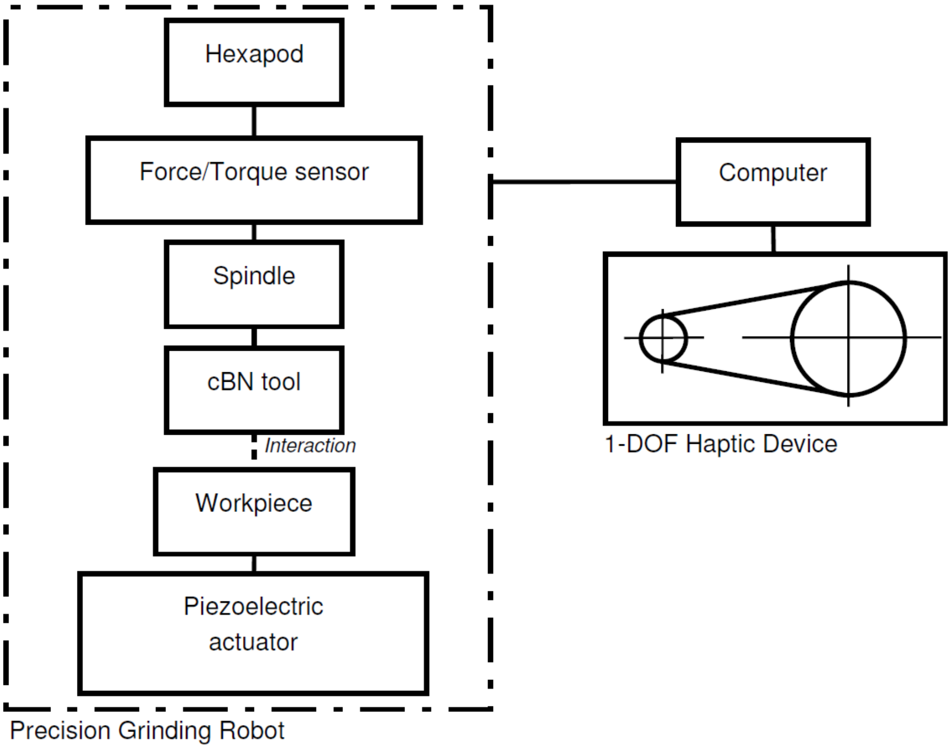
Hexapod
Force/Torque sensor
Spindle
cBN tool
Interaction
Workpiece
Piezoelectric actuator
Precision Grinding Robot
Computer
1-DOF Haptic Device

Figure 6.4: The connectivity diagram of the overall system

During the experiments, a human operator rotates the knob of the haptic device. This rotation is translated into motion of piezoelectric actuator. Since piezoelectric actuator is connected to the workpiece, human knob rotation actually moves the workpiece back and forth. Simultaneously, the hexapod moves the spindle from left to right in a constant speed. By default, the tool does not touch the workpiece. The cutting action is only possible if the operator moves the workpiece towards the tool. Due to the sinusoidal geometry of the workpiece, the operator has to follow the geometry (otherwise the forces will become too small or too much for cutting) while tracking the cutting forces from the monitor and feeling them from the haptic device's force feedback. The workpiece and tool positions is given in Figure 6.5.

The hexapod only moves in Y-axis and carries force/torque sensor, spindle and the cBN tool. Since hexapod can only move with 1 mm/s speed, it is not suitable to track the human hand motion. However, piezoelectric actuator is fast enough so that it can follow even the fastest hand movements.

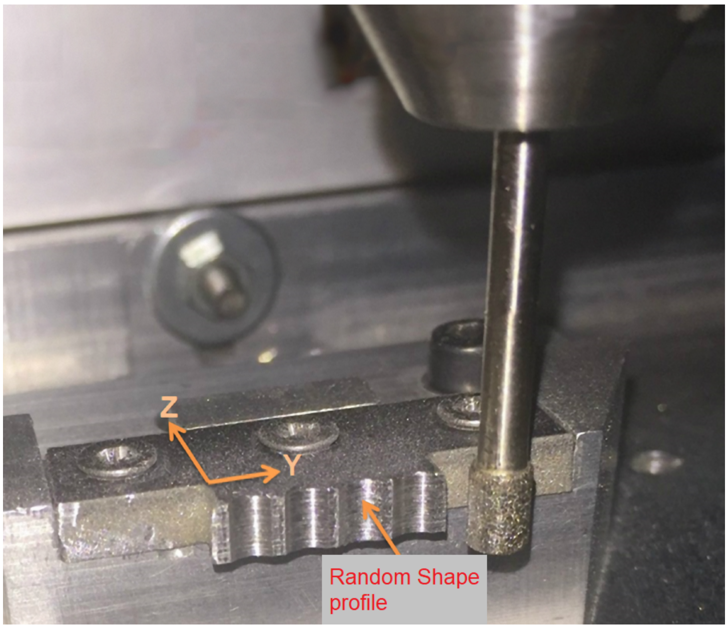

Figure 6.5: Upper front view of the workpiece and the tool tip

There are two kinds of feedback for the operator to track the forces namely following forces from a display and actually feeling the forces from the haptic device's force feedback. Forces coming from the cutting operation is translated to the voltages for the motor in the 1DOF haptic device. If the operator moves the workpiece toward the tool and a force is resulted, this force is converted to the knob motion for operator to feel. Note that, this force is not the actual force resulting from the operation, but proportional (increased) to it. Moreover, if the forces are too high, operator cannot move the knob or move it in the reverse direction for reducing the force.

After completing an experiment, all forces, knob motion, and piezoelectric actuator motion are saved and post-processed.

6.3 Model Verification

It is asked to each participant to hold the knob of the 1DOF haptic device and try to move it clockwise or counterclockwise in order to stay the normal force in the safe range. The participant should also look at the screen of the computer to see the instantaneous normal force. Safe range is the normal force limitation that causes acceptable depth of cut variance. In this study, it is asked from participants to fix the normal force on 10 N.

By analyzing the experiments, it is understood that, while performing an experiment, each participant has the safe range in their own subconscious. Almost all of them try to move their wrist counterclockwise or clockwise to decrease or increase the normal force when they think they are out of their safe range.

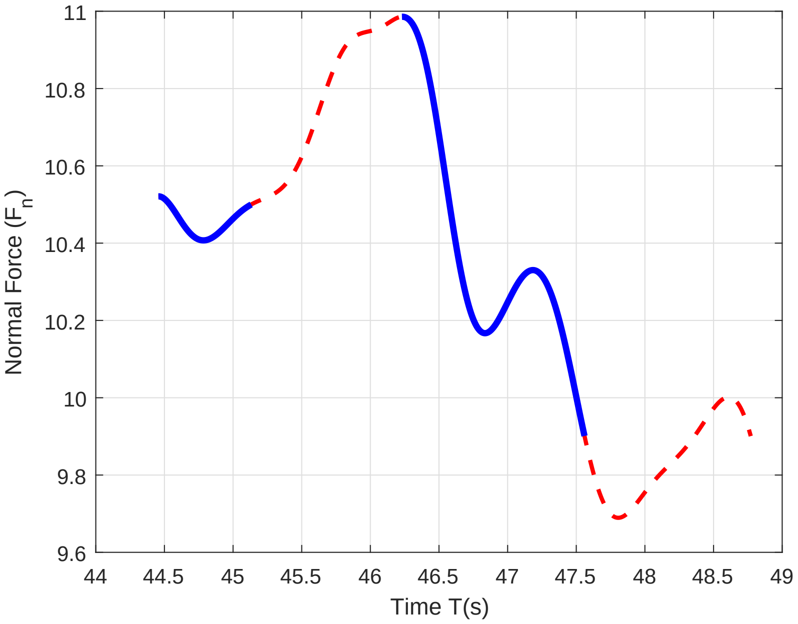

Figure 6.6: Example of the segmentation for the 1st participant in a random normal force of experiment

This reaction of participants shows that the trajectory of response starts from the first minimum value of normal force when participant notices that the value of normal force in screen is less than desired normal force value, 10 N. Also, the response can start from the maximum value of normal force when he/she notices that the value of normal force in screen is higher than 10 N. We should mention that the reaction movement ends when the exerted normal force is same as desired force.

Figure 6.6 shows the segmentation of the reaction forces exerted by each participant separately. This segmentation is obtained by determining the range of 9.8 N and 10.5 N. By observing the reactions of participants in experiments, it is understood that this range is the unconscious limitation for them.

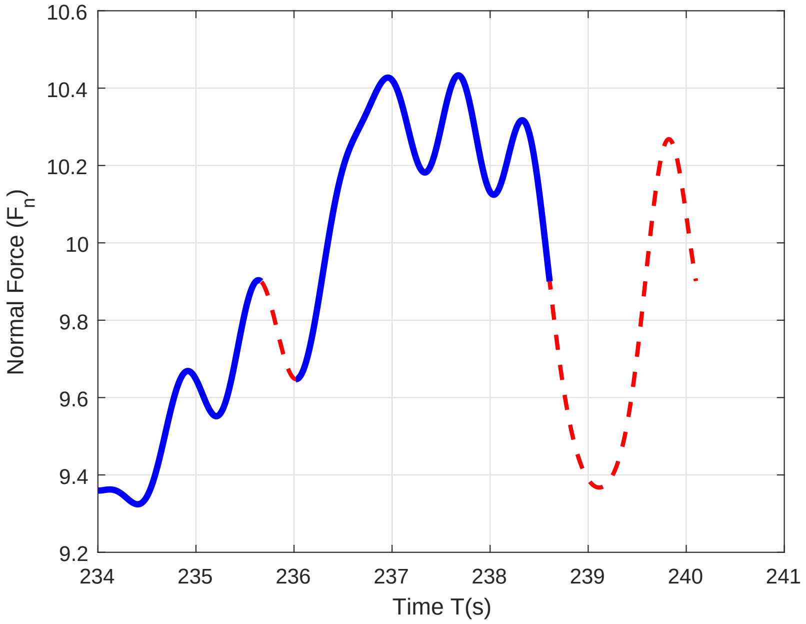

Figure 6.7: Example of the segmentation for the 2nd participant in a random normal force of experiment

Figures 6.6 and 6.7 show that each participant notices the changes of normal force in different ranges of values of them. Therefore, each participant has different reactions with respect to different normal forces. Figures 6.8 and 6.9 are the examples of all reactions of the participants in different normal forces.

Each participant has specific reactions in this experiment which is the characteristics of him/her. By using the segmentation of the reaction of a participant

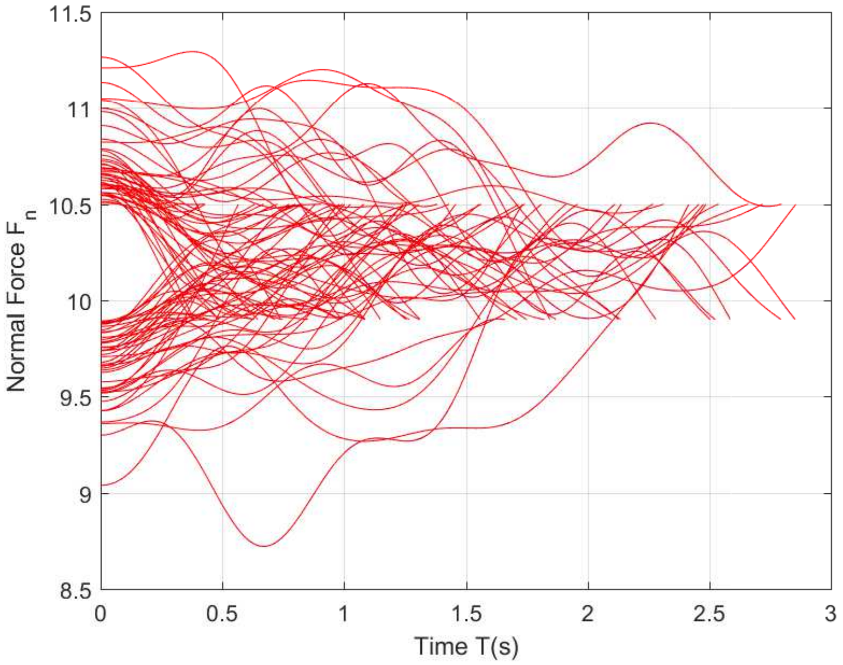

Figure 6.8: All normal force reactions of 1st Participant

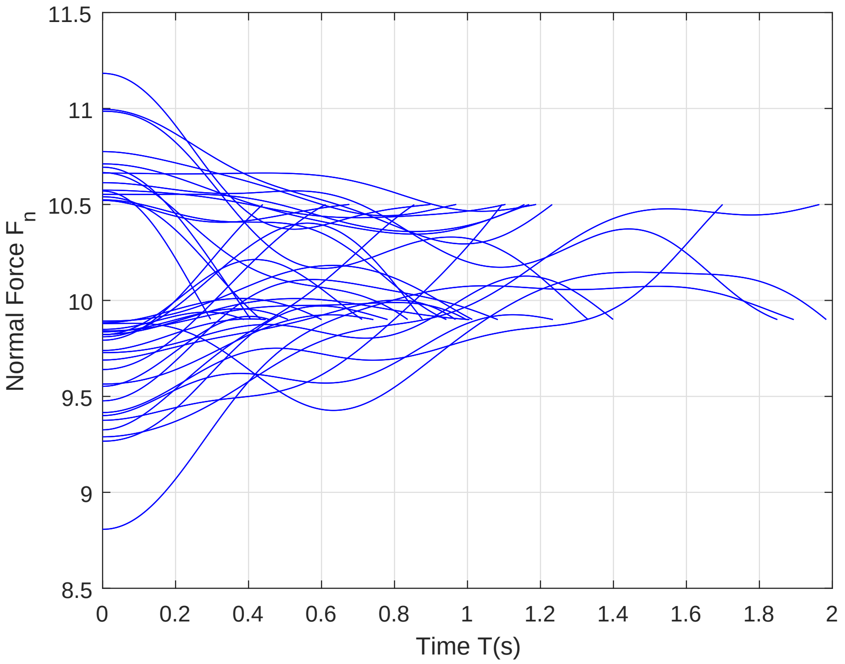

Figure 6.9: All normal force reactions of 2nd Participant

in 3 experiments and having a variation of normal forces of all experiments, we can use transformation trajectory system of DMP to compare different reactions of a participant and choose the best one.

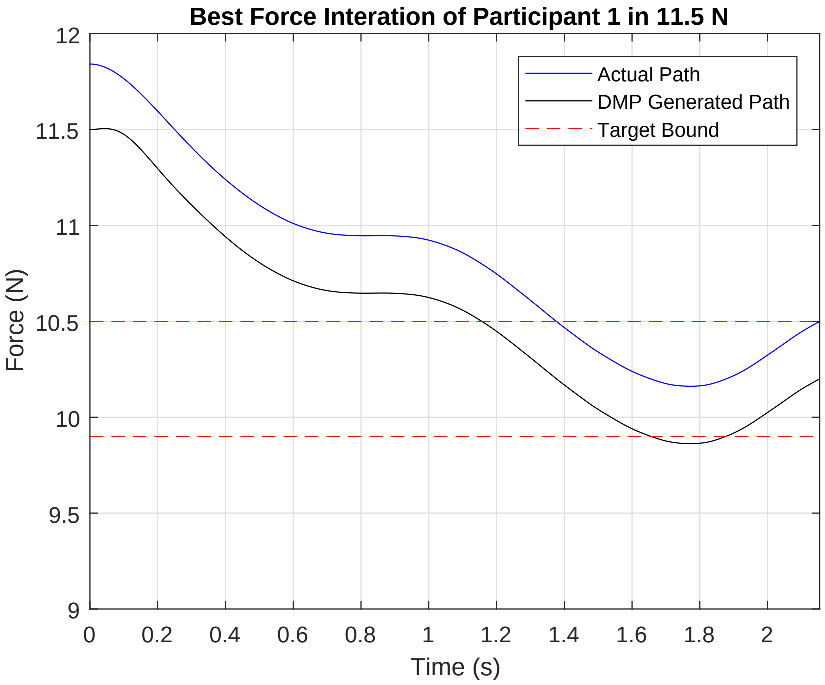

Figure 6.10: Best reaction of 1st Participant for 11.5 N disturbance force

In addition, we can learn the best reaction of each participant for different normal forces. The best reaction is the reaction which has faster motion through the desired normal force.

Also, we can have the collection of Dynamic movement primitives parameters and weights. This can help us to obtain the human controller just like other controllers. However, this controller is much more slower and may not have stable response. Figures 6.12 and 6.13 are the best response of each and all participants in all the experiments performed by them.

We can obtain the best responses and respective DMP parameters of the participants automatically, considering their time span. A database based on best DMP responses of experts can serve as a building block for a human active con-

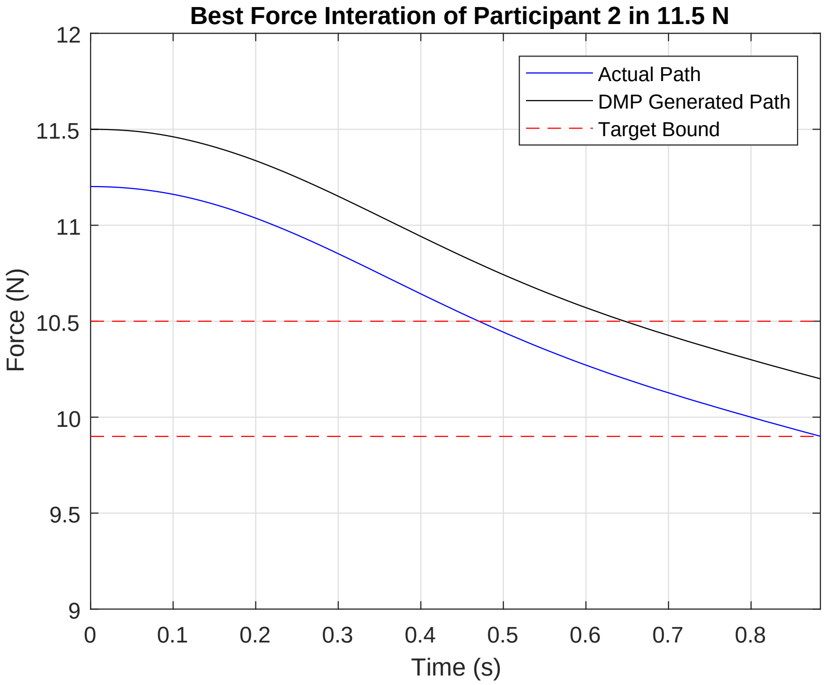

Figure 6.11: Best reaction of 2nd Participant for 11.5 N disturbance force

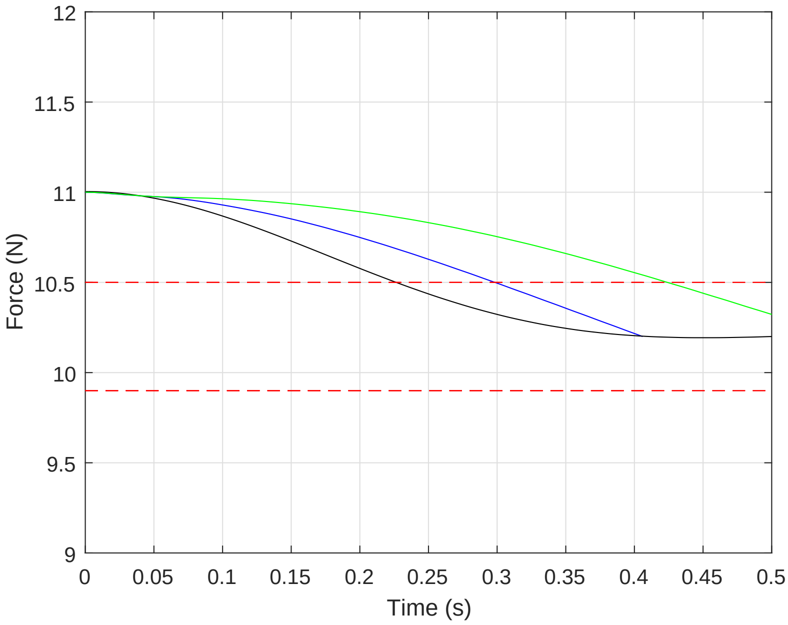

Figure 6.12: Best reaction of normal force for each participants with respect to random disturbance force (each color represent each participant)

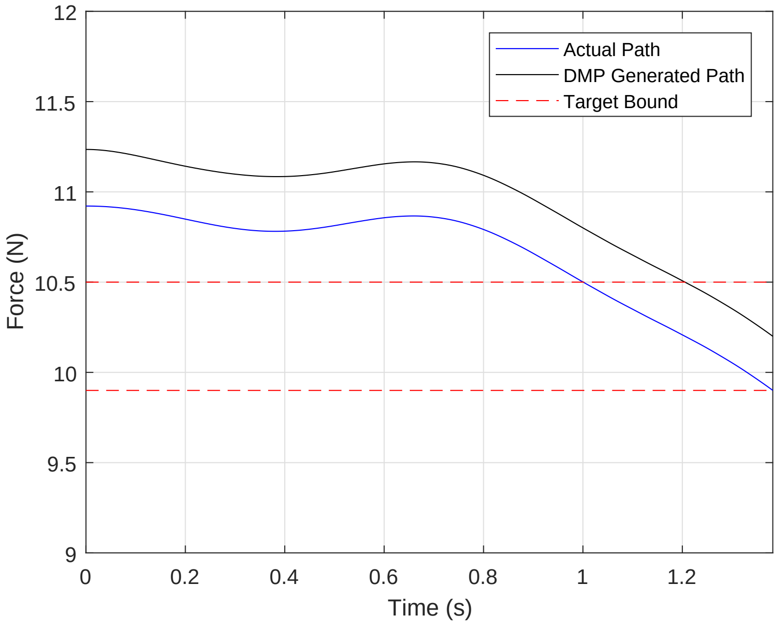

Figure 6.13: Best reaction of normal force for all participants with respect to random disturbance force

troller. This controller can work as an outer loop (a supervisory controller) for a Proportional Integral Derivative (PID) controller and may make it robust for sudden high and low force cases. In other words, such a controller would be important for automated deburring robots since it creates human-like reactions for sudden changes that a PID controller cannot handle. Our findings can be used to build such a controller. However, the purposes of this study are the extraction of the primitives, creating a database and simulation of human responses.

6.4 Conclusion

We successfully extracted force trajectories of human participants in DMP form. Our approach allows automatic segmentation of force data to obtain individual DMPs used by participants. These DMPs are collected in a database. Also, a simulation environment utilizing the DMPs is built. In simulations, a force specified outside the safe range is moved inside the range using a suitable DMP pattern drawn from the DMP database. This corresponds to a reaction of one of the participants around that specific force. Note that, the chosen pattern is the best DMP among all of the participants. Mainly, each participant has potential to react to a random force better than others. Since a participant sometimes reacts better than others for a specific force; even though, his/her overall performance may be poor compared to others. Using a teleoperation scheme for the experiments, we eliminated the correspondence problem. Participants were able to follow the sinusoidal initial form of the workpiece during the experiments. This is only possible by the normal force calculation method we presented. Our future work is to use our DMP controller as supervisory control scheme steering a PID controller to perform deburring.

CHAPTER 7

BASIC CONCEPTS

One of the tasks of this study is to automatize our robotic deburring setup. Although DMP concept is very important and the fundamental studies related to it have been done in chapter 5 and 6, we also have to consider other subjects such as tool deflection, collision, workpiece obscurity, selection of optimal feed-rate of the hexapod and generated rhythmic DMP movement. Each of the above subjects should be considered very carefully as the process is in micron-size resolution. Any mistakes can cause tool fraction, damage on F/T sensor and deformation on the calibration of the setup.

7.1 Tool deflection

During the grinding/deburring process, the interaction between tool tip and workpiece generates normal and tangential forces. Since the tool of the spindle is not rigid, there will be a deflection in two dimensions with respect to two-dimensional forces.

Deflection of the tool changes in the normal and tangential direction of the workpiece with respect to the tool which causes the change on the desired surface of the machined workpiece. In addition, excessive deflection causes plastic deformation of the tool which yields to wrong data-read for upcoming experiments. For this reason, calculation of the one-dimensional angle of deformation of a tool on a workpiece that is related to interaction normal force should be considered.

Therefore, as it is known from the experiments, forces that are higher than the maximum normal force of specified experiment should be avoided in order to eliminate excessive deformations of a tool on a workpiece which increases form error.

7.2 Collision

Collision is another important issue that has to be considered before automatizing deburring robot. Collision is created when the tool and the workpiece exert excessive force on each other in a relatively short period of time. The momentum and kinetic energy that is conserved by a tool and the workpiece during the collision, cause damages on them and creates failures on the calculation of force during the grinding/deburring process. Experiment related to force with and without collision has been performed and their differences are analyzed. Figure 7.1 shows the critic example of normal force for specific experiment.

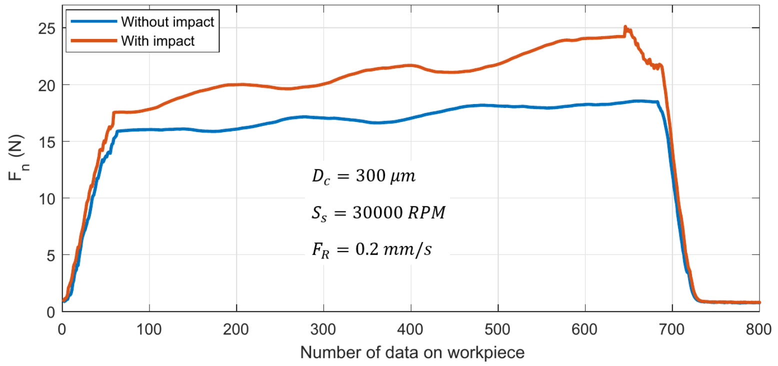

Figure 7.1: Normal force with and without collision on same characteristic experiments

As it can be seen from figure 7.1, experiments with collision generate higher force than experiments without collision. In order to be able to avoid the collision, the magnitude of a normal force and tangential force between tool and the workpiece in specified experiments have to be considered. Since, during the experiments, the depth of cut D_c, feed-rate F_R and spindle speed S_s are known, we can calculate the range of the normal and tangential forces that have to be created. Therefore, the forces that are higher than a specified force range are excessive forces. By eliminating these forces, we can avoid tool failure and damages on the profile of the workpiece.

7.3 Optimal feed-rate selection

In robotic deburring, feed-rate of the manipulator, spindle speed and depth of cut are relative to each other. Also, they create normal and tangential forces which are specific to them. In this part, it is wanted to find the optimal feed-rate with respect to load percent L_p, depth of cut and spindle speed. Before, selecting the optimal feed-rate, grinding model related to this experimental setup should be considered.

7.3.1 Grinding Model

In case of obtaining the desired depth of cut and high quality on the surface of the workpiece, there has to be a model to provide correct normal and tangential forces. In [5], the general form of model of grinding force is investigated. In this study, a physical model is used based on chip formation energy and sliding energy.

The grinding force is dependent on depth of cut D_c, feed rate F_R, velocity of tool wheel periphery S_s, tool width b and tool diameter d_e.

We should also mention that the deflection of the tool is assumed to be rigid in this study. Normal and tangential force equations obtained as follow;

$$
\begin{aligned}
F_t = & -4.67 - 37.1(\frac{bD_cF_R}{S_s}) + 0.505(\frac{bD_cF_R}{S_s})ln(\frac{{S_s}^{1.5}}{{D_c}^{0.25}{F_R}^{0.5}}) \\
& + 0.0228(b\sqrt{d_eD_c}) + 1631(\frac{bF_R\sqrt{d_eD_c}}{S_sd_e}) \\
& + 0.465(\frac{A_{1fn}}{t_{1fn}}) - 1.15(\frac{A_{2fn}}{t_{2fn}}) + 0.311(L_p\frac{F_{pn}}{L_{pmax}})
\end{aligned}
\tag{7.1}
$$

$$
\begin{aligned}
F_n = & -4.42 - 155(\frac{bD_cF_R}{S_s}) + 10.5(\frac{bD_cF_R}{S_s})ln(\frac{{S_s}^{1.5}}{{D_c}^{0.25}{F_R}^{0.5}}) \\
& + 2317(\frac{bF_R\sqrt{d_eD_c}}{S_sd_e}) + 1.49(\frac{A_{1fn}}{t_{1fn}}) - 4.24(\frac{A_{2fn}}{t_{2fn}}) \\
& + 1.79(L_p\frac{F_{pn}}{L_{pmax}})
\end{aligned}
\tag{7.2}
$$

$$
\begin{aligned}
\bar{r}^* = & e^{\tilde{u}_3\theta_1}[\bar{u}_1(a_2cos\acute{\theta}_2 + a_3cos\acute{\theta}_{23} - d_4sin\acute{\theta}_{23}) \\
& + \bar{u}_3(-a_2sin\acute{\theta}_2 + a_3sin\acute{\theta}_{23} - d_4cos\acute{\theta}_{23})]
\end{aligned}
\tag{7.3}
$$

In this study, the tool is penetrated to the workpiece in normal direction. As it can be seen from equations 7.1-3 and figure 7.2, A_{1fn} and A_{2fn} are the areas under F_n before and after the peak time. Also, t_{1fn} and t_{2fn} are respectively, the time difference between start and peak time and between peak time and end time. In addition, L_{pmax} is the peak value of percent load of the spindle, and F_{pn} is the peak F_n value.

The developed model in this study can efficiently be used for prediction of the grinding forces and obtained the relation between the depth of cut, spindle speed, feed-rate and normal and tangential force values. Also, from this inspiring academic paper, we can say that there are three regimes created during the experiments. Figures 7.3-5 show the examples of each regime with respect to normal force F_n.

In the experiment of regime 1, shown in figure 7.3, the magnitude of feed-rate F_R is low. Because of the slow velocity of the hexapod, the burr removal process

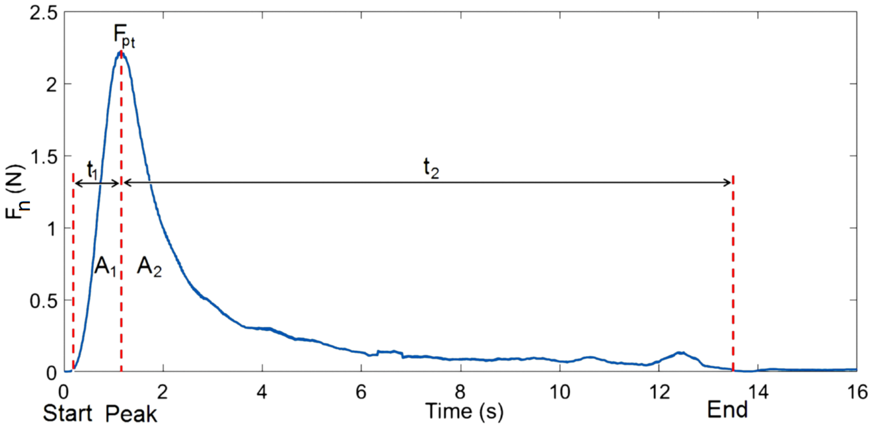

Figure 7.2: Normal force profile in time domain

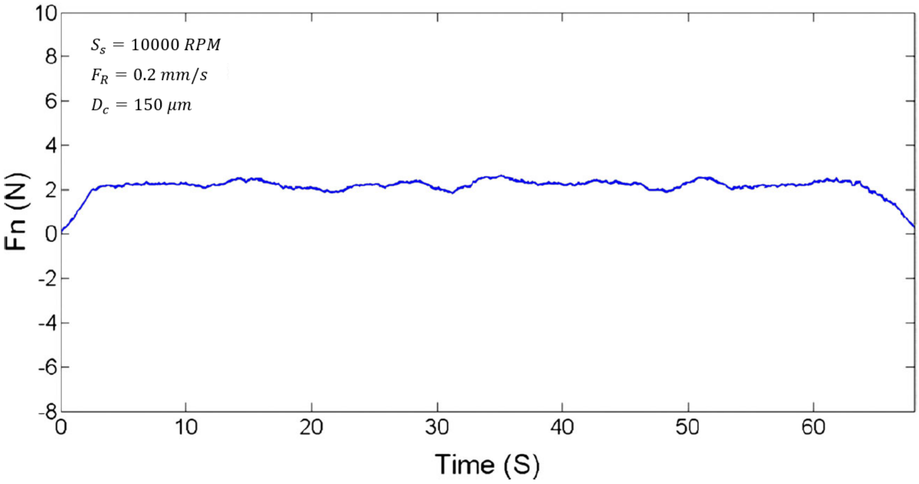

Figure 7.3: Example of regime 1

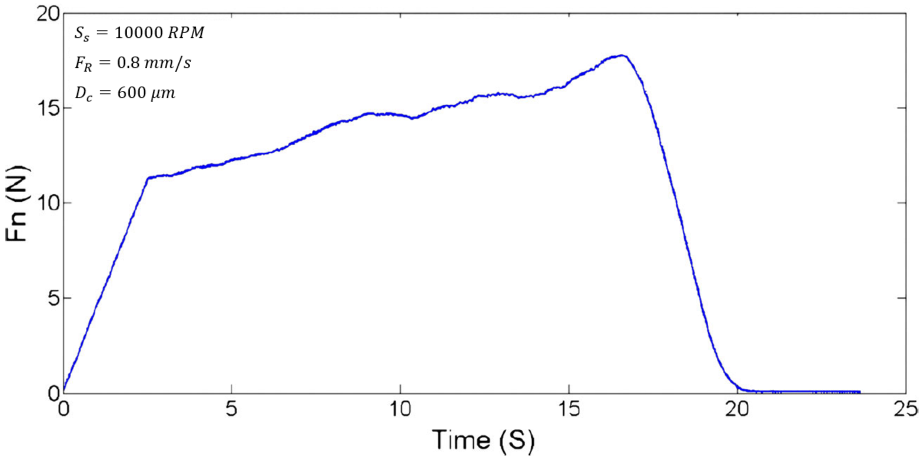

Figure 7.4: Example of regime 2

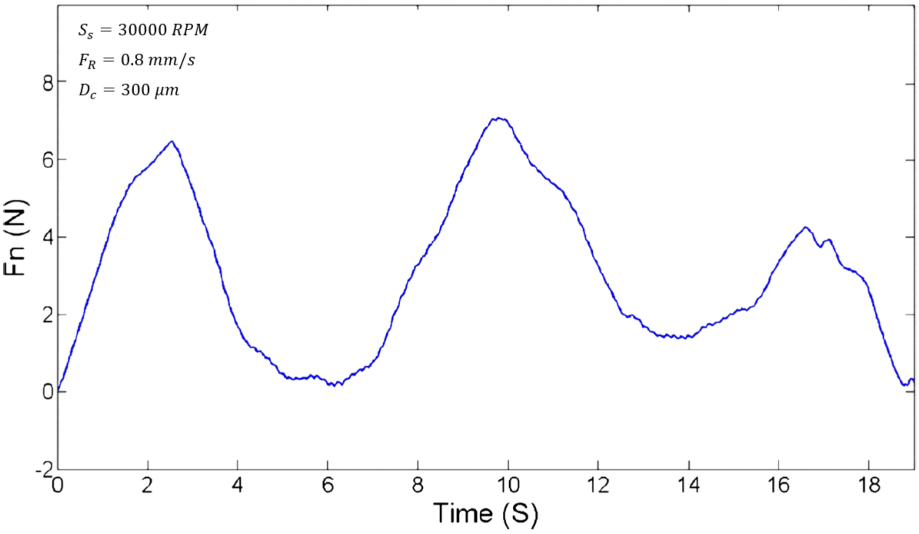

Figure 7.5: Example of regime 3

will happen at the moment of touch. However, in regime 3, by increasing the F_R, velocity of the hexapod increases and the burr removal process becomes harder because of the tool deflection and its compensation. Also, in regime 2, as force increases and S_s is not high enough to help the tool to cut the profile, tool deflects through the deburring/grinding process and is not able to compensate. Because of this reason, the experiments have to be with low F_R or high S_s in order to have stable normal force and prevent tool deflection.

7.3.2 Artificial Neural Network model

By utilizing the grinding model, it is understood that the MATLAB's curve fitting toolbox can be helpful to determine the feed-rate with respect to load percent, depth of cut and spindle speed. One of the ways to approach this problem is neural network between the load percent, depth of cut, feed-rate and spindle speed. By using the current coming to the spindle of the setup, we can understand load percent of the spindle and the tool. Load percent is depended to zero load current $I_{zeroload}$, maximum current $I_{100load}$ and instant current $I_{Instant}$ of the spindle.

$$L_p = \frac{I_{Instant} - I_{ZeroLoad}}{I_{100load} - I_{ZeroLoad}} 100 \tag{7.4}$$

By giving normal and tangential forces, we can generate load percent. Therefore, by giving the depth of cut, load percent and spindle speed as an input and feed-rate as an output, we can generate a neural network in order to learn the feed-rate needed for each experiment. By using the block diagram of Figure 7.6, the feed-rate of the experimental setup can be obtained.

7.4 Generating DMP

As it is explained before about Dynamic Movement Primitives (DMP), we can generate the movements from specific start position to the point attractor (Goal

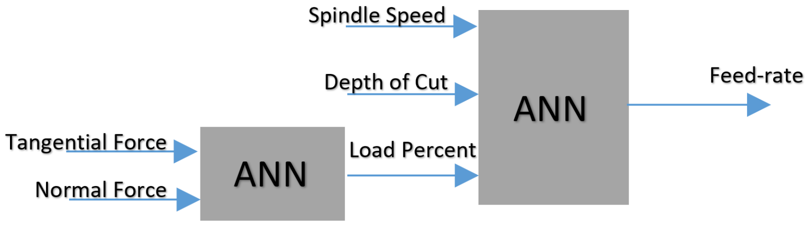

Figure 7.6: Feed-rate selection by using ANN

position). Since the human expert's movements are in two dimensions, there have to be two DMPs which work together. By utilizing chapter 4 and equations 4.1, 4.2 and 4.3, the movements of the human expert can be written as equations 7.5-8. Note that, only human expert skills in the backward rhythmic motion is analyzed in this work. Backward rhythmic motion is the trajectory of tool in 2-dimensional space to become to a new position of workpiece.

For Y-axis direction, DMP can be written as;

$$\tau_y \ddot{y} = \alpha_y(\beta_y(g_y - y) - \dot{y}) + f_y(x) \tag{7.5}$$

$$f_y(x) = \frac{\sum_{i=1}^{k} \omega_{y_i} \psi_i(x)}{\sum_{i=1}^{k} \psi_i(x)} x(g_y - y_0) \tag{7.6}$$

And, for Z-axis direction;

$$\tau_z \ddot{z} = \alpha_z(\beta_z(g_z - z) - \dot{z}) + f_z(x) \tag{7.7}$$

$$f_z(x) = \frac{\sum_{i=1}^{k} \omega_{z_i} \psi_i(x)}{\sum_{i=1}^{k} \psi_i(x)} x(g_z - z_0) \tag{7.8}$$

As it is mentioned before, parameter sets of Y-direction and Z-direction should work together. The parameter set includes τ, α, β and ω. Therefore, for generating specific two-dimensional motion, the parameters of below dataset should be chosen;

$$\begin{bmatrix} y_1 & z_1 \\ y_2 & z_2 \\ \vdots & \vdots \\ y_n & z_n \end{bmatrix} \longrightarrow \begin{bmatrix} \tau_{y_1} & \alpha_{y_1} & \beta_{y_1} & \tau_{z_1} & \alpha_{z_1} & \beta_{z_1} \\ \tau_{y_2} & \alpha_{y_2} & \beta_{y_2} & \tau_{z_2} & \alpha_{z_2} & \beta_{z_2} \\ \vdots & \vdots & \vdots & \vdots & \vdots & \vdots \\ \tau_{y_n} & \alpha_{y_n} & \beta_{y_n} & \tau_{z_n} & \alpha_{z_n} & \beta_{z_n} \end{bmatrix}$$

Also, it should be mentioned that weights are also specific to the specific task. For this reason;

$$\begin{bmatrix} y_1 & z_1 \\ y_2 & z_2 \\ \vdots & \vdots \\ y_n & z_n \end{bmatrix} \longrightarrow \begin{bmatrix} \omega_{y_1} & \omega_{z_1} \\ \omega_{y_2} & \omega_{z_2} \\ \vdots & \vdots \\ \omega_{y_n} & \omega_{z_n} \end{bmatrix}$$

Note that ω is the dataset of the weights for the specific task. Generation of DMP for specific start and point attractor can be shown in Figure 7.7 which is the block diagram of the process.

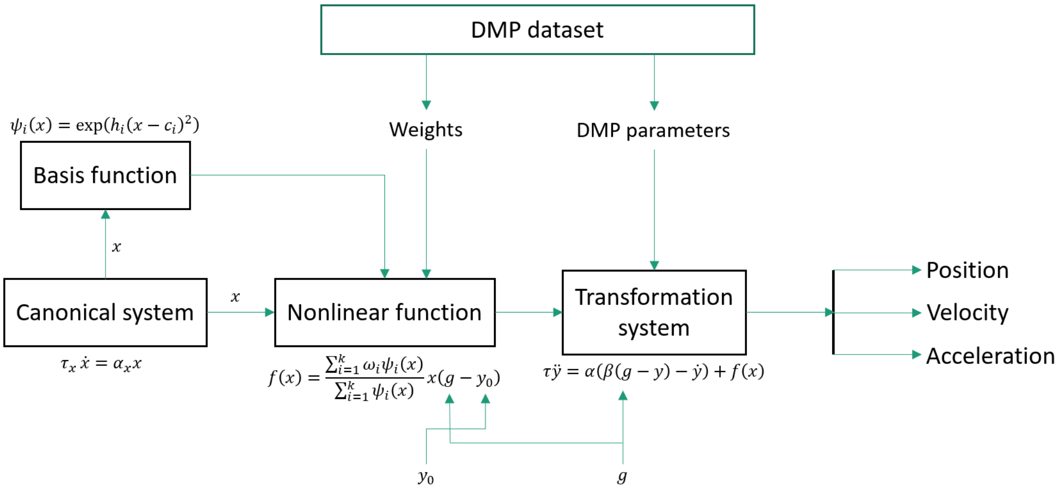
DMP dataset
Weights
DMP parameters
$\psi_i(x) = \exp(h_i(x - c_i)^2)$
Basis function
x
Canonical system
x
Nonlinear function
Transformation system
Position
Velocity
Acceleration
$\tau_x \dot{x} = \alpha_x x$
$f(x) = \frac{\sum_{i=1}^{k} \omega_i \psi_i(x)}{\sum_{i=1}^{k} \psi_i(x)} x(g - y_0)$
$\tau \ddot{y} = \alpha(\beta(g - y) - \dot{y}) + f(x)$
y_0
g

Figure 7.7: Block diagram of DMP generation

7.5 Conclusion

In robotic deburring, the obscurity of the profile of the workpiece is one of the most important issues that should be considered. In order to have automatic robotic deburring on unknown profile of the workpiece, tool deflection, collision, selection of feed-rate and generated DMP movement have to be considered carefully. Therefore, the experimental procedure and results of robotic deburring/grinding process should be based on the above-mentioned concepts.

CHAPTER 8

BASIC EXPERIMENTS AND RESULTS

8.1 Tool Deflection

As it is mentioned before, in chapter 7, tool deflection can be avoided by staying in the range of tangential and normal forces for specified task. Since calculating the tool deflection is in two dimensions and the surface of the workpiece can only be measured in normal direction, methods of beam deflection for calculating tool deflection from workpiece are not applicable. Tool angle of deformation and displacement create form error on the profile of the workpiece with respect to D_c, F_R and S_s. The experiments on smooth profile with different D_c, minimum F_R and maximum S_s have been performed. After that, the surface of the workpiece is scanned with laser scanner, shown in figure 8.1.

Task of "Making profile of workpiece flat" is given to the setup. Experiments of $150\mu m$, $300\mu m$ and $450\mu m$ with 0.2 mm/s F_R and 30000 RPM spindle speed have been performed. After that the surface of workpieces are scanned in two different x-directions. Figures 8.2-4 show the displacements on the workpiece in z-direction.

Analyzing figures 8.2-4, table 8.1 shows the maximum normal force and related maximum form error on the workpiece.

Since D_c of $150\mu m$, $300\mu m$ and $450\mu m$ create different form error in normal direction of workpiece, we can conclude that there will be a need for cleaning pass of the tool.

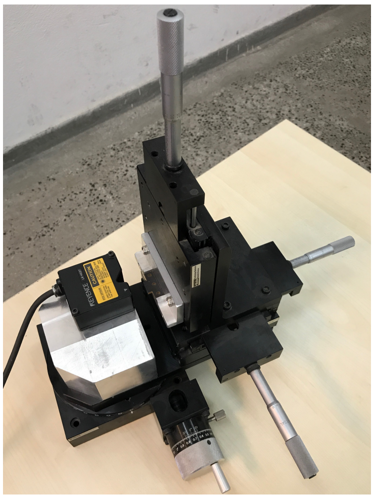

Figure 8.1: Surface scanning setup

Table 8.1: Maximum normal force and related maximum form error on workpiece

	$D_c = 150\ \mu m$	$D_c = 300\ \mu m$	$D_c = 450\ \mu m$
$F_{n_{max}}\ (N)$	8.48	12.51	20.69
$r_{max}\ (\mu m)$	57	58	66.5

8.2 Cleaning pass

In order to have smooth profile with lowest form error in Z-direction, there will be a need for cleaning pass. By utilizing maximum form error of workpiece in Z-direction from table 8.1 and performing extra deburring/grinding process, we can say that the cleaning pass can result in significant decrease in form error on workpiece. Experiments related to this study with $0.2mm/s$ F_R and 30000 RPM of S_s on workpiece is shown in table 8.2.

Before scanning the surface of the profile after cleaning pass, the surface of workpieces with 150 μm, 300 μm and 450 μm depth of cuts are scanned. 30 sections in Y-direction with two different X-directions are determined for calculation of form error on the workpiece. Also, the workpiece surface is scanned after cleaning pass motion.

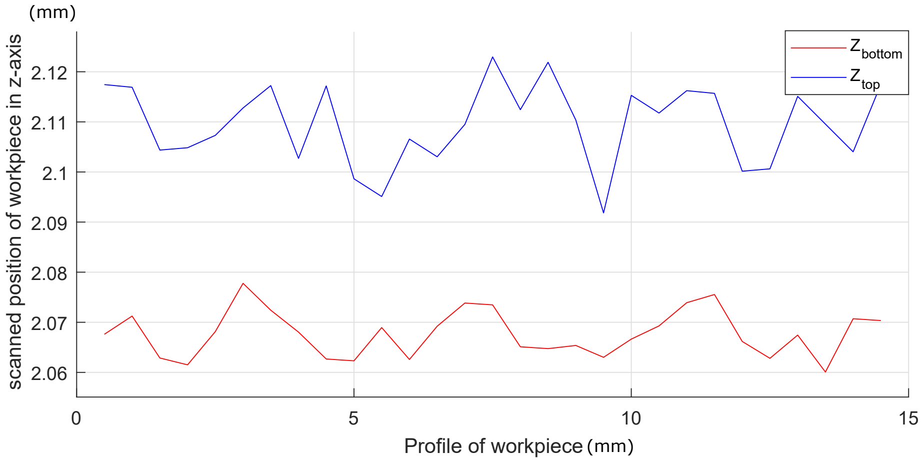

Figure 8.2: Form error due to interaction force of 150 μm depth of cut

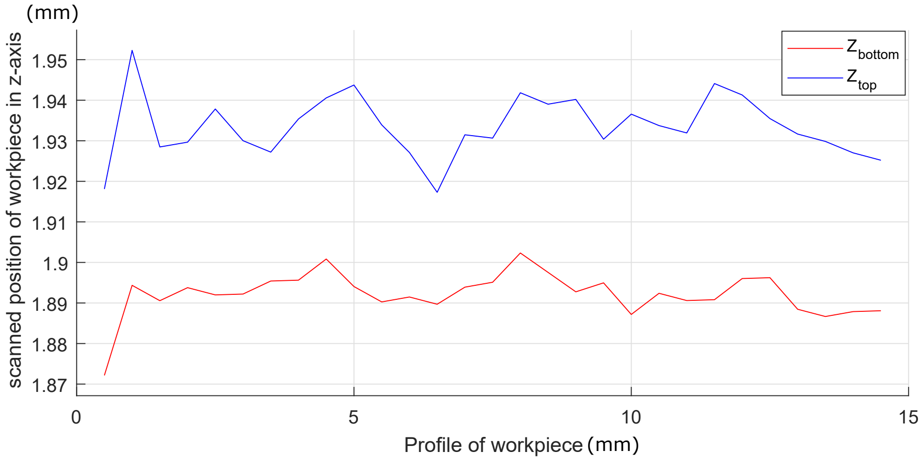

Figure 8.3: Form error due to interaction force of 300 μm depth of cut

Table 8.2: Maximum form error before and after cleaning pass

	$D_c = 150\ \mu m$	$D_c = 300\ \mu m$	$D_c = 450\ \mu m$
r_{max} (μm)	57	58	66.5
r_{max} after C.pass (μm)	16	35	39

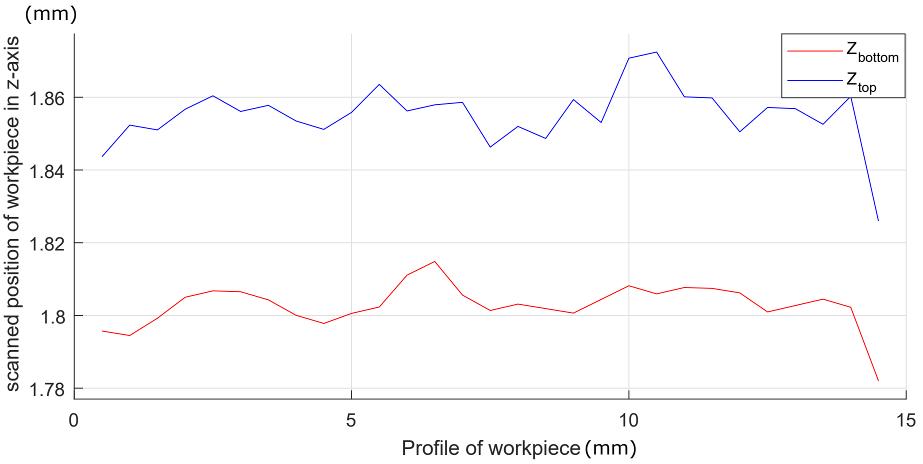

Figure 8.4: Form error due to interaction force of 450 μm depth of cut

By calculating the mean value of form error on the workpiece before and after cleaning pass, we can say that there are 72%, 39% and 41% decrease of form error for 150 μm, 300 μm and 450 μm depth of cuts respectively.

8.3 Collision and burr size relation

It is mentioned before in section 7.2 that collision should be eliminated somehow in experiments. However, as the profile of the workpiece is unknown and experiments have to be blind, the collision of the tool with workpiece should be identified.

Burrs are very small pieces of materials that when tool comes to them, they should not be misunderstood with profile of the workpiece. Also, since it is wanted to have blind robotic deburring, we do not want our robot to have extra grinding process for D_c's of less than 150μm which will be explained in chapter 9. For this reason, the $F_{resultant}$ which is the interaction resultant force between tool and workpiece should be considered carefully. It can be seen from table 8.3 that F_R, S_s and D_c have important influence on $F_{resultant}$

Experiments have been done on 150 μm, 300 μm and 450 μm depth of cuts with 0.2 mm/s, 0.4 mm/s and 0.6 mm/s feed-rate and 10000 RPM, 20000 RPM and 30000 RPM spindle speed. Table 8.3 shows the above-mentioned experiments with their average and maximum resultant forces.

Table 8.3: Maximum and average resultant force of specific task

Exp. No	D_c (μm)	S_s (rpm)	F_R (mm/s)	$F_{result_{max}}$ (N)	$F_{result_{avg}}$ (N)
. 1	150	10000	0.2	6.978	6.568
2	150	20000	0.4	8.986	8.825
3	150	30000	0.2	8.477	5.929
4	150	30000	0.6	7.004	6.681
5	300	10000	0.4	39.646	36.729
6	300	20000	0.2	18.724	17.33
7	300	30000	0.2	12.53	9.153
9	450	30000	0.2	20.84	15.471

As it can be seen from table 8.3, when giving specific F_R, S_s and D_c to the setup, if generated force is more than maximum $F_{resultant}$, it should be considered as excessive force and should be avoided. The avoidance process is explained in the flowchart of figure 9.6.

8.4 ANN training for optimal F_R selection

It is mentioned in chapter 7.3.1 that normal force is more reliable and smooth when it is in regime 1. Because of that, the value of F_R must be low to make a tool be able to cut in a moment of touch. Therefore, our ANN has to work with F_R in a range of $0.2 - 0.6$ mm/s and S_s has to be in a range of $10000 - 30000$ RPM.

We performed two ANN training on our data. the first training is for obtaining the relation between "normal and tangential forces" as an input and "load percent L_p" as an output. Also, the second training is between "the load percent L_p, D_c

and S_s" as an input and "F_R" as output.

8.4.1 ANN training for L_p and forces

Load percent of the spindle has the same reaction with resultant force. As it can be seen from Figure 8.5, the neural network curve fitting between them can be determined easily.

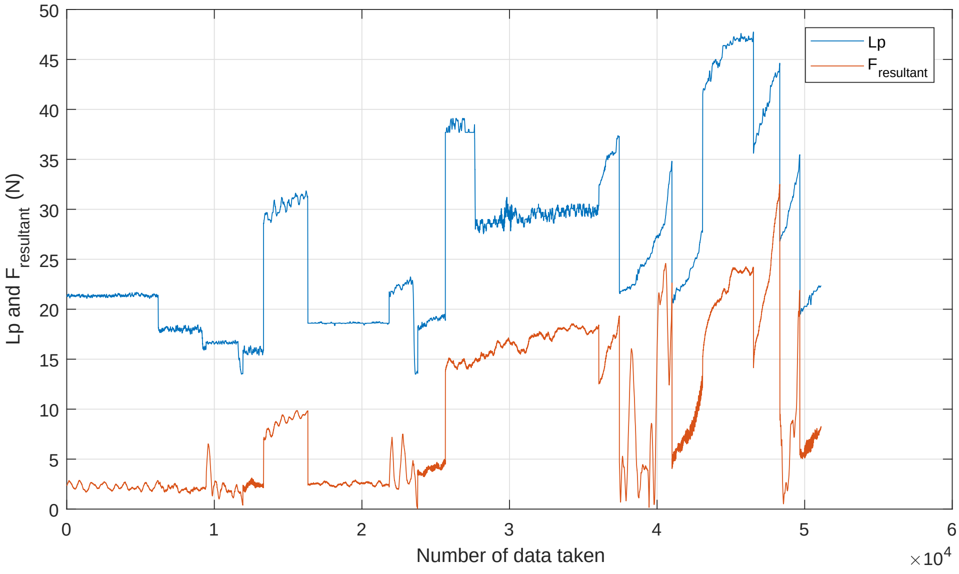

Figure 8.5: Example of the relation between L_p and $F_{resultant}$

In this work, L_p, F_t and F_n are approximated using two layer feed-forward neural network that is trained by Bayesian regularization back-propagation algorithm by using MATLAB Neural Network Toolbox [34]. The block diagram of ANN of L_p is available in figure 8.6. Considering the offered methods in [35], the number of hidden neurons of neural network is determined.

Figure 8.7 shows the verification of the curve fitting of our ANN by giving 10 hidden neurons. Also, it shows that load percent, normal force and tangential force have direct relations.

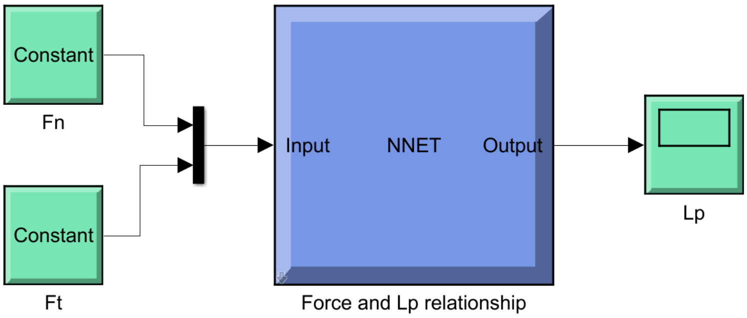

Figure 8.6: ANN block digram of force inputs and L_p output

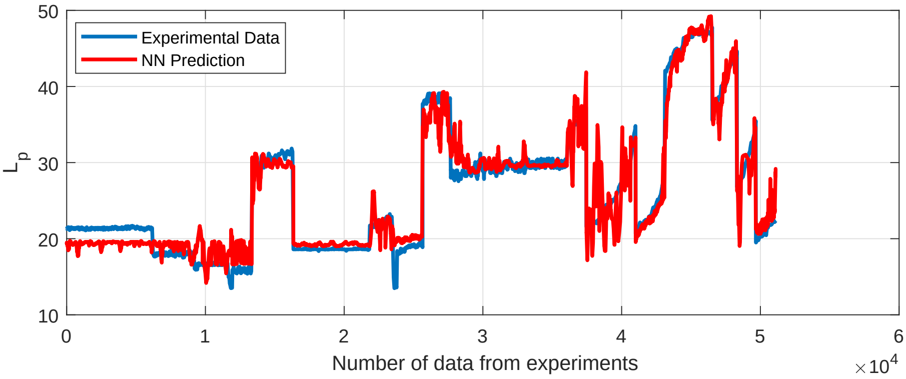

Figure 8.7: ANN prediction of L_p and trained L_p

8.4.2 Overall ANN training

It is known from grinding model equations mentioned in section 7.3.1 that forces are relative to S_s, F_R and D_c. Also, it is known from previous section that load percent is related to normal and tangential forces. Therefore, we can say that neural network between L_p, D_c, F_R and S_s is applicable.

Since there are three inputs and one output, the number of hidden layers of 3, 6 and 10 are checked, where 10 gives the least error. The block diagram that is generated in MATLAB neural network toolbox can be seen in figure 8.8.

The results of the block diagram, shown in figure 8.9, shows that the curve fitting works pretty well.

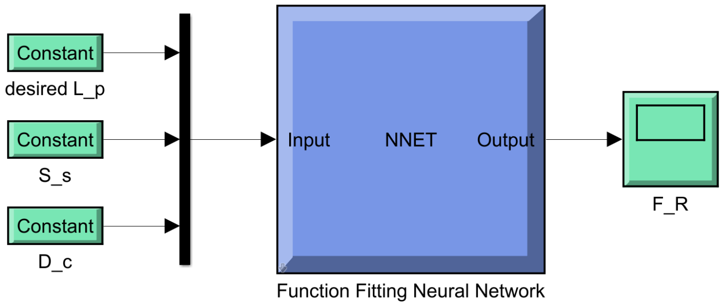
Constant
desired L_p
Constant
S_s
Constant
D_c
Input
NNET
Output
Function Fitting Neural Network
F_R

Figure 8.8: Block diagram of overall ANN for feed-rate selection

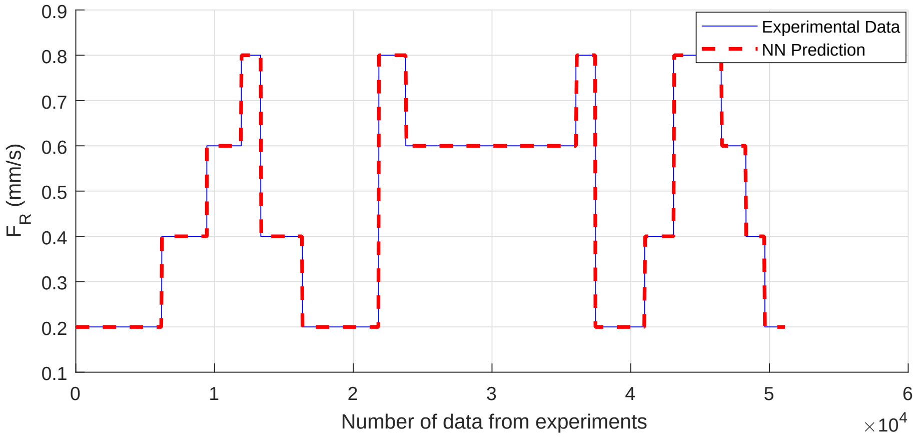

Figure 8.9: ANN prediction of F_R and trained F_R

By the help of this block diagram, we can change the F_R of parallel manipulator (hexapod) with respect to given D_c, S_s and L_p. As it is known from previous section, L_p is relative with normal and tangential forces. Therefore, By giving the desired L_p, we can avoid excessive loads on tool and spindle.

8.5 Dynamic Movement Primitives generation

As it is mentioned before, the generation of Dynamic movement Primitives needs the parameters of α, β, θ and ω for specific experiments. In order to have movements in two dimensions, experiments have been performed by using 6DOF haptic device.

8.5.1 Experiments related to DMP generation

In this section, the backward trajectory of the tool tip of 6DOF haptic device on the surface of the sinusoidal workpiece, shown in figure 8.11, is examined and the movements of experienced participants and deburring expert hand are recorded.

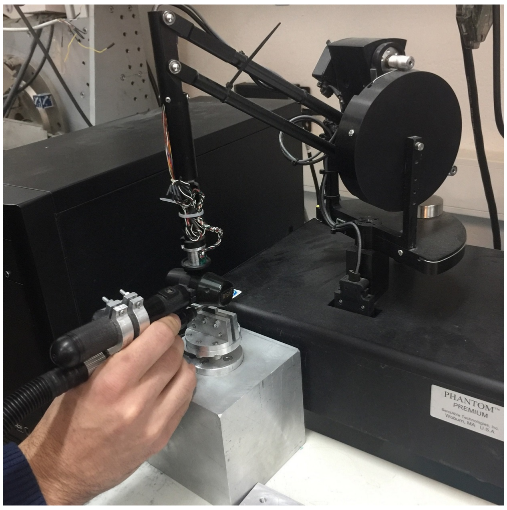

Figure 8.10: Participant holding spindle of 6-DOF haptic device

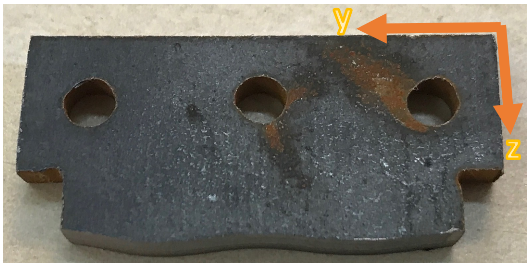

Figure 8.11: sinusoidal profile

It is asked from experienced participants and deburring expert to perform deburring on the workpiece. Movements of tool on the workpiece in Y-direction and Z-direction are recorded. The trajectory of a tool is fit to DMP model and the parameters of it are collected as DMP dataset. By utilizing this dataset, we can generate trajectory from desired start position to desired end position. Tool movements on the workpiece can be seen from figure 8.10.

The rhythmic backward movements of experienced participants in order to do the task of deburring pass are almost same in all participants, however, it is different for human expert. Experts perform this rhythmic backward movement in a very optimal way, that is, when tool comes to the surface of the workpiece or comes out, it moves tangentially to the surface of the workpiece which decreases the normal force. In order to be able to analyze these rhythmic movements, the segmentation of them is performed.

8.5.2 Elliptical fit from hand movements

It is understood from experiments that the expert and participants hand movements in deburring process are in an elliptical form, however, the characteristics of them are different. So, the least-square criterion for estimation of the best fit to an ellipse from tool movements is utilized. Conic representation of an ellipse is;

$$ay^2 + byz + cz^2 + dy + ez + f = 0 \tag{8.1}$$

The tilt factor b is used for rotation matrix to have a better fit. With the help of elliptic fit, we can reduce the number of points in movements. In each rhythmic experiments there are more than 100 points available for movement. However by utilizing the elliptic fit, we can make human movement smoother, shown in figure 8.12. Hexapod should not have unnecessary movements which can be eliminated.

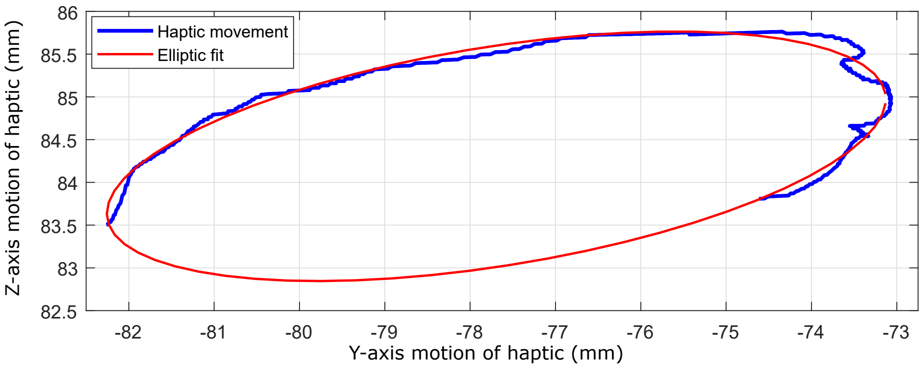

Figure 8.12: Example of elliptic fit of rhythmic movement of experienced participants

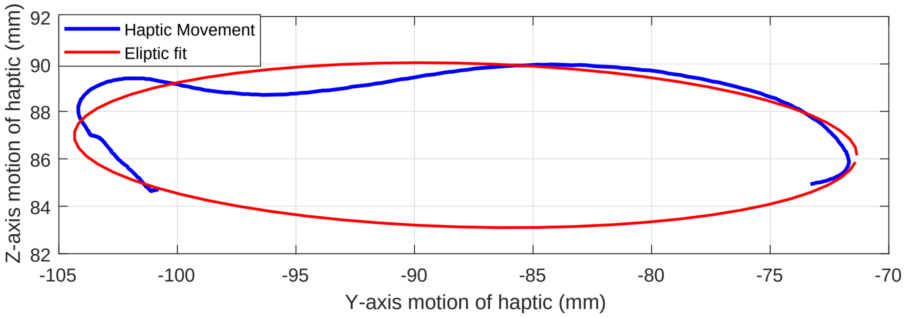

Figure 8.13: Example of elliptic fit of rhythmic movement of deburring expert

8.5.3 Extraction of DMP

Since robotic deburring is in micron-size resolution, the generated trajectory of DMP should have trajectory with an exact start and end point. Because of that, the maneuvers of a tool during experiment should be in a specific range. However, since DMP method is goal oriented and we can just change the start and goal positions, asking for specific trajectory is not applicable. As it can be seen in figure 8.14, rhythmic backward movement of a tool on the workpiece works pretty well, however, there is a possible collision between the tool and workpiece. In order to be able to prevent any collisions and control the range of the trajectory, the elliptic movement is segmented. The segmentation of elliptic fit is divided in approaching trajectory and curved trajectories, shown in figure 8.15 and 8.16. In experienced participant's hand movements, by utilizing approaching trajectory, tool moves until the end Y-position of the workpiece and then curved trajectory performs the arc movement to the goal position, shown in figure 8.15. However, in deburring expert movement, there is a curved trajectory for moving away from the workpiece, and then with approaching trajectory same task performs, then, by using the second curved trajectory, it moves to the goal position, shown in figure 8.16.

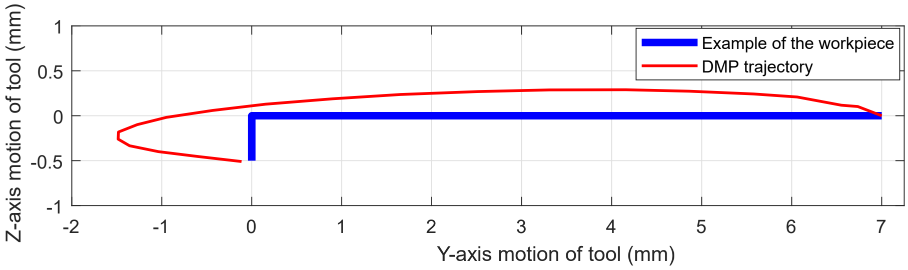

Figure 8.14: DMP with elliptical trajectory generation

Approaching and curved trajectories are different movements and generation of each of them needs specific DMP parameters and weights. Utilizing the segmentation, we can use differet DMPs for each trajectory. So, by the help of this, we can increase the number of possible solutions (by using 2 trajectory combinations for experienced participant and 3 for deburring expert). In addition, we can have movements in the range of Y and Z-directions that we desire.

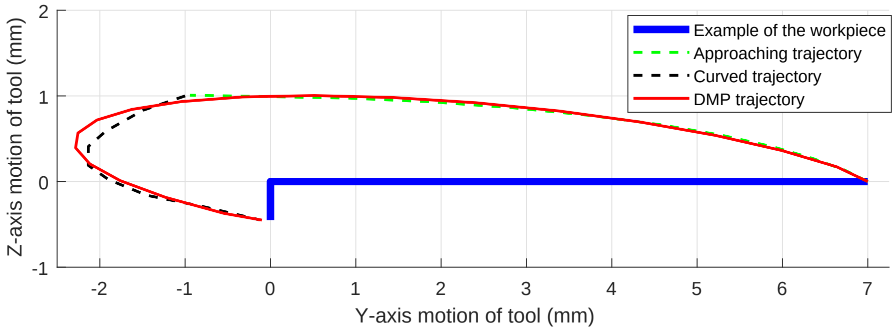

Figure 8.15: Generating trajectory of experienced participant

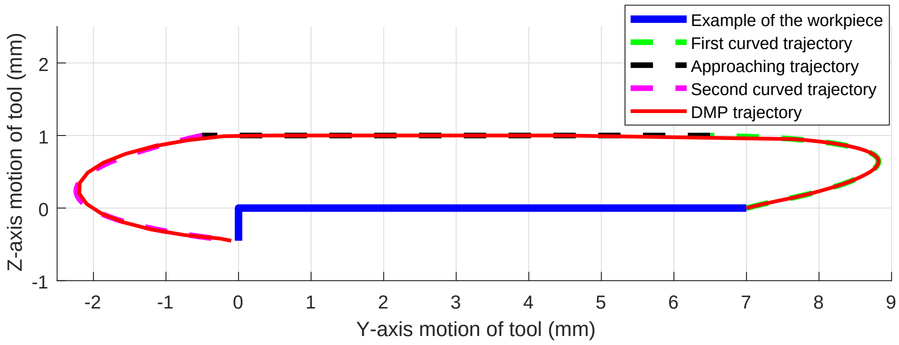

Figure 8.16: Generating trajectory of deburring expert

Note that, only parameters, weights, and length between the start and end point of experiments are collected in DMP dataset. When asking for trajectory from desired start position to desired end position, we cannot generate a trajectory by using the data of position taken from experiments which decelerates the process. Each trajectory recorded from the experiments have a vector from start to end points. The length of vectors are analyzed and the vector which has the closest length with desired start and end point is the best case for a generation. In addition, if the generated trajectory is outside the desired range in two dimensions, the next vector (next dataset taken from experiments) will be utilized.

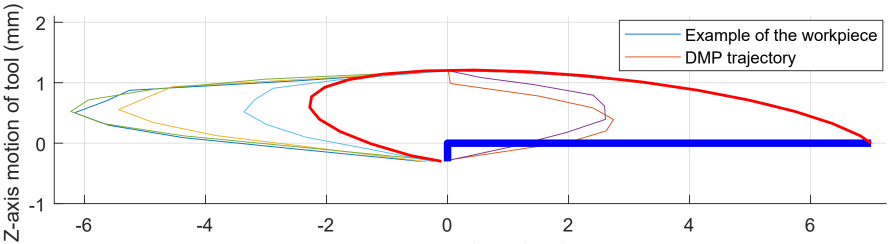

Figure 8.17: Example training to choose DMP in the desired range for experienced participants

Figure 8.17 shows that the generated trajectories are considered with respect to the range of the movement. Range of movement is very important because of avoiding collision, unnecessary movements and help to reduce the duration of deburring/grinding process.

8.6 Conclusion

Since our deburring robot is sensitive and works in micron-size resolution, there should be some basic experiments and analyses performed in order to not harm our setup. Normal and tangential forces, D_c, F_R, S_s are important factors, thus, selection of them should be done before. Also, the tool deflection changes the profile of the workpiece which should be avoided in order to not harm the setup and reduce the form error. In addition, excessive and extra movements increase the duration of experiments and probability of collision which should be avoided by selecting the true trajectories by using DMP generator.

CHAPTER 9

EXPERIMENTAL PROCEDURE

The aim of this thesis is to reach the flat profile with a constant depth of cut of the unknown workpiece by using the automatic deburring/grinding process. In order to obtain this, we first have to specify the desired length of the workpiece in Z-direction after deburring process. For obtaining the smooth surface, we need to know the desired start and end point of the workpiece in Y and Z-directions. In order to do that, the tool touches the workpiece in the start point P_{start} and the desired end point P_{end}, shown in figure 9.1.

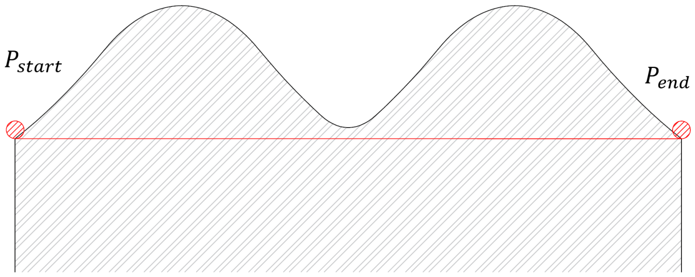

Figure 9.1: The Y-direction movement of the tool on the workpiece

As we know P_{start} and P_{end}, we can create the straight line with respect to them. This path can be 2-dimensional because of the possible calibration error, so we can learn the slope of the motion. However, in this work, we assume that the calibration error is zero.

For deburring/grinding process, we ask the robot to move toward the end point with specific depth of cut D_c, feed-rate F_R and tool rotation velocity S_s. During the motion, when force increases, we find out that during the motion there are some obstacles on the way. These obstacles can be burrs or the profile of the workpiece. Therefore, the value of the force generated during the deburring/grinding process is very important in order to cut unknown profile and not harm the setup.

9.1 Ramp step search

The motion of the tool is through $+Y$ direction. Figure 9.2 shows that if we want to learn the profile of the workpiece, we need to have ramp step search. In this search, when tool comes to workpiece which creates excessive force, it moves one step backward and one step upward, and then moves again through $P_{y_{end}}$.

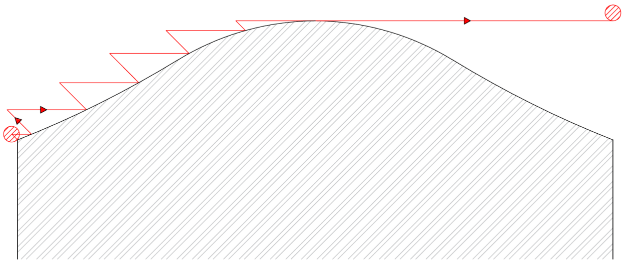

Figure 9.2: Ramp step search in order to find profile shape

The reason why the ramp step search is used is to be able to recognize the profile of the workpiece and prevent any collisions during motion. In some profiles, there can be a wall-shaped obstacles come to the tool. In figure 9.3 we can see that ramp step helps to skip the wall-shaped obstacles.

The $150\mu m$ ramp step movement has been chosen for this study because it is the minimum D_c that is given in the experiments.

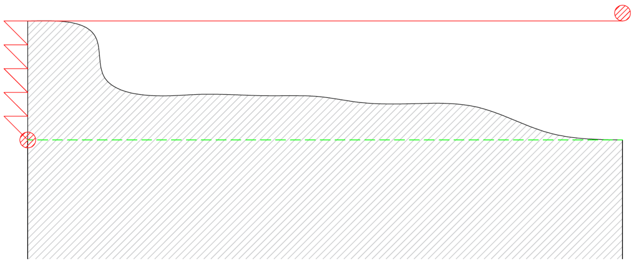

Figure 9.3: wall shaped workpiece

9.2 Generation of DMP

As the tool finds the peak of the unwanted part of the workpiece, by using step ramp search, it will have backward and downward motions (DMP trajectory) and then grinding occurs again and again until it reaches desired P_{end}, shown in figure 9.4.

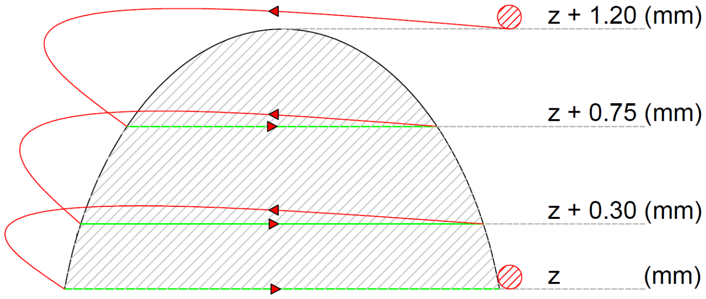

Figure 9.4: DMP generation of the tool with respect to the desired depth of cut

However, it is known that the backward motion to the new position should be considered in this part. tool starts the trajectory from the peak of the unwanted part and moves downward to go back to the desired Z position. Therefore, in this part, the movement primitives of the human expert are transferred to the robot in order to have backward rhythmic motions. These movement primitives can change with respect to different start and goal positions.

Since the length of the peak of the workpiece in Z-direction changes in different profiles, the layer selection of deburring/grinding process which is explained in section 9.4, should be considered.

9.3 Touching motion

In the experiments, generated trajectory does not exactly finish in the Y desired position which is taken from ramp step process. It is chosen to finish $100\mu m$ far from the desired position in order to prevent collision. Then tool moves exactly parallel to the desired $P_{y_{end}}$ chosen in section 9.1. When tool touches the workpiece and force become more than 0 N, we understand that it touches the workpiece. By performing this motion we can prevent collision.

9.4 Grinding on the layers

The experiments that have been performed in this study are for depth of cuts of $150\mu m$, $300\mu m$ and $450\mu m$. The length of the peak of the workpiece in Z-direction is different for different profiles. So, the selection of layers from peak starts from $450\mu m$ and if this value is larger than the value of the peak length, it will choose $300\mu m$ and $150\mu m$ respectively. Figure 9.5 shows the examples of the layer selection for peak length of $z + 1.20$ (mm).

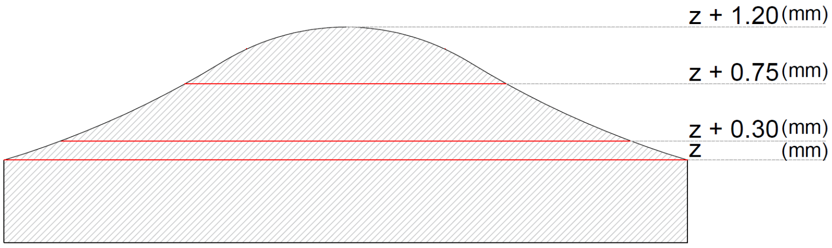

Figure 9.5: Layer selection

In figure 9.5, we can figure out that, for reaching the peak point of $z + 1.20$ μm, step ramp search will perform 8 steps. However, by utilizing the layer selection method, instead of choosing 8 layers of 150 μm D_c, we will have two grinding process with 450 μm D_c and one 300 μm D_c . By using layer selection, we will have less grinding process and less duration of process, respectively.

9.5 F_R selection by using ANN

Since we know the position of tool after being generated the trajectory, we can deduce the D_c of the process. Neural network which trained before, can be helpful to choose F_R of the process with respect to D_c and desired S_s and L_p.

9.6 Overall experimental procedure

The experimental procedure which is chosen helps the setup to have automatic robotic deburring/grinding process without knowing the profile of the workpiece. Utilizing this, we can reduce the tool deflection by eliminating the collision and not passing the excessive force of specific task. The flow chart of the overall experiment is given in figure 9.6.

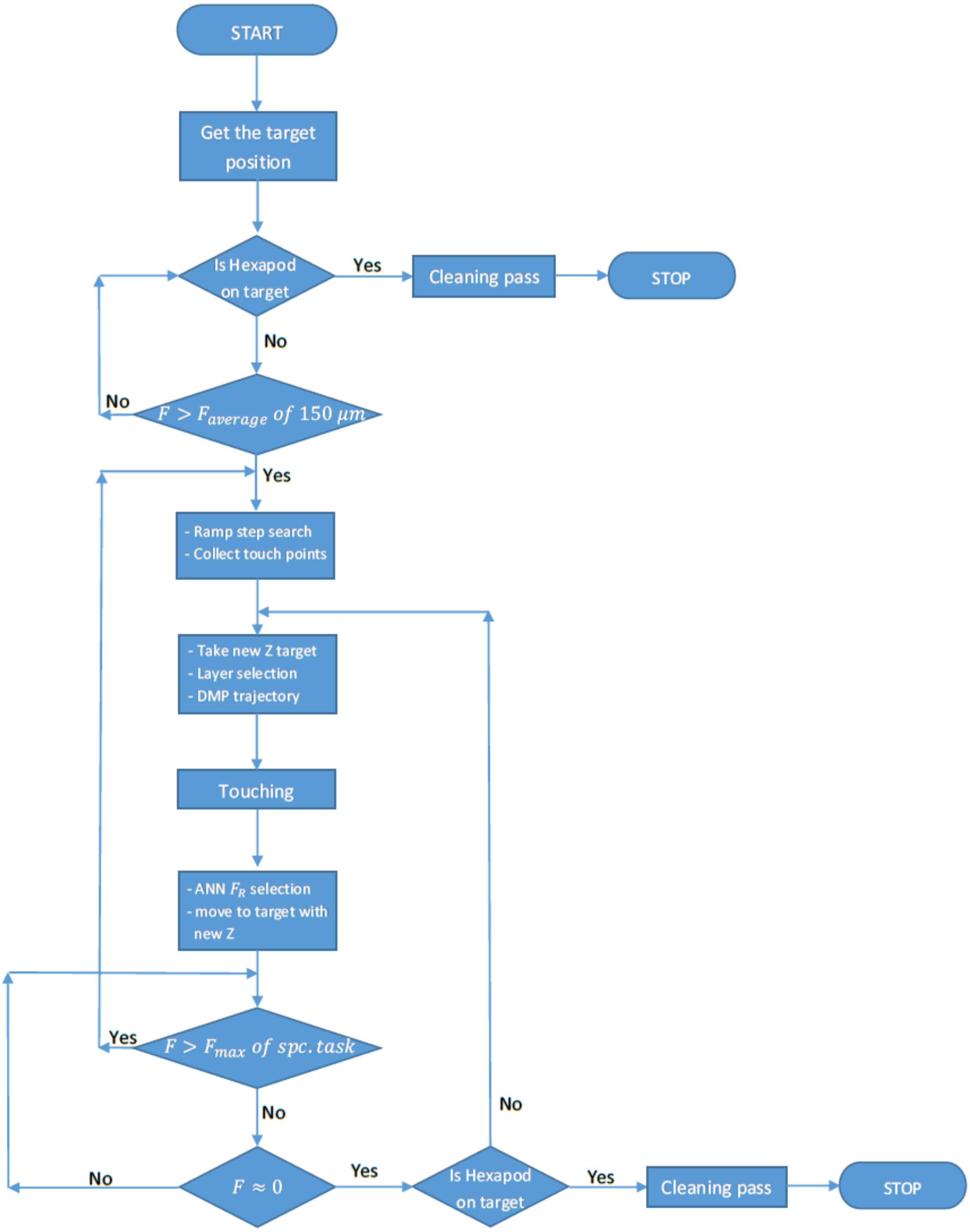
START
Get the target position
Is Hexapod on target
Yes
Cleaning pass
STOP
No
No
$F > F_{average}$ of 150 μm
Yes
- Ramp step search
- Collect touch points
- Take new Z target
- Layer selection
- DMP trajectory
Touching
- ANN F_R selection
- move to target with new Z
Yes
$F > F_{max}$ of spc. task
No
No
No
$F \approx 0$
Yes
Is Hexapod on target
Yes
Cleaning pass
STOP

Figure 9.6: overall flowchart of the experiments

CHAPTER 10

RESULTS AND DISCUSSION

In this chapter, the duration of experiments on automatic robotic deburring/ grinding process will be analyzed and compared with an alternative process. In addition, the surface of the workpiece will be scanned before and after the automatic grinding/deburring process and form error on wokpieces will be analyzed. Note that, the results of experiments of tool deflection, collision, Neural network of F_R selection and DMP generation have been explained before in chapter 8.

10.1 Duration of process

Duration of the automatic robotic deburring/grinding process is very important because during the process, thermal effects increase. When a tool gets warmer causes the spindle and F/T sensor get warmer. This can damage the calibration of setup permanently. Also, when the duration of the process gets faster, it will be more valuable. In mass production, saving time means more production. There is an alternative deburring/grinding process other than our process which will be analyzed. By comparing with the alternative approach, we want to prove the success of our process.

10.1.1 Process with zigzag movement

This process is completely different from our process. In this process, we can ask our robot to have kind of zigzag movements, shown in figure 10.1. Note that, in this process, we still need ramp step search in order to find the peak of the workpiece in Z-direction.

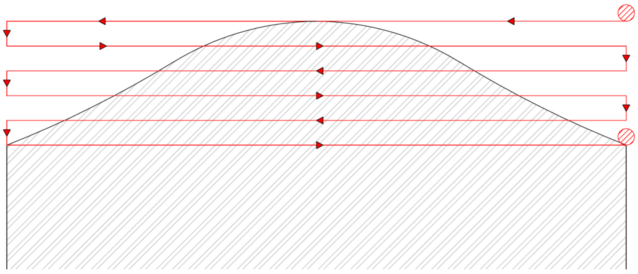

Figure 10.1: Example of zigzag movement

Process with zigzag movement eliminates the backward movement which decreases the duration of the process substantially. However, as we want to have deburring/grinding process on unknown profile of workpiece, this process has different performance with respect to different profiles. To illustrate, figure 10.3 shows that this process is very useful and the duration of the process is low in comparison with our process.

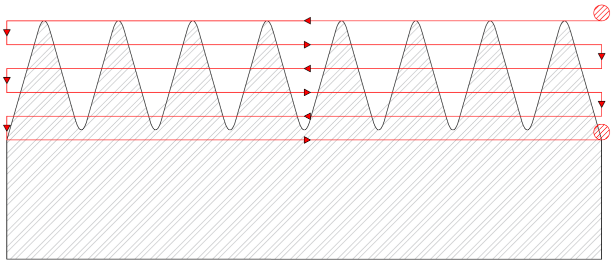

Figure 10.2: Significant zigzag motion on workpiece

However, for profiles which have shapes same as shown in figure 10.4, process of zigzag is not suitable because of loosing time in paths with no deburring/grinding passes and it is better to use DMP trajectory as shown in figure 10.5.

Not that, while doing the process same as profile of figures 10.3 and 10.4, we may come across with the following issues;

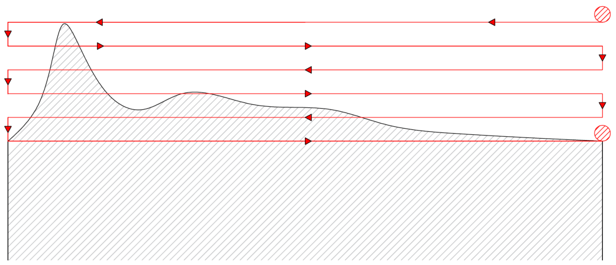

Figure 10.3: Nonsense zigzag motion on workpiece

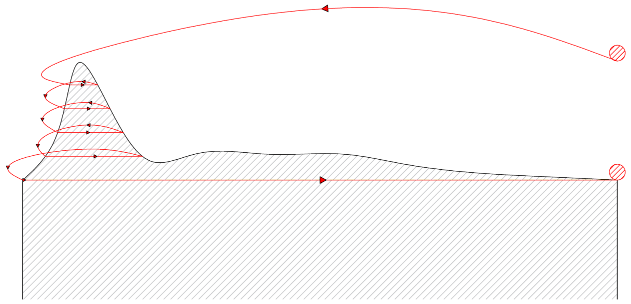

Figure 10.4: DMP trajectory on the workpiece

- Not considering the collision which creates a tool deflection during deburring/grinding process.
- Unnecessary maneuvers can happen based on the profile of the workpiece.

Therefore, it can be said that, although process with DMP trajectory generation may sometimes have longer duration process, it can prevent items mentioned above. Also, DMP trajectory generation is applicable for all unknown workpiece profiles.

10.2 Form error of workpiece

In this section, the form error on the workpiece is analyzed with laser scanner after deburring/grinding process. In automatic deburring/grinding process, the last layer of the motion of tool may be one of $150, 300$ and 450 μm depth of cuts.

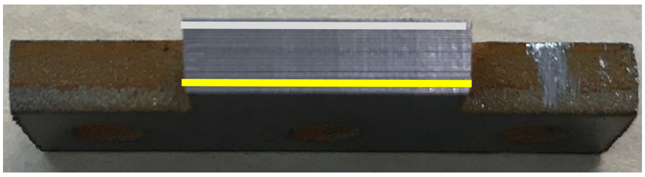

Figure 10.5: profile scanning in two different paths

10.2.1 Experiment with last layer D_c of 150 μm

In this part, experiment of deburring/grinding process on random shape workpiece is performed. In this experiment, the last layer was 150 μm. The surface of the profile is scanned before automatic robotic deburring/grinding process in 30 sections in Y-direction and two different X-directions. After that, the surface is scanned after the process. Figure 10.6 shows the shape of the workpiece before and after the process. Data of this experiment is available in figure B.1.

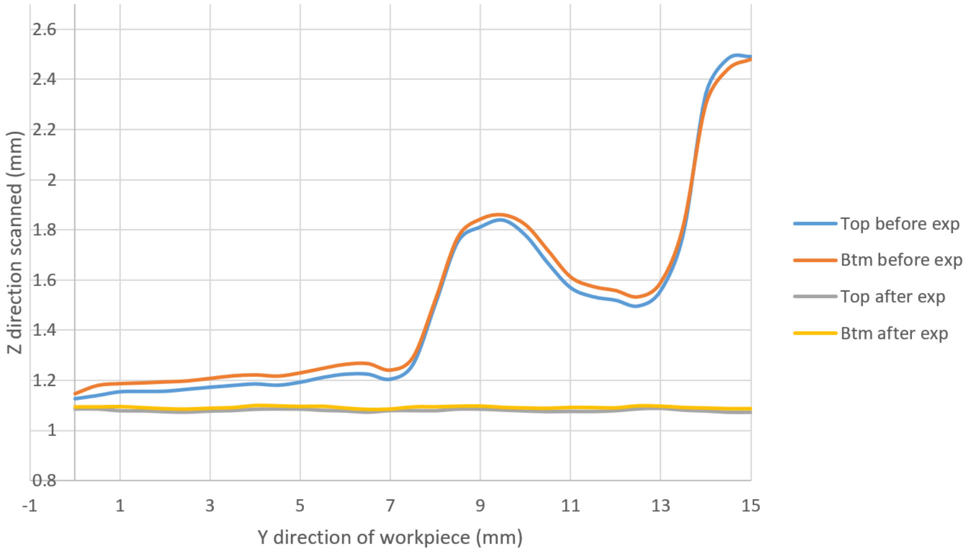

Figure 10.6: Workpiece before and after experiment with last layer of 150 μm

Data of figure B.1 shows that the maximum form error on the workpiece is 16 μm. The mean form error is 11.7 μm with the variance of 5.91 μm^2.

10.2.2 Experiment with last layer D_c of 300 μm

In this part, another experiment of deburring/grinding process on random shape workpiece is performed. In this experiment, the last layer was 300 μm. Figure 10.8 shows the shape of the workpiece before and after process. Data of this experiment is available in figure B.2.

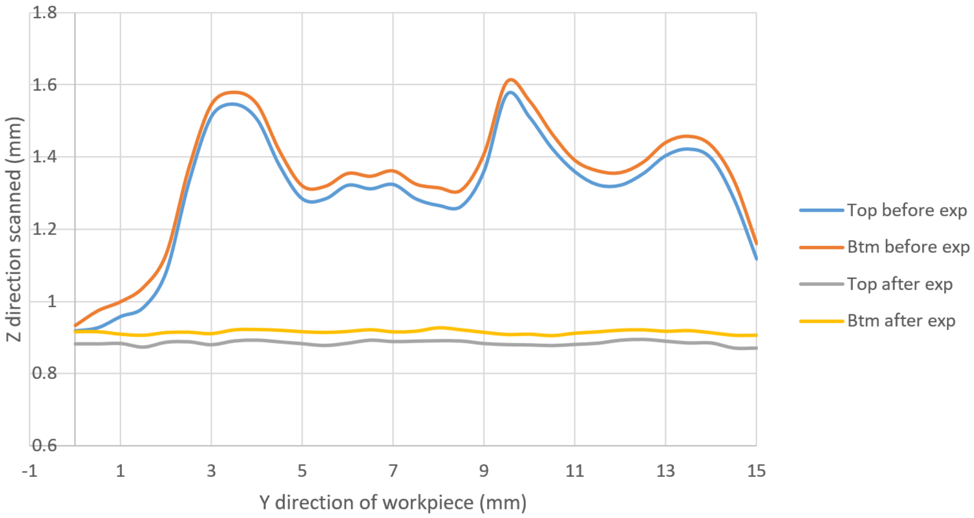

Figure 10.7: Workpiece before and after experiment with last layer of 300 μm

By analyzing figure B.2, we can conclude that the maximum form error on the workpiece after grinding process is 35 μm. Also, the mean form error is 29 μm with the variance of 9.54 μm^2.

10.2.3 Experiment with last layer D_c of 450 μm

Another experiment of deburring/grinding process on random shape workpiece is performed. In this experiment, the last layer was 450 μm. Figure 10.9 shows the shape of the workpiece before and after process. Data of this experiment is available in figure B.3.

Using figure B.3 which is taken by scanning the surface of the workpiece after grinding process, the maximum form error became 39 μm, also, the mean value

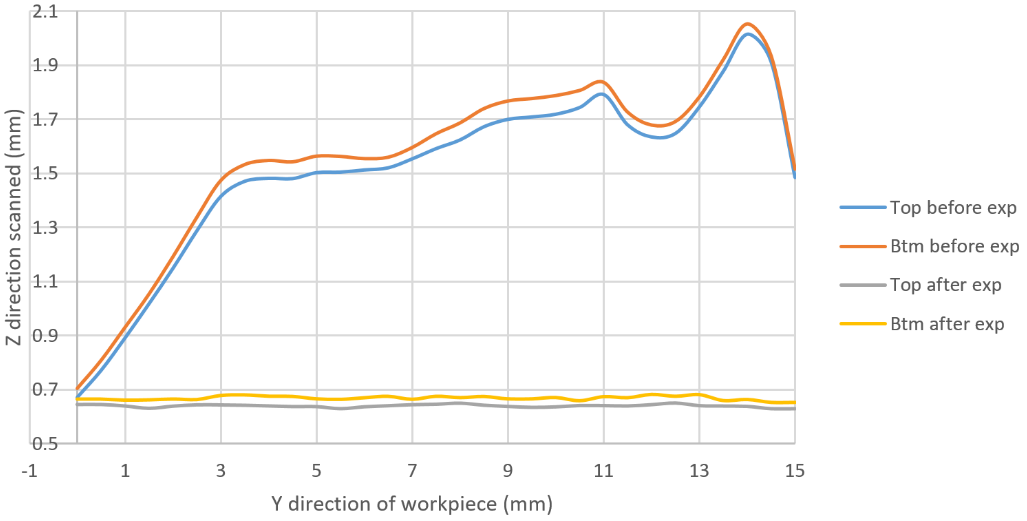

Figure 10.8: Workpiece before and after experiment with last layer of 450 μm

of 27.9 μm with the variance of 45.26 μm^2.

CHAPTER 11

CONCLUSION AND FUTURE WORK

11.1 Conclusion

In this study, automatic robotic deburring/grinding process is performed on unknown shape workpieces by utilizing the movement primitives of human skill model. It is observed that backward rhythmic movements of a human expert can be fitted to a conic representation of ellipse by using least-square criterian. This ellipse shape human movements are extracted by using Dynamic Movement Primitives (DMP), and then by using particle swarm optimization, parameters and weights are collected. By utilizing dataset of parameters and weights and giving desired start and end positions, we can generate trajectory of backward rhythmic movement.

However, for automatic robotic deburring/grinding process, besides DMP, there are some issues that are considered such as tool deflection, layer selection, ramp step search, collision and feed-rate selection.

It is shown from experiments that tool deflection increases form error on the profile of the workpiece, which by using cleaning pass, it can be reduced to minimum 39%. Also, a collision between the workpiece and tool increases interaction forces which increases the tool deflection. So, in experiments, collisions are eliminated. In addition, By using MATLAB artificial neural network toolbox, the relation between forces and load percent, and depth of cut, spindle speed and feed-rate are obtained. Furthermore, the layer selection and ramp step search helped experiments to eliminate excessive forces.

Finally, we mentioned an alternative process that can be replaced with our process. It is proven that zigzag movement is not suitable for our tasks because of the possibility of collision and unnecessary maneuvers. In addition, the surface of the workpieces is scanned before and after automatic deburring/grinding process. It can be seen that we can obtain flat surfaces with a surface form error of maximum 39 μm and mean value of 27.9 μm with the variance of 45.26 μm^2.

Note that, we have presented two fundamental studies related to this study. In deburring/grinding process, there is an interaction force between tool and a workpiece. Thereby, in general concentrated DMP model, we modified DMP model in order to have model of movement primitives of human expert and his/her forces. However, since there is a correspondence problem between the links and joints of human expert and our robot, we solved this problem by performing teleoperation between 1DOF haptic device and the robot. DMP which is dependent to position and its derivatives modified to DMP of force trajectory since we required to move through desired force. By utilizing this local DMP, we can generate human-like controller in order to have reaction to force changes.

11.2 Future work

In this study, DMP is used for backward rhythmic movements to place the tool in a suitable position to have deburring passes. In the future, beside backward movement, grinding/deburring process of human expert will be transferred to our setup. In this process, a nonlinear learn-able differential equation of DMP method have force feedback which generates the trajectory of motion with respect to interaction normal and tangential forces. Right now, ANN is used in this study, but above-mentioned DMP can be replaced with it. The fundamental study related to modification of DMP have been explained in detail in chapters 5 and 6.

REFERENCES

[1] L. K. Gillespie, *Deburring and edge finishing handbook.* Society of Manufacturing Engineers, 1999.

[2] H. Kazerooni, J. Bausch, and B. Kramer, "An approach to automated deburring by robot manipulators," *Journal of dynamic systems, measurement, and control*, vol. 108, no. 4, pp. 354–359, 1986.

[3] R. W. Paine and J. Tani, "Motor primitive and sequence self-organization in a hierarchical recurrent neural network," *Neural Networks*, vol. 17, no. 8, pp. 1291–1309, 2004.

[4] X. Shusong and H. Jiefeng, "Biologically inspired robot behavior design," in *Industrial Informatics, 2008. INDIN 2008. 6th IEEE International Conference on.* IEEE, 2008, pp. 63–67.

[5] M. Latifinavid and E. ilhan Konukseven, "Hybrid model based on energy and experimental methods for parallel hexapod-robotic light abrasive grinding operations," *The International Journal of Advanced Manufacturing Technology*, vol. 93, no. 9-12, pp. 3873–3887, 2017.

[6] A. J. Ijspeert, J. Nakanishi, and S. Schaal, "Learning attractor landscapes for learning motor primitives," in *Advances in neural information processing systems*, 2003, pp. 1547–1554.

[7] S. Schaal, "Dynamic movement primitives-a framework for motor control in humans and humanoid robotics," in *Adaptive motion of animals and machines.* Springer, 2006, pp. 261–280.

[8] N. Hogan and S. P. Buerger, "Impedance and interaction control, robotics and automation handbook," 2005.

[9] N. Hogan and D. Sternad, “Dynamic primitives of motor behavior,” *Biological cybernetics*, pp. 1–13, 2012.

[10] J. Kober, M. Gienger, and J. J. Steil, “Learning movement primitives for force interaction tasks,” in *Robotics and Automation (ICRA), 2015 IEEE International Conference on.* IEEE, 2015, pp. 3192–3199.

[11] S. Liu and H. Asada, “Adaptive control of deburring robots based on human skill models,” in *Decision and Control, 1991., Proceedings of the 30th IEEE Conference on.* IEEE, 1991, pp. 348–353.

[12] P. Pastor, H. Hoffmann, T. Asfour, and S. Schaal, “Learning and generalization of motor skills by learning from demonstration,” in *Robotics and Automation, 2009. ICRA’09. IEEE International Conference on.* IEEE, 2009, pp. 763–768.

[13] H. Hoffmann, P. Pastor, D.-H. Park, and S. Schaal, “Biologically-inspired dynamical systems for movement generation: automatic real-time goal adaptation and obstacle avoidance,” in *Robotics and Automation, 2009. ICRA’09. IEEE International Conference on.* IEEE, 2009, pp. 2587–2592.

[14] B. E. Perk and J.-J. E. Slotine, “Motion primitives for robotic flight control,” *arXiv preprint cs/0609140*, 2006.

[15] A. Paraschos, C. Daniel, J. R. Peters, and G. Neumann, “Probabilistic movement primitives,” in *Advances in neural information processing systems*, 2013, pp. 2616–2624.

[16] A. D. Dragan, K. Muelling, J. A. Bagnell, and S. S. Srinivasa, “Movement primitives via optimization,” in *Robotics and Automation (ICRA), 2015 IEEE International Conference on.* IEEE, 2015, pp. 2339–2346.

[17] A. Colomé, G. Neumann, J. Peters, and C. Torras, “Dimensionality reduction for probabilistic movement primitives,” in *Humanoid Robots (Humanoids), 2014 14th IEEE-RAS International Conference on.* IEEE, 2014, pp. 794–800.

[18] T. Matsubara, S.-H. Hyon, and J. Morimoto, "Learning parametric dynamic movement primitives from multiple demonstrations," *Neural networks*, vol. 24, no. 5, pp. 493–500, 2011.

[19] M. Kallmann, R. Bargmann, and M. Mataric, "Planning the sequencing of movement primitives," in *proceedings of the international conference on simulation of adaptive behavior (SAB)*, 2004, pp. 193–200.

[20] P. Parvizi, M. C. Ugurlu, K. Acikgoz, and E. I. Konukseven, "Parametrization of robotic deburring process with motor skills from motion primitives of human skill model," in *Methods and Models in Automation and Robotics (MMAR), 2017 22nd International Conference on.* IEEE, 2017, pp. 373–378.

[21] M. Ewerton, G. Neumann, R. Lioutikov, H. B. Amor, J. Peters, and G. Maeda, "Learning multiple collaborative tasks with a mixture of interaction primitives," in *Robotics and Automation (ICRA), 2015 IEEE International Conference on.* IEEE, 2015, pp. 1535–1542.

[22] S. Niekum, S. Osentoski, G. Konidaris, and A. G. Barto, "Learning and generalization of complex tasks from unstructured demonstrations," in *Intelligent Robots and Systems (IROS), 2012 IEEE/RSJ International Conference on.* IEEE, 2012, pp. 5239–5246.

[23] N. Figueroa, A. L. Pais Ureche, and A. Billard, "Learning complex sequential tasks from demonstration: A pizza dough rolling case study," in *The Eleventh ACM/IEEE International Conference on Human Robot Interaction.* IEEE Press, 2016, pp. 611–612.

[24] K. Acikgoz, "Prediction of the cutting forces for robotic grinding processes with abrasive mounted bits." Master's thesis, Middle East Technical University, 2015.

[25] A. Pervez, A. Ali, J.-H. Ryu, and D. Lee, "Novel learning from demonstration approach for repetitive teleoperation tasks," in *World Haptics Conference (WHC), 2017 IEEE.* IEEE, 2017, pp. 60–65.

[26] A. J. Ijspeert, J. Nakanishi, H. Hoffmann, P. Pastor, and S. Schaal, "Dynamical movement primitives: learning attractor models for motor behaviors," *Neural computation*, vol. 25, no. 2, pp. 328–373, 2013.

[27] R. Eberhart and J. Kennedy, "A new optimizer using particle swarm theory," in *Micro Machine and Human Science, 1995. MHS'95., Proceedings of the Sixth International Symposium on.* IEEE, 1995, pp. 39–43.

[28] R. Poli, J. Kennedy, and T. Blackwell, "Particle swarm optimization," *Swarm intelligence*, vol. 1, no. 1, pp. 33–57, 2007.

[29] H. Huang, A. Hoorfar, and S. Lakhani, "A comparative study of evolutionary programming, genetic algorithms and particle swarm optimization in antenna design," in *Antennas and Propagation Society International Symposium, 2007 IEEE.* IEEE, 2007, pp. 1609–1612.

[30] M. Clerc and J. Kennedy, "The particle swarm-explosion, stability, and convergence in a multidimensional complex space," *IEEE transactions on Evolutionary Computation*, vol. 6, no. 1, pp. 58–73, 2002.

[31] M. H. Raibert and J. J. Craig, "Hybrid position/force control of manipulators," *Journal of Dynamic Systems, Measurement, and Control*, vol. 102, no. 127, pp. 126–133, 1981.

[32] G. Ziliani, A. Visioli, and G. Legnani, "A mechatronic approach for robotic deburring," *Mechatronics*, vol. 17, no. 8, pp. 431–441, 2007.

[33] A. Donder, "Active compliance control structure design for a robotic-grinding machine," Master's thesis, Middle East Technical University, 2017.

[34] C.-T. Kim and J.-J. Lee, "Training two-layered feedforward networks with variable projection method," *IEEE Transactions on Neural Networks*, vol. 19, no. 2, pp. 371–375, 2008.

[35] K. G. Sheela and S. N. Deepa, "Review on methods to fix number of hidden neurons in neural networks," *Mathematical Problems in Engineering*, vol. 2013, 2013.

APPENDIX A

MATLAB SIMULINK MODEL

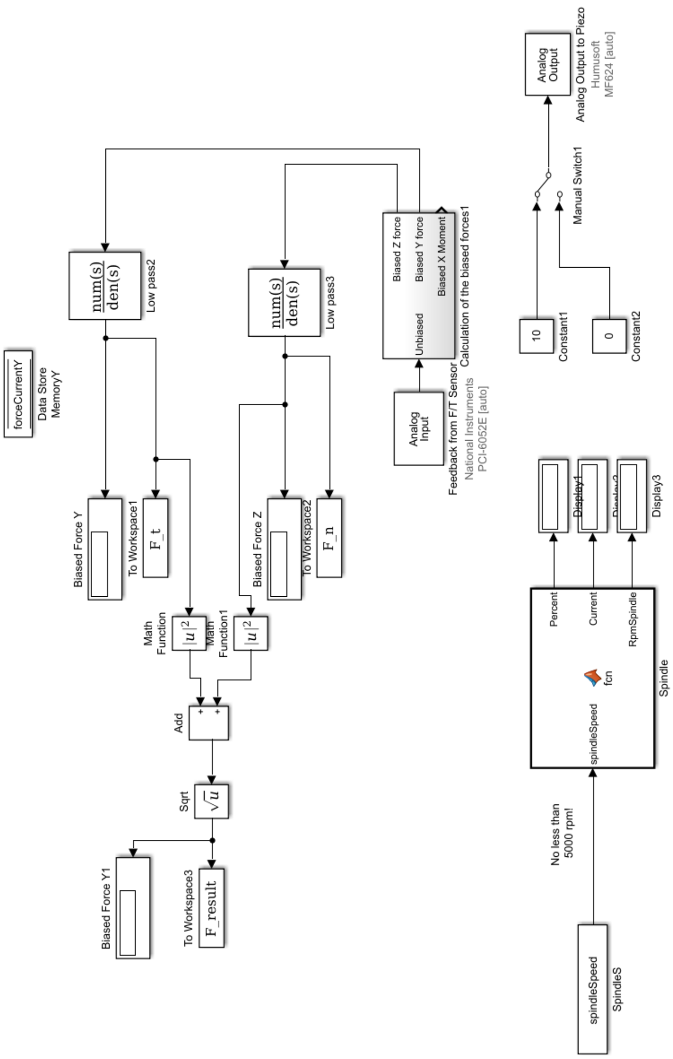
forceCurrentY
Data Store MemoryY
num(s)/den(s)
Low pass2
num(s)/den(s)
Low pass3
Biased Z force
Biased Y force
Biased X Moment
Unbiased
Calculation of the biased forces1
Analog Input
Feedback from F/T Sensor
National Instruments
PCI-6052E [auto]
Analog Output
Analog Output to Piezo
Humusoft
MF624 [auto]
Manual Switch1
10
Constant1
0
Constant2
Biased Force Y
To Workspace1
F_t
Biased Force Z
To Workspace2
F_n
Math Function
Math Function1
$|u|^2$
$|u|^2$
Add
Sqrt
$\sqrt{u}$
Biased Force Y1
To Workspace3
F_result
Display1
Display2
Display3
Percent
Current
RpmSpindle
spindleSpeed
fcn
Spindle
No less than 5000 rpm!
spindleSpeed
SpindleS

Figure A.1: Matlab Simulink of F/T sensor, Piezoelectric actuator and spindle speed (Work simultaneously)

APPENDIX B

DATA OF EXPERIMENTS

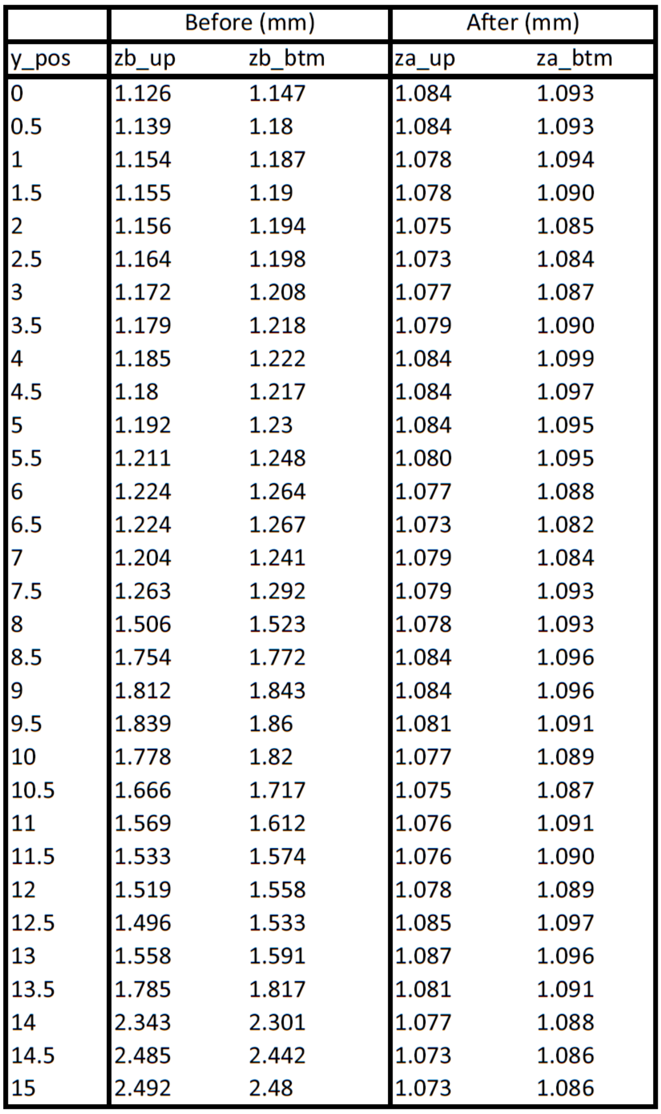

	Before (mm)		After (mm)	
y_pos	zb_up	zb_btm	za_up	za_btm
0	1.126	1.147	1.084	1.093
0.5	1.139	1.18	1.084	1.093
1	1.154	1.187	1.078	1.094
1.5	1.155	1.19	1.078	1.090
2	1.156	1.194	1.075	1.085
2.5	1.164	1.198	1.073	1.084
3	1.172	1.208	1.077	1.087
3.5	1.179	1.218	1.079	1.090
4	1.185	1.222	1.084	1.099
4.5	1.18	1.217	1.084	1.097
5	1.192	1.23	1.084	1.095
5.5	1.211	1.248	1.080	1.095
6	1.224	1.264	1.077	1.088
6.5	1.224	1.267	1.073	1.082
7	1.204	1.241	1.079	1.084
7.5	1.263	1.292	1.079	1.093
8	1.506	1.523	1.078	1.093
8.5	1.754	1.772	1.084	1.096
9	1.812	1.843	1.084	1.096
9.5	1.839	1.86	1.081	1.091
10	1.778	1.82	1.077	1.089
10.5	1.666	1.717	1.075	1.087
11	1.569	1.612	1.076	1.091
11.5	1.533	1.574	1.076	1.090
12	1.519	1.558	1.078	1.089
12.5	1.496	1.533	1.085	1.097
13	1.558	1.591	1.087	1.096
13.5	1.785	1.817	1.081	1.091
14	2.343	2.301	1.077	1.088
14.5	2.485	2.442	1.073	1.086
15	2.492	2.48	1.073	1.086

Figure B.1: Scanned surface of experiment of figure 10.7

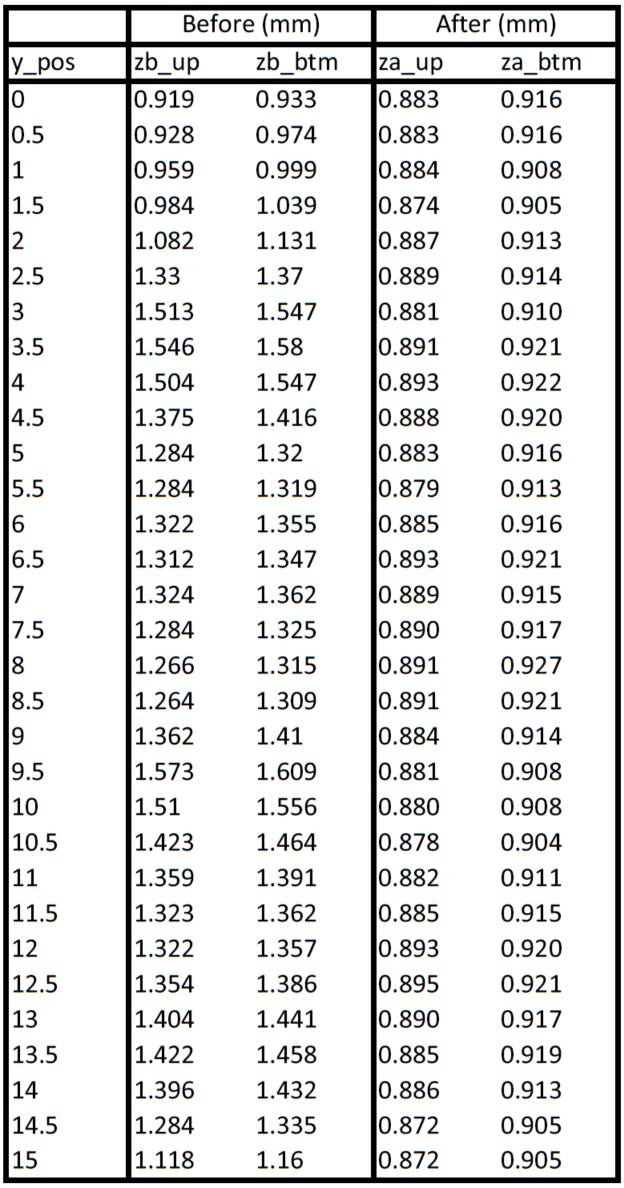

	Before (mm)		After (mm)	
y_pos	zb_up	zb_btm	za_up	za_btm
0	0.919	0.933	0.883	0.916
0.5	0.928	0.974	0.883	0.916
1	0.959	0.999	0.884	0.908
1.5	0.984	1.039	0.874	0.905
2	1.082	1.131	0.887	0.913
2.5	1.33	1.37	0.889	0.914
3	1.513	1.547	0.881	0.910
3.5	1.546	1.58	0.891	0.921
4	1.504	1.547	0.893	0.922
4.5	1.375	1.416	0.888	0.920
5	1.284	1.32	0.883	0.916
5.5	1.284	1.319	0.879	0.913
6	1.322	1.355	0.885	0.916
6.5	1.312	1.347	0.893	0.921
7	1.324	1.362	0.889	0.915
7.5	1.284	1.325	0.890	0.917
8	1.266	1.315	0.891	0.927
8.5	1.264	1.309	0.891	0.921
9	1.362	1.41	0.884	0.914
9.5	1.573	1.609	0.881	0.908
10	1.51	1.556	0.880	0.908
10.5	1.423	1.464	0.878	0.904
11	1.359	1.391	0.882	0.911
11.5	1.323	1.362	0.885	0.915
12	1.322	1.357	0.893	0.920
12.5	1.354	1.386	0.895	0.921
13	1.404	1.441	0.890	0.917
13.5	1.422	1.458	0.885	0.919
14	1.396	1.432	0.886	0.913
14.5	1.284	1.335	0.872	0.905
15	1.118	1.16	0.872	0.905

Figure B.2: Scanned surface of experiment of figure 10.8

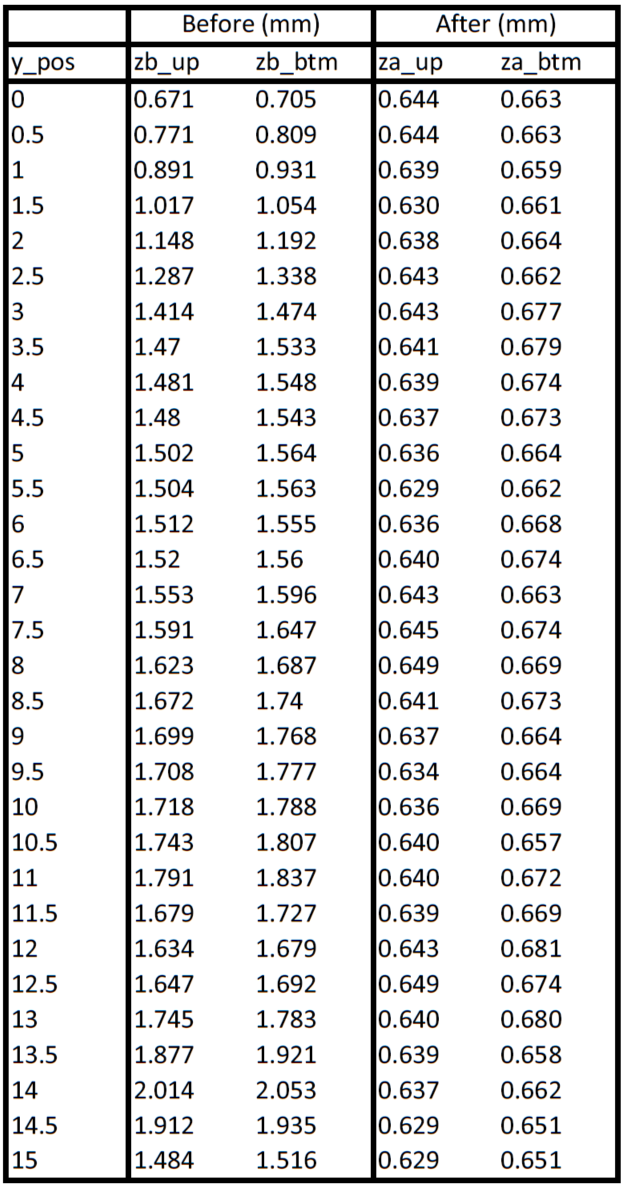

	Before (mm)		After (mm)	
y_pos	zb_up	zb_btm	za_up	za_btm
0	0.671	0.705	0.644	0.663
0.5	0.771	0.809	0.644	0.663
1	0.891	0.931	0.639	0.659
1.5	1.017	1.054	0.630	0.661
2	1.148	1.192	0.638	0.664
2.5	1.287	1.338	0.643	0.662
3	1.414	1.474	0.643	0.677
3.5	1.47	1.533	0.641	0.679
4	1.481	1.548	0.639	0.674
4.5	1.48	1.543	0.637	0.673
5	1.502	1.564	0.636	0.664
5.5	1.504	1.563	0.629	0.662
6	1.512	1.555	0.636	0.668
6.5	1.52	1.56	0.640	0.674
7	1.553	1.596	0.643	0.663
7.5	1.591	1.647	0.645	0.674
8	1.623	1.687	0.649	0.669
8.5	1.672	1.74	0.641	0.673
9	1.699	1.768	0.637	0.664
9.5	1.708	1.777	0.634	0.664
10	1.718	1.788	0.636	0.669
10.5	1.743	1.807	0.640	0.657
11	1.791	1.837	0.640	0.672
11.5	1.679	1.727	0.639	0.669
12	1.634	1.679	0.643	0.681
12.5	1.647	1.692	0.649	0.674
13	1.745	1.783	0.640	0.680
13.5	1.877	1.921	0.639	0.658
14	2.014	2.053	0.637	0.662
14.5	1.912	1.935	0.629	0.651
15	1.484	1.516	0.629	0.651

Figure B.3: Scanned surface of experiment of figure 10.9